

Production of actinide atomic and molecular ion beams at CERN-ISOLDE

Dissertation
zur Erlangung des Grades

“Doktor der Naturwissenschaften”

im Promotionsfach Chemie
am Fachbereich Chemie, Pharmazie, Geographie und Geowissenschaften
der Johannes Gutenberg-Universität in Mainz

Mia Au

geb. in Edmonton, Canada

Mainz, 2023



Examiners (Gutachter)

Supervisor (Berichterstatter): Prof. Dr. Christoph E. Düllmann

Supervisor (Berichterstatter): Dr. Sebastian Rothe

Prof. (adj.) Dr. Jens Lassen

Date of the oral examination: 13 September 2023



This project has received funding from the European Union's Horizon 2020 Research and Innovation Program under grant agreement number 861198 project 'LISA' (Laser Ionization and Spectroscopy of Actinides) Marie Skłodowska-Curie Innovative Training Network (ITN).

Abstract

The Isotope Separation On-Line method is used to produce, extract, ionize and deliver a wide variety of radionuclides/radioisotopes as ion beams at the CERN-ISOLDE facility. This work investigates the application of the ISOL method towards the production of nuclides in the elusive actinide region of the nuclear chart.

Actinide nuclides were produced in nuclear reactions with 1.4-GeV protons incident on a bulk target. They were extracted, delivered to different experimental stations and identified through measurements of their unique properties. The production of atomic ion beams was investigated for the elements with atomic numbers 89-94. Actinium was ionized using resonance laser ionization and delivered as an atomic ion beam, facilitating experimental studies of the isotopes $^{224-231}\text{Ac}$. The elements neptunium and plutonium were identified for the first time at ISOLDE. Extracted and mass-separated ion beam rates for $^{235-241}\text{Np}$ and $^{234-241}\text{Pu}$ were measured and compared with predictions from simulations.

Molecular formation via injection of CF_4 gas was used to extract actinide nuclides in the form of molecular fluoride ion beams. Ac^+ , AcF^+ , and AcF_2^+ were identified by α - and γ -decay spectroscopy measurements as well as by time-of-flight mass measurements. Successful production of AcF^+ enabled the first laser spectroscopy studies of the AcF molecule. Uranium, neptunium, and plutonium molecules were observed. Molecules were also formed from the mass-separated ion beams in a helium-buffer-gas-filled radio-frequency-quadrupole cooler-buncher ion trap by reactions with residual gas impurities. Varying the interaction time in the trap was shown to affect the formation rates of molecular species, providing a method to produce molecules of interest at ambient temperature.

The study of radiogenically produced species is prioritized at ISOLDE, thus technical developments often need to be pursued at “offline” facilities without direct irradiation. ISOLDE’s offline 2 mass separator facility features copies of key ISOLDE infrastructure, making it ideal to develop the next generation of ion beams. To enable systematic studies of molecular formation, ionization, breakup and fundamental properties, ISOLDE’s offline 2 mass separator facility has been upgraded with two new gas systems and time-resolved single-ion-counting data acquisition.

Thank you so much to all the people in my life who have helped me get to this point. You have my deepest gratitude.

Contents

List of Tables	vi
List of Figures	vii
List of Acronyms	viii

Preamble

Introduction	1
1.1 Radionuclide production	3
1.1.1 The ISOL method	5
1.1.2 The ISOLDE facility	5
1.1.3 Release from ISOL targets	7
1.2 Molecular beams	9
1.2.1 Nuclear physics observables in molecules	12
1.2.2 Searches for physics beyond the Standard Model	13
1.3 Ion sources	14
Experimental techniques	19
2.1 Resonance laser ionization	20
2.2 Ion trapping	22
2.2.1 Time-of-flight mass measurements	22
2.2.2 Trapping of non-isobaric species	23
2.3 Radioactive decay spectroscopy	24
2.4 Techniques for studies of molecular beams	27
2.5 Experimental requirements	29

Results and Discussion

The actinide mass region	34
---------------------------------	-----------

Production of actinide atomic ion beams	36
4.1 Actinium	36
4.2 Thorium	38
4.3 Protactinium	39
4.4 Uranium	40
4.5 Publication I: Production of neptunium and plutonium nu- clides from uranium carbide using 1.4-GeV protons	40
Extraction and production of molecular ion beams containing an actinide nucleus	56
5.1 Publication II: In-source and in-trap formation of molecular ions in the actinide mass range at CERN-ISOLDE	57
5.2 Publication in preparation: Actinium fluorides	64
5.3 Thorium molecular ions	72
5.4 Protactinium molecular ions	72
5.5 Uranium molecular ions	73
5.6 Transuranium molecular ions	74
Offline developments for studies of molecular beams	80
6.1 Introduction	80
6.2 Publication III: Developments at CERN-ISOLDE's OFFLINE 2 mass separator facility for studies of molecular ion beams . .	81
Conclusions	87
7.1 Target and ion source operation for molecular beams	87
7.1.1 In-source molecular formation	88
7.1.2 Injection of reactive gases	88
7.2 Availability of actinides	90
7.2.1 Actinium	90
7.2.2 Thorium	91
7.2.3 Protactinium	92
7.2.4 Uranium	92
7.2.5 Transuranium elements	93
7.3 Radioactive molecular beams	94
Outlook	95
Complete List of Publications	97
Bibliography	102
Curriculum Vitæ	122

List of Tables

5.1	Purity of AcF_x^+ beams	68
5.2	Yields from collections of $^{225}\text{Ac}^{19}\text{F}_2^+$	70
5.3	Yields from collections of $^{234,238}\text{Np}^{19}\text{F}_x^+$	77

List of Figures

1.1	Periodic table of the elements	1
1.2	Chart of the nuclides	2
1.3	ISOLDE experiments	6
1.4	Release from ISOL targets	7
1.5	Nuclear chart of production at CERN-ISOLDE	10
1.6	The molecular landscape	11
1.7	MK1 and VD5 ion sources	17
1.8	Experimental schematic	18
2.1	GLM TISD chamber	20
2.2	Mass scans with and without RILIS for U	22
2.3	FTS alpha detector	25
2.4	LA1 collection chamber assembly	26
2.5	Target and ion source assembly	27
3.1	ToF spectra of isobaric contaminants	35
4.1	Resonance laser ionization of ^{225}Ac	37
4.2	RILIS schemes of Pa	39
4.3	Resonance ionization of $^{235,238}\text{U}$	41
4.4	RILIS scheme of U	41
5.1	$^{225}\text{Ac}^{19}\text{F}_2^+$ α -decay spectrum	65
5.2	ToF spectrum of $^{225}\text{AcF}_2^+$	67
5.3	ToF spectra of $^{226}\text{AcF}_x^+$ sidebands	69
5.4	$^{225}\text{AcF}_2$ sample decay	70
5.5	Mass scan with and without 532-nm laser light	73
5.6	ToF spectra of $A = 234, 238, 250, 252, 258, 273, 276$	75
5.7	ToF spectra with molecular formation for Ta and U	76
5.8	ToF spectra of Np, Pu fluorides	79

List of Acronyms

ALTO	Accélérateur Linéaire auprès du Tandem d'Orsay
AME	Atomic Mass Evaluation
ARIEL	Advanced Rare Isotope Laboratory
BSM	Beyond the Standard Model
COLLAPS	COLlinear Laser Spectroscopy
<i>C,P,T</i>	Charge, Parity, Time
CRIS	Collinear Resonance Ionization Spectroscopy
DC	Direct Current
EDM	Electric Dipole Moment
FC	Faraday Cup
FEBIAD	Forced Electron Beam Induced Arc Discharge
FLUKA	FLUktuierende KAskade
FRIB	Facility for Rare Isotope Beams
FTS	Fast Tape Station
FWHM	Full-Width at Half-Maximum
GANIL	Grand Accélérateur National d'Ions Lourds
GEANT4	GEometry ANd Tracking
GPS	General Purpose Separator
GSI	Gesellschaft für Schwerionenforschung
HIE-ISOLDE	High Intensity and Energy ISOLDE
HPGe	High Purity Germanium detector
HRS	High Resolution Separator
IGISOL	Ion Guide Isotope Separator On Line
ISAC	Isotope Separator and ACcelerator
ISCOOL	ISOLDE cooler
ISOL	Isotope Separation On-Line
ISOLDE	Isotope Separator On-Line DEvice
ISOLTRAP	The ISOLTRAP experiment
IUPAC	International Union of Pure and Applied Chemistry
MEDICIS	MEDical Isotopes Collected from ISOLDE
MR-ToF MS	Multi-Reflection Time-of-Flight Mass Spectrometer

MYRRHA	Multi-purpose hYbrid Research Reactor for High-tech Applications
PI-LIST	Perpendicularly-Illuminated Ion Source and Trap
PIPS	Passively-Implanted Planar Silicon
PNPI	Petersburg National Physics Institute
PSB	Proton Synchrotron Booster
REX	Radioactive beam Experiments
RF	Radio Frequency
RFQ	Radio Frequency Quadrupole
RFQcb	Radio Frequency Quadrupole cooler and buncher
RIB	Radioactive Ion Beam
RIBF	Radioactive Ion Beam Factory
RIKEN	Rikagaku Kenkyujyo
RILIS	Resonance Ionization Laser Ion Source
RISP	Rare Isotope Science Project
SPES	Selective Production of Exotic Species
SRIM	Stopping and Range of Ions in Matter
ToF	Time-of-Flight
Ti:Sa	Titanium Sapphire laser
TISD	Target and Ion Source Development
TRIUMF	TRI University Meson Facility
VADIS	Versatile Arc Discharge Ion Source

Preamble

Introduction	1
1.1 Radionuclide production	3
1.2 Molecular beams	9
1.3 Ion sources	14
Experimental techniques	19
2.1 Resonance laser ionization	20
2.2 Ion trapping	22
2.3 Radioactive decay spectroscopy	24
2.4 Techniques for studies of molecular beams	27
2.5 Experimental requirements	29

1. Introduction

The periodic table of the elements describes all the elements discovered so far (Fig. 1.1). Central to the definition of each element is the nucleus, a configuration of protons and neutrons that defines each element by its unique proton number Z . In a neutral atom, the proton number corresponds to the number of electrons each element has, giving elements their unique chemical properties.

1 H Hydrogen																	2 He Helium
3 Li Lithium	4 Be Beryllium											5 B Boron	6 C Carbon	7 N Nitrogen	8 O Oxygen	9 F Fluorine	10 Ne Neon
11 Na Sodium	12 Mg Magnesium											13 Al Aluminium	14 Si Silicon	15 P Phosphorus	16 S Sulphur	17 Cl Chlorine	18 Ar Argon
19 K Potassium	20 Ca Calcium	21 Sc Scandium	22 Ti Titanium	23 V Vanadium	24 Cr Chromium	25 Mn Manganese	26 Fe Iron	27 Co Cobalt	28 Ni Nickel	29 Cu Copper	30 Zn Zinc	31 Ga Gallium	32 Ge Germanium	33 As Arsenic	34 Se Selenium	35 Br Bromine	36 Kr Krypton
37 Rb Rubidium	38 Sr Strontium	39 Y Yttrium	40 Zr Zirconium	41 Nb Niobium	42 Mo Molybdenum	43 Tc Technetium	44 Ru Ruthenium	45 Rh Rhodium	46 Pd Palladium	47 Ag Silver	48 Cd Cadmium	49 In Indium	50 Sn Tin	51 Sb Antimony	52 Te Tellurium	53 I Iodine	54 Xe Xenon
55 Cs Cesium	56 Ba Barium	57-71 Lanthanides	72 Hf Hafnium	73 Ta Tantalum	74 W Tungsten	75 Re Rhenium	76 Os Osmium	77 Ir Iridium	78 Pt Platinum	79 Au Gold	80 Hg Mercury	81 Tl Thallium	82 Pb Lead	83 Bi Bismuth	84 Po Polonium	85 At Astatine	86 Rn Radon
87 Fr Francium	88 Ra Radium	89-103 Actinides	104 Rf Rutherfordium	105 Db Dubnium	106 Sg Seaborgium	107 Bh Bohrium	108 Hs Hassium	109 Mt Meitnerium	110 Ds Darmstadtium	111 Rg Roentgenium	112 Cn Copernicium	113 Nh Nihonium	114 Fl Flerovium	115 Mc Moscovium	116 Lv Livermorium	117 Ts Tennessine	118 Og Oganesson

57 La Lanthanum	58 Ce Cerium	59 Pr Praseodymium	60 Nd Neodymium	61 Pm Promethium	62 Sm Samarium	63 Eu Europium	64 Gd Gadolinium	65 Tb Terbium	66 Dy Dysprosium	67 Ho Holmium	68 Er Erbium	69 Tm Thulium	70 Yb Ytterbium	71 Lu Lutetium
89 Ac Actinium	90 Th Thorium	91 Pa Protactinium	92 U Uranium	93 Np Neptunium	94 Pu Plutonium	95 Am Americium	96 Cm Curium	97 Bk Berkelium	98 Cf Californium	99 Es Einsteinium	100 Fm Fermium	101 Md Mendelevium	102 No Nobelium	103 Lr Lawrencium

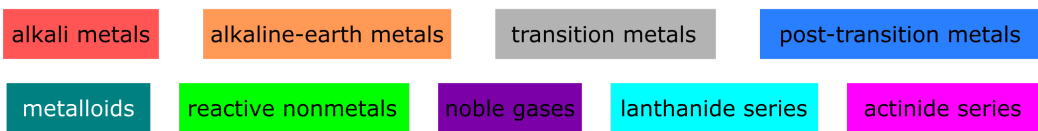


Figure 1.1: The periodic table of the elements classified unofficially according to behaviour. There is no standard agreement on the definition of the “metalloids” (semimetals), which display mixed properties of both metals and non-metals. While “lanthanoid” and “actinoid” are the IUPAC-recommended terms for the elements 57-71 and 89-103 respectively [1], “lanthanide” and “actinide” are widely used and are used in this work.

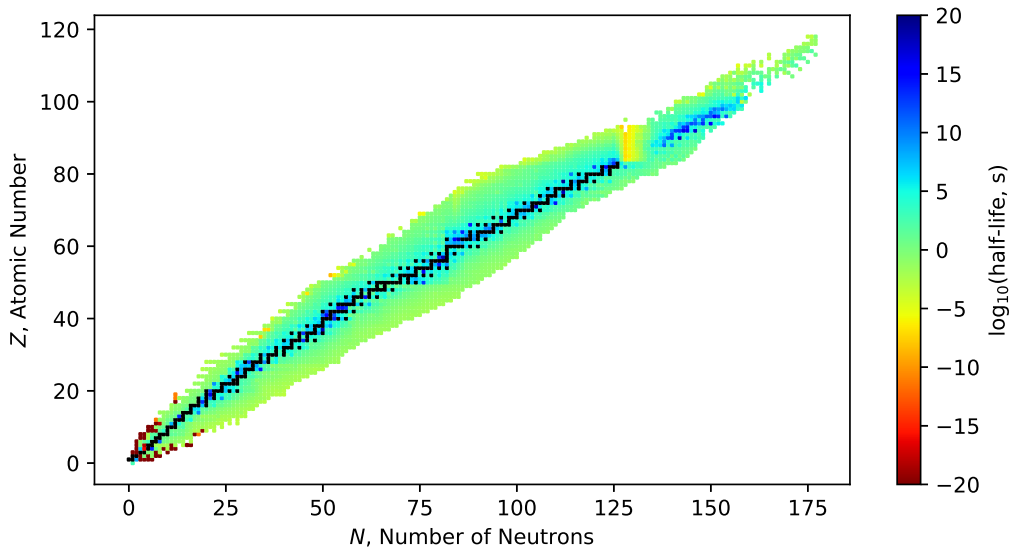


Figure 1.2: The chart of the nuclides as of the 2021 Atomic Mass Evaluation (AME) [2], with 3340 squares each indicating a discovered nucleus with proton number Z and neutron number N . The colour represents the half-life of the ground state in logarithmic scale, with stable nuclides shown in black.

While each element has a fixed number of protons, there exist multiple possibilities for the corresponding number of neutrons (N). This range of nuclear configurations over which the combination of protons and neutrons are bound into a nucleus gives rise to *isotopes*: nuclides of the same element with a different number of neutrons in the nucleus. Many of these configurations are unstable (Fig. 1.2)—after a finite half-life, they transform into other nuclei through the processes of radioactive decay.

The actinide series refers to the elements with atomic numbers $Z = 89 - 103$. None of the actinide elements are stable. They feature unique nuclear and chemical properties, in addition to their potential applications. There are open questions in the actinide region of the nuclear chart about topics including the modeling of astrophysical isotopic abundances and the rapid-neutron capture process [3], as well as nuclear fission properties [4, 5]. Experimental measurements of nuclear masses, β -decay, neutron capture, and fission properties are required to benchmark theoretical nuclear structure models but are, so far, missing for many nuclei [6, 7]. Some actinides can be applied for diagnostics or treatment in nuclear medicine [8, 9, 10], while others find a variety of potential uses in fields such as environmental monitoring [11] and energy production [12]. The factor that currently limits

both the study and use of the actinides is the availability of many desired isotopes in a form accessible for these experiments and applications.

There are very few naturally occurring isotopes of the actinide elements on Earth, making them difficult to study or use. With the exception of several thorium and uranium isotopes, the actinides available on Earth are produced naturally in the decay of other actinides, or artificially through nuclear reactions. Their radioactivity and lack of availability pose a challenge for extracting information about atomic or nuclear structure from these nuclides. The first necessary step towards advancements in the actinide region is to produce these radioactive nuclides in a usable form for experiments. The Isotope Separation On-Line (ISOL) technique is used worldwide to produce radioactive isotopes. In this work, the ISOL technique is explored for production of actinide nuclides as a radioactive ion beam (RIB) of atomic and molecular ions.

1.1 The production of radioactive nuclides

Since the discovery of the atomic nucleus, experimental studies of its properties have shaped the field of nuclear science. While more than 3000 nuclides are known (see Fig. 1.2), and approximately 7000 are predicted to be bound, only 288 of these are stable [2, 13]. To study the majority of these nuclides, they must first be produced through nuclear reactions. Generator systems make use of radioactive nuclear decay to produce nuclides in decay chains, while reactor-based and accelerator-based techniques are used to drive other nuclear reactions needed to produce radioactive nuclides.

Generator systems make use of radioactive decay chains to obtain a supply of a particular radioactive nucleus by maintaining a supply of the radioactively decaying parent nucleus. Some generator systems are used for the production of medical radionuclides, such as ^{99}Mo as a parent of the ^{99m}Tc used in diagnostic imaging. Generators for actinide isotopes include ^{223}Ra and ^{227}Th from ^{227}Ac [14]. This process is dependent on the half-lives and decay pathways of the parent nucleus, and as such, is feasible only for a selection of pairs or chains of isotopes.

In reactors, fissile nuclides such as ^{235}U or ^{239}Pu split into smaller fragment nuclides through neutron-induced fission. This process generates radioactive fission fragments along with high-energy and, upon thermalization, thermal neutrons, and γ -radiation. Samples can be placed in this neutron flux and irradiated, which can induce nuclear reactions such as neutron capture and subsequent radioactive decay. An example includes the production of the parent for the previously mentioned ^{99m}Tc generator system: the ^{99}Mo is

most commonly produced from the neutron activation of stable ^{98}Mo [15]. Sizeable amounts of other radioactive species can be produced through irradiation in this environment, called “reactor breeding”, and collected for further processing [16].

Accelerator-based techniques use accelerated, energetic particles to induce nuclear reactions, which create the radioactive nuclides of interest. Accelerator-based radionuclide production is often called an “online” technique, i.e., a continuous irradiation and production process that typically requires the operation of a driving accelerator. Proton driver beams are, e.g., used at CERN-ISOLDE [17, 18] (Geneva, Switzerland), TRIUMF-ISAC (Vancouver, Canada) [19, 20], GANIL (Caen, France) [21, 22], RAON-RISP (Daejeon, Korea) [23, 24], and will also be used at INFN-SPES (Legnaro, Italy) [25, 26] and ISOL@MYRRHA (Mol, Belgium) [27, 28]. Electron driver beams are used for photofission at ALTO (Orsay, France) [29, 30] and TRIUMF-ARIEL (Vancouver, Canada). Other driver beams such as neutrons, deuterons, light and/or heavy-ion beams are used at IGISOL (Jyväskylä, Finland) [31, 32], FRIB (Michigan, USA) [33, 34], GSI (Darmstadt, Germany) [35, 36], RIKEN-RIBF (Wako, Japan) [37, 38], PNPI (Gatchina, Russia) [39, 40] and also at GANIL, ALTO, and RAON in addition to their other beams. From this non-exhaustive list of worldwide facilities, many are operational, while others are under construction.

While some of these facilities, particularly those with proton driver beams, use the ISOL technique for radioisotope production, others use in-flight fragment separation techniques [41] to provide access to a wide range of very short-lived isotopes. The in-flight technique uses high-energy projectiles on thin targets, creating reaction products that typically retain a large forward momentum from the primary beam without the need for reacceleration. The desired reaction products must then be separated from the primary beam and the other reaction products, typically using energy degraders and electromagnetic mass separators. Unlike the ISOL method, the in-flight process is independent of chemical properties and radioisotope half-life. In-flight facilities can also stop reaction fragments in a gas cell or catcher, followed by extraction and re-acceleration of a lower-energy beam for subsequent mass-separation.

Online facilities may also generate radioactive species in symbiotic installations for a range of applications, e.g., ISOLDE-MEDICIS [42]. Separation of the reaction products can then be employed “offline”—without continuous irradiation—to obtain comparatively longer-lived isotopes for medical and related research purposes.

1.1.1 The ISOL method

Since its first use in 1950 [43], the ISOL method has been applied at many RIB facilities worldwide for the production and study of radioactive isotopes across the nuclear chart. ISOL facilities produce radioactive nuclei through reactions between the beam of accelerated particles and target materials, predominantly inducing fission, fragmentation, and spallation of the target nucleus. The nuclei generated in these reactions are typically lighter (lower nucleon number A) than the nucleon number of the target nucleus. Following the creation of nuclear reaction products in the target, the nuclei of interest are extracted from the target matrix through a complex process known as release. After the nuclei of interest are released from the target unit, they arrive at the ion source, where they are ionized and extracted across an electrical potential difference to form a RIB.

The ions produced in this process are then separated. In online operation, the separation occurs during continuous irradiation and production. Mass separators typically use a magnetic field, in which the ions follow a curved path with a radius corresponding to their mass-to-charge ratio m/q . A specific bending radius corresponds to a selected m/q . During the separation step, only species in the ion beam with the selected m/q will be transmitted, with a resolution given by the separator's mass-resolving power $R = m/\Delta m$. With sufficient mass-resolving power, such separation can often limit the transmission to a single isobar—singly-charged species with the same given number of nucleons. The mass-separated beam can then be delivered to experimental end stations.

In the actinide region, only ^{232}Th and ^{238}U are available in practical quantities for the preparation of bulk ISOL targets, which typically require grams of material. The applicability of the ISOL method to the production and subsequent study of actinide elements remains to be evaluated, and is the focus of this work.

1.1.2 The ISOLDE facility

The ISOLDE facility at CERN [17] is a radioactive ion beam facility that uses 1.4-GeV protons from the Proton Synchrotron Booster (PSB) to induce nuclear reactions in thick targets. With the ISOL technique, the ISOLDE facility has provided more than 1000 isotopes from 76 elements [44, 45]. ISOLDE provides radioactive ion beams of atomic or molecular species for experiments that address a broad range of interdisciplinary scientific questions. Experimental infrastructure available at the facility (Fig. 1.3) allows studies ranging from solid-state physics research [46] and chemistry [47], to nu-

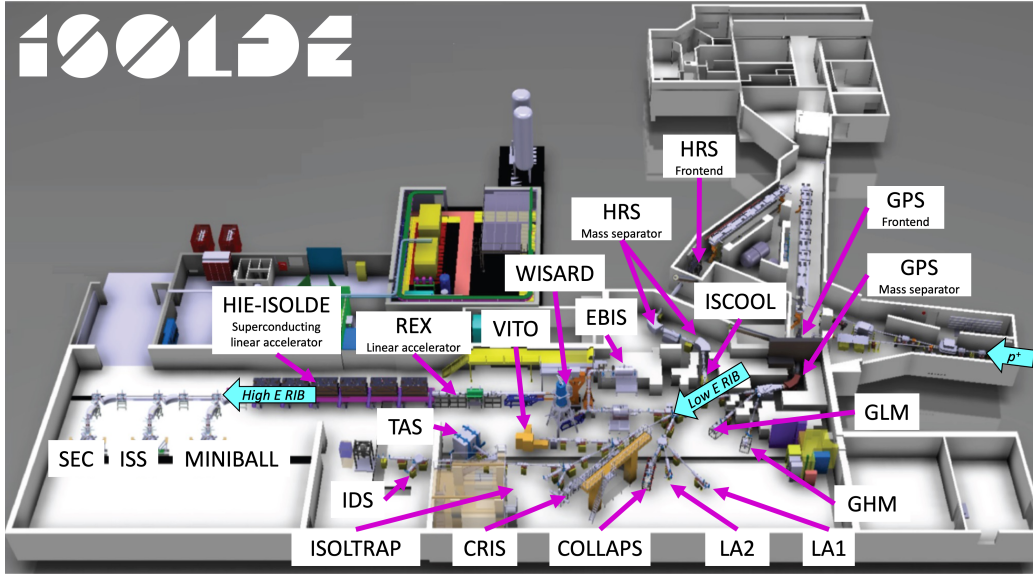


Figure 1.3: ISOLDE experimental hall

clear physics research through techniques including decay spectroscopy [48], ion trapping [49, 50, 51], laser spectroscopy [52, 53, 54], and nuclear reactions [55, 56, 57].

At the target station, the target material and attached ion source are contained within a hermetically-sealed vacuum vessel biased to a voltage between 30 and 60 kV. The proton beam impacts the target nuclei within the target and ion source unit, generating radioactive isotopes which are released from the target material. During the release process, nuclei diffuse randomly through the target material and experience many collisions with surfaces of the target container as well as collisions and interactions with surfaces and grain boundaries within the target material itself. In typical operation, the process is promoted by resistively heating the target container to temperatures in the vicinity of 2000 °C to facilitate diffusion and effusion. The diffusing atoms reach the ion source, where they are ionized, typically by removing an electron to form a singly-charged atomic ion. The ions are then extracted to ground potential at energies of 30-60 keV and can be further accelerated through Radioactive beam Experiments (REX) and High Energy and Intensity ISOLDE (HIE-ISOLDE) to energies of up to 10 MeV/u [58].

ISOLDE's two online target stations are coupled to two mass separators known as the General Purpose Separator (GPS) and the High-Resolution Separator (HRS). With approximate mass resolving powers $R = 800$ for the GPS and $R = 6000$ for the HRS [17], the separators nominally transmit one

isobar. The mass-separated ions are then sent into the experimental beam lines shown in Figure 1.3. The HRS includes a radio-frequency quadrupole cooler-buncher (RFQcb) called the ISOLDE cooler (ISCOOL), which uses direct current (DC) potentials to confine ions along the beam axis and oscillating potentials for radial confinement. Ions are typically trapped in the ISCOOL and cooled by repeated collisions with atoms of a constantly injected buffer gas maintained at higher pressures ($\approx 10^{-6}$ mbar) than the rest of the facility beam line via differential pumping. While both separators can provide continuous beam, the HRS separator can also deliver cooled and bunched beams through the ISCOOL.

ISOLDE also hosts two irradiation points located after the primary target at each target station, where standard ISOLDE targets or material samples can be irradiated. Irradiated targets or samples can be coupled to the CERN-MEDICIS facility for offline extraction of medical isotopes [42] or coupled to the ISOLDE target stations to deliver long-lived isotopes. This mode of operation can deliver RIBs to experiments without protons continuously hitting the target material, and is therefore independent from the operation of the CERN accelerator complex.

1.1.3 Release from ISOL targets

Nuclides produced in reactions between the accelerated protons and the target nuclei are created through a variety of nuclear reactions, many of which could result in the reaction product forming at the site of the original target nucleus, within the bulk material of the ISOL target. The reaction product then leaves the target material through the so-called release process, illustrated in Fig. 1.4.

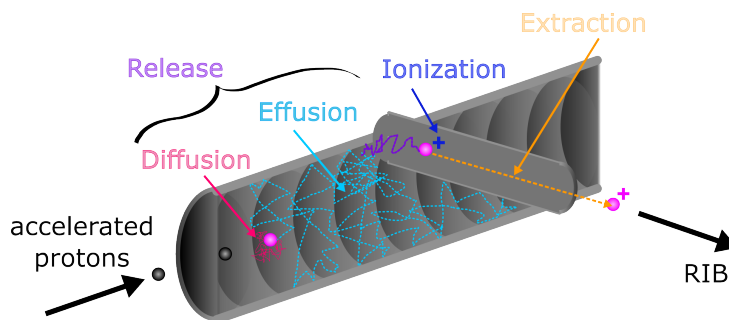


Figure 1.4: Schematic of the release process, showing the incoming accelerated beam (black) creating the nuclide of interest (pink) which undergoes diffusion (red) and effusion (light blue) before being released from the target (purple), ionized (dark blue) and finally extracted (orange) as a RIB.

The first step of the release process is diffusion of the reaction product, which is typically assumed to take the form of a neutral atom. The target material is installed within a cylindrical tantalum container that is heated resistively using a current of several hundred amperes to operating temperatures near 2000 °C. At these temperatures, diffusion through the bulk target material governs the transport of the nuclide to grain surfaces or pore boundaries. The diffusion process depends on the chemical properties of the target material, the reaction product, and the target structural materials, as well as the materials' properties. Numerous diffusion mechanisms including bulk diffusion, surface diffusion, grain boundary diffusion, and lattice diffusion can occur.

At grain surfaces and pore boundaries, desorption of the nuclide may occur, depending again on the chemical properties between the surface and the radionuclide as well as on the vapor pressure of the element of interest. After desorption, the atoms effuse out of the material as a gas. During the effusion process, the radionuclide may undergo many collisions with the target and container materials, such that the residence (“sticking”) time on these surfaces governs the transport out of the target. Strong reactivity between the isotope and target material results in long sticking times and poor release. Similarly, strong interactions with the tantalum container material will prevent quick effusion of the nuclide of interest into the ion source.

Each reaction product undergoes many such interactions on average before the nucleus of interest is released and reaches the ion source. Each component of the release process has a characteristic time scale, contributing to an overall length of the process which sets a lower limit on the time with which a radioactive isotope can still be successfully released. This, in turn, dictates a minimum half-life with which an isotope can be extracted. The dependence of release time on the target material is an area of constant development, with recent focus on enhancement of open porosity and reduction of characteristic length scales in the bulk target material. Several studies on nanomaterials show an improvement in yield for some short-lived isotopes, with recent reviews [59, 60] describing attempts and advances in the field of engineered target materials.

Refractory species, with high melting and boiling points and low vapor pressures even in vacuum at 2000 °C, are notoriously difficult to release from thick ISOL-type targets as demonstrated in Fig. 1.5. Elements such as carbon, boron, silicon, vanadium, and the refractory metals are released with prohibitively low efficiencies for measurement or experiments. The actinides present a similar challenge and require developments in extraction techniques.

1.2 Molecular beams

Molecular beams have been studied for decades at ISOLDE [61, 62, 63, 64, 65] as a way to enhance volatility of reactive species and provide high-purity beams of isotopes of interest such as carbon [66, 67] and boron [45, 68]. This method to efficiently deliver beams of release-limited, refractory elements is known as molecular sideband extraction. Additionally, extraction using a molecular sideband is used as a technique to improve beam purity by shifting the species of interest away from background-dominated isobars into mass regions with fewer ionized contaminants.

In addition to their uses for isotope extraction, molecular beams provide new opportunities for fundamental physics studies at RIB facilities. The study of molecules containing short-lived radioactive isotopes has received attention as a promising pathway for progress in fundamental and applied science, recently drawing together an international research community with multidisciplinary interests outlined in Ref. [69]. Molecular species offer greater sensitivity by orders of magnitude to observables associated with searches for new physics Beyond the Standard Model (BSM) [70, 71]. Additionally, new techniques for studies of nuclear structure such as charge radii and nuclear moments using experimental observables in molecules offer alternative methods to the nuclear physics research already being conducted at RIB facilities [72].

Molecular formation can occur along the path followed by the radioactive species, adding another step to the release process. Molecules can be formed from reactants in the target material, e.g. oxide molecules forming between a radioactive isotope and an oxide target material. In some cases this can be beneficial; refractory radioactive carbon is more easily extracted as volatile CO^+ from CaO targets [68]. In other cases, oxide and carbide molecules forming from the ceramic oxide and carbide materials commonly employed as ISOL targets may be more refractory than the radioactive atomic species, observed, for example, in the case of Ac_2O_3 formation, which results in higher required temperatures for extraction of actinium from ThO_2 matrices [73]. Alternatively, reactants for molecular formation can be added to the target and ion source environment deliberately. Previous studies have explored providing reactive gases to different target and ion source combinations via calibrated leaks or vapors from solids, observing the formation of molecules and molecular ions [74].

Molecules will have different volatility, vapor pressure and adsorption enthalpy than their constituent radioactive atoms, giving them different release and ionization properties. Refractory elements, including e.g. Si, B, C, and transition metals Nb, Mo, Tc, W, Re, Os, are not successfully extracted

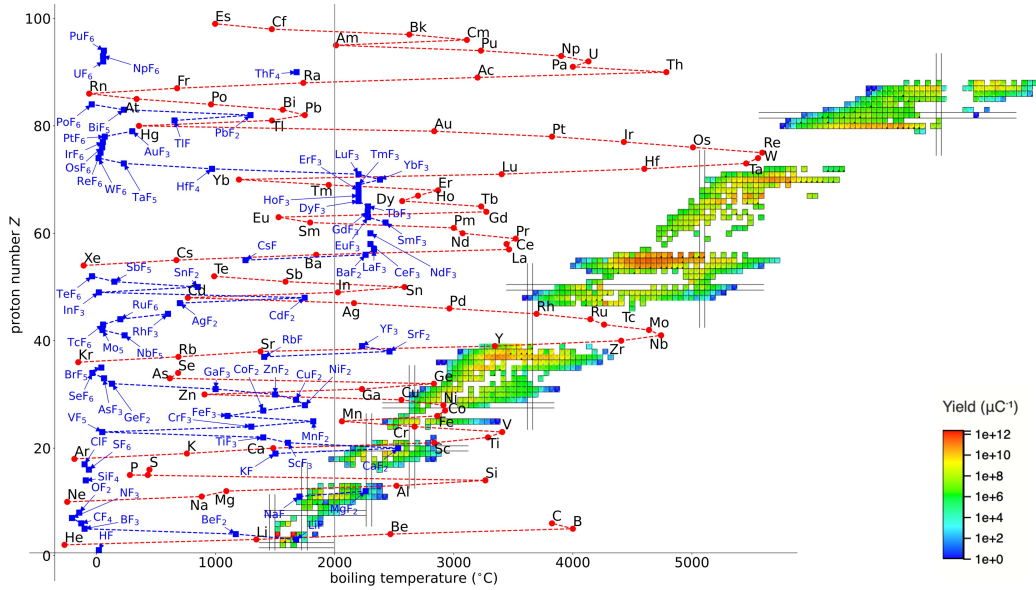


Figure 1.5: The nuclear chart of isotopes produced and measured at CERN-ISOLDE, with colours indicating the measured extraction rate of each nuclide in ions per μC of 1.4-GeV protons incident on the target. Horizontal gaps in the data are an indication of elements that are not easily extracted. Overlay: literature boiling temperatures of the elements (red) and literature boiling temperatures of selected fluoride compounds of the elements (blue), aligned by proton number Z . The grey vertical line indicates the typical operating temperature of target and ion source units at the ISOLDE facility. Adapted from [75].

as a monatomic gas, corresponding to the absence of these elements from ISOLDE's catalogue of available RIBs (see Fig. 1.5). Some of these form molecular species that are more volatile than the monatomic gas, enabling extraction of these elements that would otherwise be too refractory. The volatile species may then travel through the target as a neutral molecule before reaching the ion source, where it can ionize or dissociate, enhancing yield by breaking up larger molecules, or decreasing yield by dissociating the molecule of interest. The distribution of the nucleus of interest into molecular sidebands depends both on the chemical equilibrium within the target and ion source environment and on the employed ionization mechanism.

Fluorine, the most electronegative element, reacts with many species to form molecules that are stable in the environment of the ISOL target and ion source as well as potentially more volatile species of otherwise refractory elements as highlighted in Fig. 1.5. Radioactive beams of fluoride molecules

have been observed as sidebands or contaminants in several experiments (BaF, BF_x, RaF, SrF), some even without the presence of reactive fluorine gas. With only one stable isotope (¹⁹F), fluorine simplifies the distribution of molecular sidebands across different masses, compared to other halogens such as chlorine, which would either require isotopically purified sources or split the population of radioactive molecules across two masses according to the natural isotopic abundances of ^{35,37}Cl. Other such sidebands have been observed and noted over years of operation (Figure 1.6 shows some of these along with others that have yet to be seen), making them promising potential candidates to the study of radioactive molecules. The injection of reactive gases was applied for the formation of volatile fluoride molecules in this work.

1																	2
H																	He
3	4											5	6	7	8	9	10
Li	Be											B	C	N	O	F	Ne
11	12											13	14	15	16	17	18
Na	Mg											Al	Si	P	S	Cl	Ar
19	20	21	22	23	24	25	26	27	28	29	30	31	32	33	34	35	36
K	Ca	Sc	Ti	V	Cr	Mn	Fe	Co	Ni	Cu	Zn	Ga	Ge	As	Se	Br	Kr
37	38	39	40	41	42	43	44	45	46	47	48	49	50	51	52	53	54
Rb	Sr	Y	Zr	Nb	Mo	Tc	Ru	Rh	Pd	Ag	Cd	In	Sn	Sb	Te	I	Xe
55	56	57-71	72	73	74	75	76	77	78	79	80	81	82	83	84	85	86
Cs	Ba	Lanthanides	Hf	Ta	W	Re	Os	Ir	Pt	Au	Hg	Tl	Pb	Bi	Po	At	Rn
87	88	89-103	104	105	106	107	108	109	110	111	112	113	114	115	116	117	118
Fr	Ra	Actinides	Rf	Db	Sg	Bh	Hs	Mt	Ds	Rg	Cn	Nh	Fl	Mc	Lv	Ts	Og

57	58	59	60	61	62	63	64	65	66	67	68	69	70	71
La	Ce	Pr	Nd	Pm	Sm	Eu	Gd	Tb	Dy	Ho	Er	Tm	Yb	Lu
Lanthanum	Cerium	Praseodymium	Neodymium	Promethium	Samarium	Europium	Gadolinium	Terbium	Dysprosium	Holmium	Erbium	Thulium	Ytterbium	Lutetium
89	90	91	92	93	94	95	96	97	98	99	100	101	102	103
Ac	Th	Pa	U	Np	Pu	Am	Cm	Bk	Cf	Es	Fm	Md	No	Lr
Actinium	Thorium	Protactinium	Uranium	Neptunium	Plutonium	Americium	Curium	Berkelium	Californium	Einsteinium	Fermium	Mendelevium	Nobelium	Lawrencium

HX ⁺	BeX ⁺	AlX ⁺	SiX ⁺	NX ⁺	XO ⁺	XCO ⁺	XS ⁺	XF ⁺	XCl ⁺
NaX ⁺	MgX ⁺				XO ₂ ⁺	XO ₃ ⁺		XF ₂ ⁺	XBr ⁺
KX ⁺	CaX ⁺							XF ₃ ⁺	
	SrX ⁺							XF ₄ ⁺	
	BaX ⁺								

Figure 1.6: Summary of potential radioactive molecular ion beams seen and predicted from ISOL targets and ion sources [76]. Some of the molecules (e.g. the transition metal carbonyl or oxide compounds or COTe) are conceptual and would require ion source developments. The actinides other than U are predicted to form compounds with a variety of valence states and require beam developments. Plasma or electron bombardment ion sources may cause molecular fragmentation.

Multiple diatomic species have been produced historically at ISOLDE, with success especially in the cases of molecules that are stable at high temperatures. Recent experiments on the RaF molecule mark a milestone as the first laser spectroscopy conducted of a short-lived radioactive molecule [77, 78], performed by producing ion beams of radium fluoride and delivering them to ISOLDE’s Collinear Resonance Ionization Spectroscopy (CRIS) [53] experiment. The radioactive radium isotope was generated by proton impact on the uranium target nucleus. The radium must move through the target material to find a corresponding fluorine atom, where it can then form a molecule. RaF is then ionized using surface ionization in a hot cavity ion source, after which it can be extracted as a RIB. For long-lived isotopes, it is possible to irradiate the target without heating, thus limiting diffusion of the produced species and collecting activity of the isotope of interest within the thick target matrix. Such targets can then be stored and used as sources of long-lived radioactive molecular beams. As was done in the RaF study, the target unit containing the long-lived activity can then be heated to release the remaining isotopes, allowing operation without proton beam.

Polyatomic molecules, with three or more atoms, can offer advantages for precision measurements of fundamental physics [79]. For some of the more fragile molecules, the high-temperature environment of the various ISOLDE targets and ion sources can cause dissociation and breakup. An alternative route to the production of volatile molecules is the use of ion traps to facilitate molecular formation. Ion traps are a staple tool frequently employed at ISOLDE for experiments with radioactive isotopes, and in the preparation of beams for further study [80]. Molecular formation from the primary mass-separated beam has already been observed in both the ISCOOL RFQcb and the ISOLTRAP RFQcb at ISOLDE, likely due to collisions with contaminants in the buffer gas. Ion preparation with buffer gas lends itself to deliberate injection of reactive gases for molecular formation with the radioactive species. Formation of $^{226}\text{RaOH}^+$ has already been observed in an ion trap environment [81]. By injecting trace amounts of reactive gases into ion traps, ISOLDE could develop the capability to intentionally form and deliver species such as polyatomic symmetric-top and chiral molecules from radioactive beams.

1.2.1 Nuclear physics observables in molecules

The rich electronic structure in molecules can also be employed for nuclear-structure studies using resonance laser ionization, in a similar manner to that discussed previously in the context of atomic systems. Molecular structure can be sensitive to the nuclear size [77], electromagnetic moments [82], and

in some cases may allow spectroscopy experiments to extract nuclear observables that are challenging to obtain in atomic systems [83, 84]. Studies on stable molecules demonstrate successful extraction of nuclear information such as nuclear quadrupole moments from molecules, but the application of such techniques to molecules containing a radioactive nucleus are only beginning to be implemented [72].

1.2.2 Searches for physics beyond the Standard Model

The Standard Model (SM) of particle physics has remained the best description of fundamental particles, interactions, and forces for decades. Despite this notable success, it does not accurately explain all fundamental observations. The baryonic matter we know forms only a very small fraction of the total energy density in the Universe (around 5%), while dark matter is responsible for about 26% [85, 86]. The rest may or may not be what we term “dark energy”, the existence of which has yet to be fully understood. Another puzzle is the baryon asymmetry problem [87]—*why is there more matter than antimatter in our universe?* For this asymmetry to exist, there must be strong charge–parity (CP) violation [88, 89]. Theories are being constructed to better capture these observations, often by proposing new particles. While searches for such new particles can be done using TeV-scale particle colliders, such as the LHC at CERN, nuclear, atomic and molecular physics offer complementary possibilities. Some hypothesized particles are predicted to interact with Standard Model particles in a way that introduces or alters properties that can manifest as experimental observables, e.g. an electric dipole moment (EDM). New approaches based on high-precision investigations at low energy, such as searches for an EDM of the neutron [90], proton [91], or electron [92, 93], or precision studies of radioisotopes involved in nuclear β -decay to search for new interactions [94], are predicted to probe equal or higher-energy scales than those accessible at the LHC. Current limits on the existence of EDMs have already excluded many models that attempt to describe the current understanding of physics. One of the best limits on the electron EDM was measured using an actinide molecule: thorium monoxide (ThO) [93]. At present, the best limit on the electron EDM was measured in hafnium monofluoride (HfF^+) [95].

Atomic systems can possess remarkable sensitivity to the effects of fundamental symmetry violations [70, 96]. Nuclear properties including the Schiff moment and magnetic quadrupole moment can be connected theoretically to underlying time and parity-violating mechanisms in the nucleus, permitting experiments to probe information about fundamental parameters involved in the matter-antimatter asymmetry problem [97].

Some molecules demonstrate further sensitivity enhancement over atoms [98]. Electric polarization can cause energy shifts that can be connected to underlying sources of CP -violation [99, 100]. Heavy polar molecules display exceptionally high internal effective electric fields (e.g. 78 GV cm^{-1} in the case of the electronic state of ThO used in Ref. [93]), resulting in an energy shift proportional to the electron EDM. Recent advances in atomic, molecular and optical precision techniques [79, 96] suggest a potential gain in sensitivity that could offset the effort to adapt the current techniques from atoms to molecules. Radioactive molecules containing heavy, octupole-deformed isotopes have been identified by ongoing theoretical efforts as being the most sensitive probes for searches of new physics using tabletop experiments [101, 102]. Molecules containing actinide nuclei are therefore of high interest for these investigations.

For most molecules containing short-lived isotopes, the electronic, vibrational, rotational, and hyperfine structures are unknown or only predicted by theoretical models. To extract information about fundamental asymmetries from these molecules, both experimental and theoretical values are needed at a high level of precision. Initial characterization and benchmarking of current theories can be conducted by techniques such as the laser spectroscopy experiments at RIB facilities, motivating the addition of radioactive molecular ion beams to the facility catalogue of ion beams available for experiments, particularly the actinide molecules produced in this work.

1.3 Ion sources

The ionization energy or ionization potential (IP) of a species is defined as the energy required to remove the most weakly bound electron from an atom or molecule. This property governs the choice of ion source used in the delivery of the species as a RIB. The ion source also affects the ionization or dissociation of molecules, which could result in isobaric contamination on the mass of interest. Additionally, the choice and operation of the ion source has an effect on the emittance of the extracted ion beam.

Surface ion sources

Surface ionizers, also known as hot cavity ion sources, are a simple method to remove electrons from a species with sufficiently low ionization potential [103]. A hot cavity is formed by typically resistive (Joule) heating by passing a high current through a cylindrical tube. Atoms colliding with the cavity walls can lose or gain electrons through processes dependent on the

specific work function of the cavity material, which can be chosen as required. These hot cavity ion sources are robust and can be operated at high temperatures [104, 105]. In addition, the cavity walls emit electrons, which, together with the positively charged particles inside the cavity, form an electrostatic potential, confining positive charges to the axial center of the ion source [106, 107]. This property leads naturally into the application of these hot cavities as laser ion sources.

Resonance Ionization Laser Ion Source (RILIS)

The ISOLDE RILIS [52] accomplishes element-selective ionization by directing photons into the ion source in the form of laser light. By tuning the frequency of the lasers to sequential electronic transitions in the atom of interest, an electron is step-wise resonantly excited from the atomic ground state or a thermally populated state of a typically neutral species into the continuum, creating an ion. The element-unique electronic structure enables the resonance ionization of a single element while leaving other elements unaffected. In some cases, ionization efficiency values up to 50% have been reported using this technique [108]. Due to the selectivity and efficiency, the RILIS is the most commonly employed ion source at ISOLDE [109]. RILIS can be employed for almost all elements, with exceptions for elements where the first excitation energies require wavelengths below 205 nm, e.g., the noble gases. For elements with IP values below ≈ 4.5 eV, surface ionization is usually very efficient inside the hot cavity, resulting in a high ratio of ions to neutrals, and therefore reducing the relative magnitude of additional effects from laser ionization schemes that promote electrons from the atomic ground state.

In addition to using resonance laser ionization for RIB production, the RILIS is employed to study nuclear properties which can be extracted from laser spectroscopy experiments, such as the charge radius and magnetic moments of the nucleus. A recent overview of the capabilities of laser spectroscopy experiments is given in Ref. [110]. In the RILIS, laser spectroscopy is performed on atomic vapors in the ion source, in contrast to other techniques of laser spectroscopy performed on mass-separated ion beams. Results obtained using this technique include the nuclear shape-staggering effect in mercury nuclei, which also notably demonstrates the efficiency of the method for very low production rates [111].

The experimental resolution of in-source laser spectroscopy is limited by the Doppler-broadening of observed transitions, influenced by the atomic mass, the ion source temperature, as well as the gas pressure within the cavity, which is typically negligible for the vacuum conditions in thick ISOL tar-

gets. To compensate for this, ion source techniques with large improvements in resolution have recently been implemented at ISOLDE with the Perpendicularly Illuminated Laser Ion Source and Trap (PI-LIST) [112]. The PI-LIST is connected to the target in the same way as other ISOLDE ion sources, such that gaseous vapors travel to the ion source through a transfer line. A small (90 mm) radio-frequency quadrupole (RFQ) ion trap provides radial confinement for a field-free ionization region inside the LIST structure. The hot atomization region is separated from the interaction region for element-selective laser ionization, suppressing the non-selective surface-ionized contamination and enhancing ion beam purity by orders of magnitude [113]. The addition of perpendicular laser illumination reduces the effective Doppler-broadening in the effusing hot vapor, enhancing spectral resolution [114].

Resonance ionization laser schemes have been developed for many actinide elements [115, 116], facilitating the use of laser ionization as a technique for efficient and element-selective production of the actinides and other radioactive ion beams. Additionally, advances in laser ion source techniques can be applied for laser spectroscopy studies of the atoms and nuclei of interest [117].

FEBIAD-type ion sources

For species with high or unknown ionization potentials or electronic transitions inaccessible by non-vacuum laser technology (e.g. noble gases, halogens, or molecules), more energetic methods of ionization are required. The Versatile Arc Discharge Ion Source (VADIS) [118] is a standard ion source at ISOLDE, and is based on the Forced Electron Beam Induced Arc Discharge (FEBIAD) design [119]. In this ion source (shown in Fig. 1.7), a cathode surface is heated to high temperature to emit thermionic electrons. A potential difference applied at the cathode surface by an anode voltage accelerates the electrons through the biased grid into an anode volume contained within an axial magnetic field induced by a current applied through an electromagnetic coil. The accelerated electrons bombard the gaseous particles in the anode volume with energies above 100 eV, ionizing atomic and molecular species with high ionization potentials such as the noble gases. For molecules, this process can also induce dissociation and fragmentation into ions or neutrals. A variety of FEBIAD-type ion sources have been implemented at different RIB facilities, with comprehensive studies performed on the operating parameters for different designs including the cathode temperature, acceleration field, and magnetic field [120, 121].

Recently a photo-cathode-driven version of the FEBIAD ion source design was proposed in Ref. [122]. The feasibility of the approach is additionally supported by a proof-of-concept experiment [123]. The design releases photo-

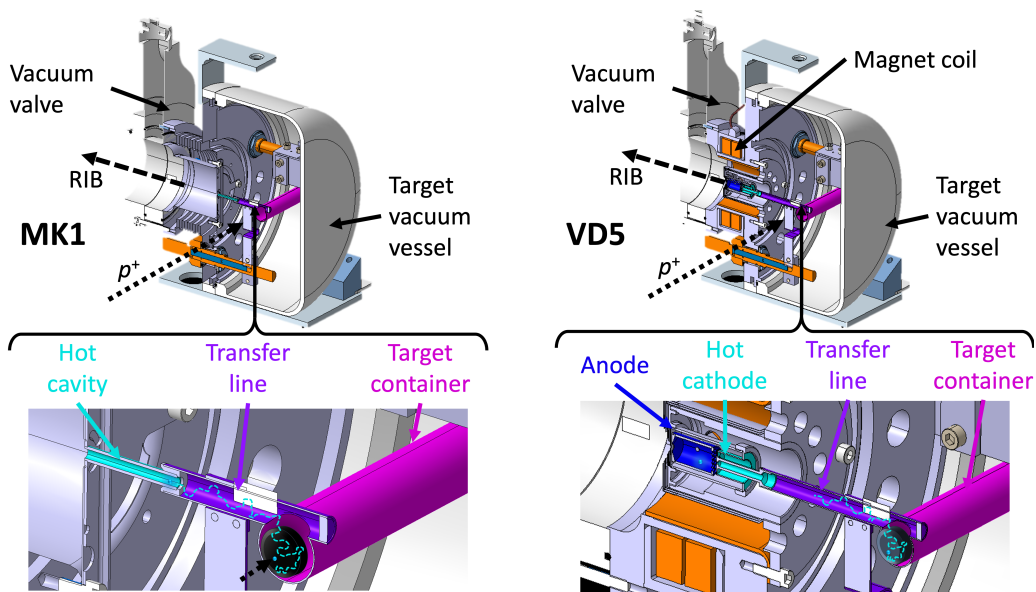


Figure 1.7: A cross-sectional view of a target and ion source unit with a MK1 surface ion source (left) and a FEBIAD-type VD5 ion source (right).

induced electrons, enabling ion source operation at ambient temperature. This has promising applications for ionization of volatile atoms and fragile molecules which could otherwise dissociate due to the high operational temperatures required for thermionic electron emission from the cathode. Further development is required to increase production of photo-electrons and achieve standard ionization efficiencies comparable to ion source designs that use thermionic emission.

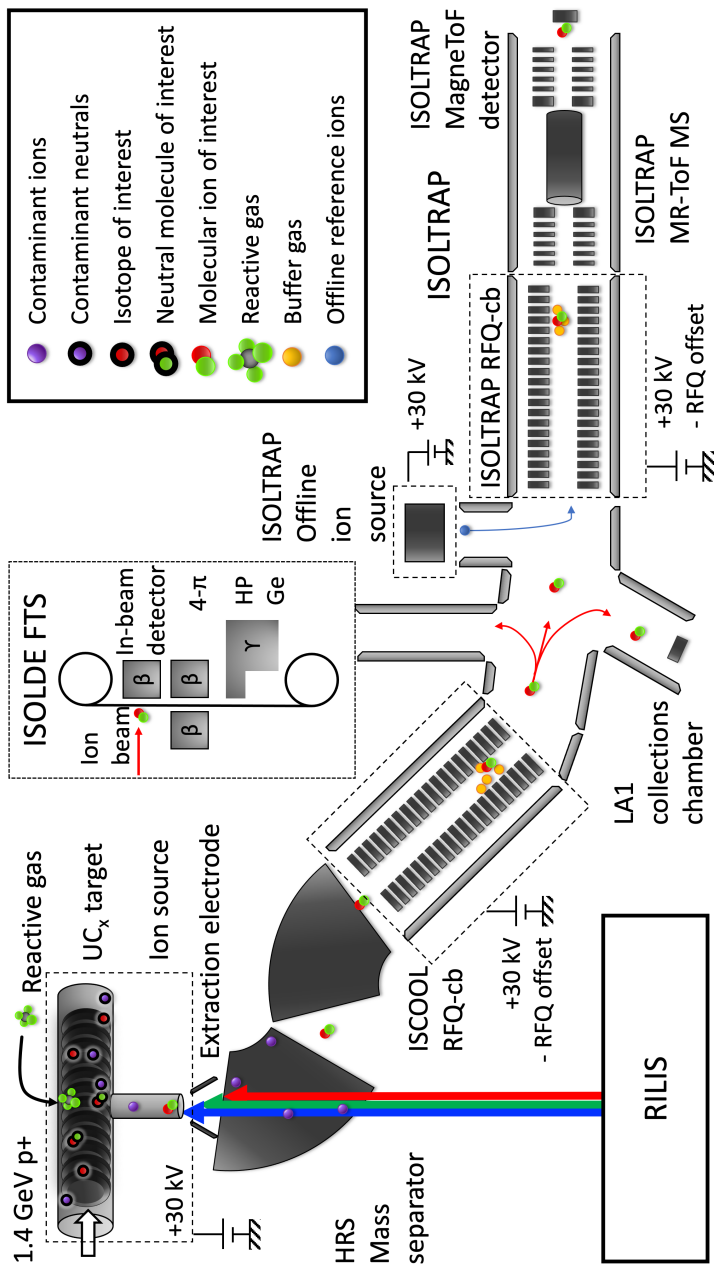


Figure 1.8: Schematic of the experimental setup for ion identification. Isotopes are generated in the target with up to $2 \mu\text{A}$ of 1.4-GeV protons from the CERN Proton Synchrotron Booster. Ions are extracted into a beam at 30-60 kV and separated by their mass-to-charge ratio in the mass separator magnets. On the HRS mass separator, the ions are then transmitted through the gas-filled ISCOOL. The cooled beams are sent to a collections chamber, to the ISOLDE FTS or to the ISOLTRAP beam line, where the ions are cooled and bunched in the ISOLTRAP RFQcb and sent to the MR-ToF MS.

2. Experimental techniques

Only two candidates for target nuclei are available in the macroscopic quantities that are required for an ISOL target with sufficient production cross-sections for the production of actinide species: ^{232}Th and depleted uranium (^{238}U). While these are available in metallic form, the dense material structure and sintering properties prohibit release of short-lived isotopes. Additionally, the metallic forms have lower melting temperatures, giving an upper limit on feasible operating temperature. Instead, carbides of both thorium and depleted uranium have been developed as ISOL target materials. In this work, uranium carbide (UC_x) and thorium carbide (ThC_x) target materials are used to produce the actinide species of interest.

Both the total and mass-separated ion current vary depending on the ion source type and the operating conditions. After transmission through the separator magnets, the mass-separated ion beams arriving to experimental end stations are mostly isobaric. Detection systems in the experimental end stations are sensitive to different sources of background. For all experiments, the ion beam purity and composition from each target and ion source combination are important metrics. To study beam composition, components in the mass-separated beam can be identified through a combination of techniques including mass spectrometry and radioactive decay spectroscopy. The following sections describe several identification and quantification techniques, all of which have been used in combination within this work for actinide atomic and molecular ion beams. A schematic of one such experiment is shown in Fig. 1.8.

The actinides have high boiling points and are known to have refractory properties, presenting a challenge for extraction from thick ISOL-type targets and the release process. Refractory elements are typically not extracted with high efficiency, corresponding to a limit in the elements available at ISOL facilities (discussed earlier in Section 1.2). To enable the detection and identification of potentially very poorly-extracted, low-intensity actinide atomic ion beams, a method of detection with higher sensitivity than typical Faraday cups was necessary. To ensure high detection sensitivity, a vacuum chamber hosting a single-ion detector (ETP MagneToF Mini 14925 [124]) was designed, purchased, assembled, and installed in ISOLDE's GLM beam

line as shown in Fig. 2.1. Many of the mass scans and laser wavelength scans presented in this work were taken using this installation. Additionally within this work, a time-to-digital converter [125] was implemented to record the time difference between a trigger signal and a channel signal, enabling the counting of single ions.

With the RILIS, ion creation happens with a time structure corresponding to the repetition rate of the pulsed laser system, i.e., a frequency of 10 kHz. The time-structure of ion generation makes time-resolution a useful characteristic for the study of low-intensity ion beams, offering diagnostics for laser ion source operation as well as for the filtering and analysis of data. The applications of the infrastructure developed for this work are discussed further in Section 4 and Publication III.

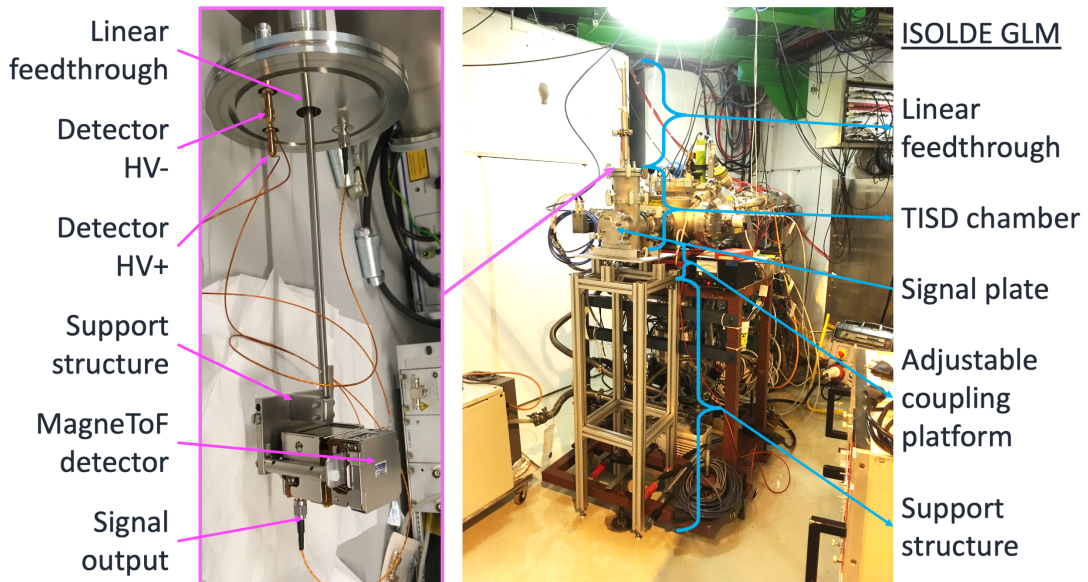


Figure 2.1: The target and ion source development (TISD) vacuum chamber with a MagneToF detector installed on a vertical linear feedthrough. Left: MagneToF detector assembly (with a protective cover) mounted on the linear feedthrough. Right: the TISD vacuum chamber connected to the beam line.

2.1 Resonance laser ionization

The element-selectivity of the RILIS technique is an advantage for identifying the presence of isobaric atomic components of the ion beam. By blocking one step of a resonance ionization laser scheme, electrons are not promoted

through the corresponding transition, and the element is not ionized. It follows that blocking the various steps of a multiple-step ionization scheme gives an element-dependent evaluation of ion intensity for species with resonance laser ionization schemes that have been developed and characterized. Similarly, scanning the frequency of a resonant laser excitation step across the a resonance frequency gives the energy of the transition, which can be compared to known information on electronic states, and the difference between resonance laser ionization and the equivalent power deposition with the laser on a wavelength sufficiently far to avoid ionizing the element of interest. Such changes in the intensity of the mass-separated ion beam therefore give the rates of the resonantly ionized element of interest on that mass. The response of an ion beam component to laser ionization can additionally be combined with techniques such as mass spectrometry to identify the presence of the resonantly ionized species (e.g. U identified in Fig. 2.2).

The selectivity of the RILIS technique requires the development and availability of a resonance ionization scheme for the element of interest that is also selective against possible contaminants. For contaminant species with low ionization potentials, photons of sufficiently high energy can cause non-resonant ionization, resulting in an observed laser response caused by a contaminant instead of the species of interest. Fig. 2.2 shows a mass spectrum of the ion beam extracted from a UC_x target without resistive heating. The target was thus heated only through conduction from the hot ion source, leading to a target temperature estimated to be several hundred degrees Celsius. ^{235}U and ^{238}U display a response to the uranium ionization scheme, as expected from the composition of the uranium carbide target material. A contaminant on mass 254 (^{238}UO) also displays a response to the laser scheme, suggesting that it is also (resonantly or non-resonantly) laser-ionized.

The laser frequency is typically optimized for one isotope. The magnitude of the isotope shift—the energy shift in an atomic transition caused by adding or removing one neutron to the nuclear system—is element- and transition-dependent. In many cases, it is not necessary to continuously or periodically adjust the laser frequency for isotope shift within the range of several mass units. In the case of the actinides, the magnitude of the isotope shift can approach the laser linewidth (typically several GHz, e.g. for Pu [126]). The isotope shift is therefore often non-negligible when studying resonantly laser-ionized actinide atomic ion beams.

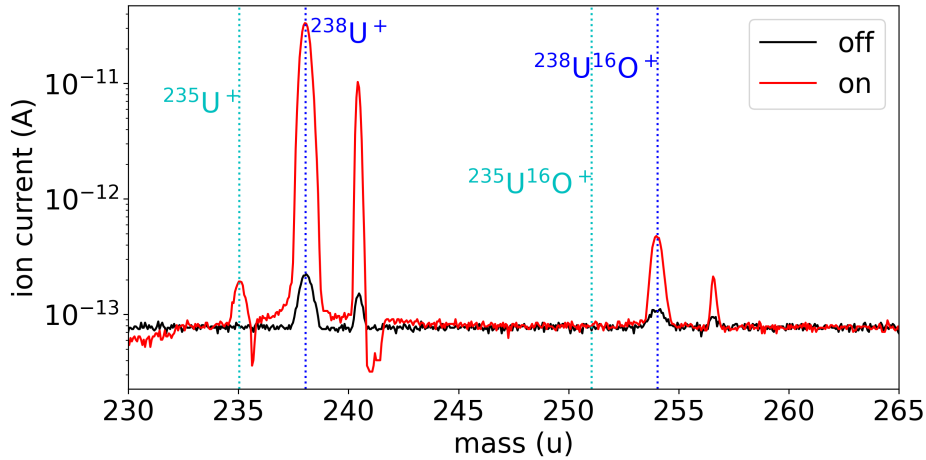


Figure 2.2: Ion current produced from a UC_x target with 0 A of heating current and the RILIS with a hot cavity at 2100°C , recorded on a Faraday cup during a mass scan using the GPS separator magnet. Red: Uranium two-step single-wavelength resonance ionization scheme in the ion source. Black: same mass scan with the laser blocked. Narrow side peaks at 240.5 and 257.7 u are thought to be artefacts caused by beamline components before the detector.

2.2 Ion trapping

As a complementary approach to the magnetic mass separation of the GPS and HRS, ion trapping techniques can be used to reach mass resolving powers capable of separating isobaric species from each other. The ISOLTRAP experiment at ISOLDE [49, 127] is designed to perform precise measurements of nuclear masses. It consists of four different ion traps in which the ion beam can be received from either the HRS or the GPS mass separator. The ion beams are decelerated, bunched, and cleaned in preparation for subsequent high-precision mass measurements [50, 51, 80, 128].

2.2.1 Time-of-flight mass measurements

Time-of-flight mass separation separates species by their mass-to-charge ratio m/q using their time of flight. Since the technique requires a relative time measurement, ion beams must be bunched. Deceleration and bunching is achieved by trapping and cooling the ions via collisions with high-purity helium gas in the ISOLTRAP radio-frequency quadrupole cooler-buncher (RFQcb) ion trap. Employing a small offset from the ion beam energy, the RFQcb is biased to a voltage typically within 200 V of the target and ion

source high voltage on which the ions are created. DC voltages applied to a set of electrodes along the beam axis provide a potential gradient to decelerate and capture the ions, while an RF potential is applied to four rods parallel to the beam direction, confining the ions perpendicularly to the direction of travel. After a predefined trapping or “cooling” time during which the ions interact with the buffer gas, the ions are released as a bunch.

Ion bunches are injected into the Multi-Reflection Time-of-Flight Mass Spectrometer (MR-ToF MS) and captured between two sets of electrostatic mirror potentials, where they are confined for up to several thousands of revolutions using the in-trap lift method [50]. The time of flight t of an ion can be related to the m/q by $t = a(m/q)^{1/2} + b$, where a and b are calibration parameters. a increases with the number of revolutions, while b is independent of trapping time. a and b are determined by at least two independent reference measurements which typically use calibration ions with known masses or different numbers of revolutions in the MR-ToF MS. By increasing their flight path, ions separate in t according to their corresponding m/q , giving typical mass-resolving powers greater than 1×10^5 [128]. With recent developments and in optimized conditions, mass resolving powers $m/\Delta m$ greater than 3×10^5 have been achieved with the MR-ToF MS [129]. The use of the subsequent Penning traps comes with a loss in efficiency but can achieve $R = 10^7$, corresponding to $10 \text{ keV}/c^2$ for medium-heavy nuclei [51].

The actinide atomic and molecular ions studied in this work are comparatively heavy with respect to typical mass ranges studied at ISOL facilities. Since the mass resolving power scales with the mass, these heavy beams require higher mass resolving power for the same absolute separation. With a nominal mass resolving power of 6000, the ISOLDE HRS can suppress most non-isobaric contaminants from the ion beam. Identification of isobaric ion beam components requires the use of more advanced techniques such as the MR-ToF MS.

2.2.2 Trapping of non-isobaric species

MR-ToF mass spectrometers provide a means to trap ions using electrostatic potentials, allowing storage times of hundreds of milliseconds in vacuum conditions of approximately 10^{-8} mbar at room temperature and thus enabling trapping of ions in a wide mass range across the nuclear chart. The use of electrostatic mirror potentials to store the ions while reflecting the trapped species back and forth is extremely flexible and gives the trap a high m/q acceptance limited only by the physical length of the cavity in time-of-flight for the ions of interest at their given energy. This high acceptance also enables the simultaneous trapping of non-isobaric contamination.

With the wide m/q acceptance for trapped species, ions of different m/q can be trapped and reflected back and forth together. At a given number of trapping revolutions, non-isobaric species can start lapping one another, resulting in a subset of revolution numbers in which species with different m/q happen to be traveling through the cavity at the same time in the same direction after each completing a different number of revolutions. If the ions are ejected from the trap on one such revolution number, the non-isobaric species will therefore hit the detector at the same time and thus appear in the same spectrum. These non-isobaric species can be identified by the difference in their dependence on the trapping revolution number [130].

Typically, the ion beam injected from ISOLDE has already been mass-separated to a single isobar, and thus the ions injected into the MR-ToF MS share only one m/q . In this case, there is no possibility to observe the lapping of non-isobaric species. The actinides are a special case. With high chemical reactivity, the actinide species studied in this work can form molecules through the process of buffer gas cooling, interacting with trace amounts of residual or contaminant gas that are present in the RFQcb even with the use of high purity (99.999%) helium. When the ions are released from the RFQcb, both the original m/q and the m/q of the molecular species can simultaneously be trapped in the MR-ToF MS.

To use the MR-ToF MS for identification in studies of actinide species, care must be taken to identify the revolution number of contaminants in the spectra. This effect is considered in Publication I. While this lapping feature adds additional complexity, the ability to observe both atomic and molecular species at a given number of revolutions lends itself to purification techniques (e.g. as in Ref. [130]) as well as in studies of molecular formation as discussed further in Publication II.

2.3 Radioactive decay spectroscopy

Radioactive decay can be used to identify short-lived components (half-lives of ms to days) in the ion beam when used in combination with the separator magnet mass separation. The ISOLDE Fast Tape Station (FTS) [17, 131] is used for online β - and γ -decay measurements of short-lived isotopes, and is the primary method for yield measurements at ISOLDE. The FTS is comprised of an in-beam β detector, a $4\text{-}\pi$ solid angle β detector, and a high-purity germanium crystal γ detector (HPGe). As part of this work, a design was developed and assembled for implementation of a detector assembly for use at a fourth measurement position, comprising a passively implanted planar silicon (PIPS) detector and a silicon photomultiplier (SiPM) detector for

α - and β - detection, respectively. The detector assembly is shown in Fig. 2.3. The FTS is described further in Ref. [131].

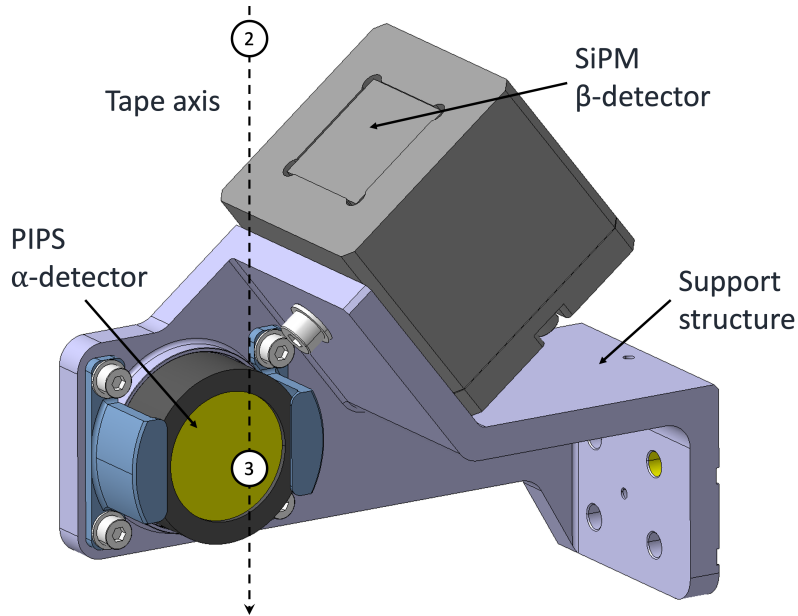


Figure 2.3: The detector assembly designed for installation in measurement positions 2 and 3 of the ISOLDE Fast Tape Station. The SiPM β -detector measures a sample placed at measurement position 2, which is in front of the HPGe γ detector (not shown here). The PIPs α -detector measures a sample at position 3. The tape axis and direction of sample travel is indicated with a dashed arrow. The full assembly of the Fast Tape Station is described in further detail in Ref. [131].

Samples of the mass-separated ion beam from either separator can be implanted into a mylar tape and transported in front of this series of detectors. Isotope identification can be done by measuring the half-life of the implanted sample through its β -decay, and additionally by detecting characteristic nuclear decays using γ -ray spectroscopy. With short collection times and short (≈ 100 ms) transport times from the implantation to the detector, the FTS is able to identify and quantify radioactive components with suitable decay mechanisms and half-lives.

For species with long half-lives, longer collection times and measurement times are more favorable. In these cases, yield measurements from ion implantations are a useful alternative. Samples of the ion beam can be implanted into a substrate and removed from the beam line to an external setup for decay spectroscopy. In this work, ion implantations were performed on

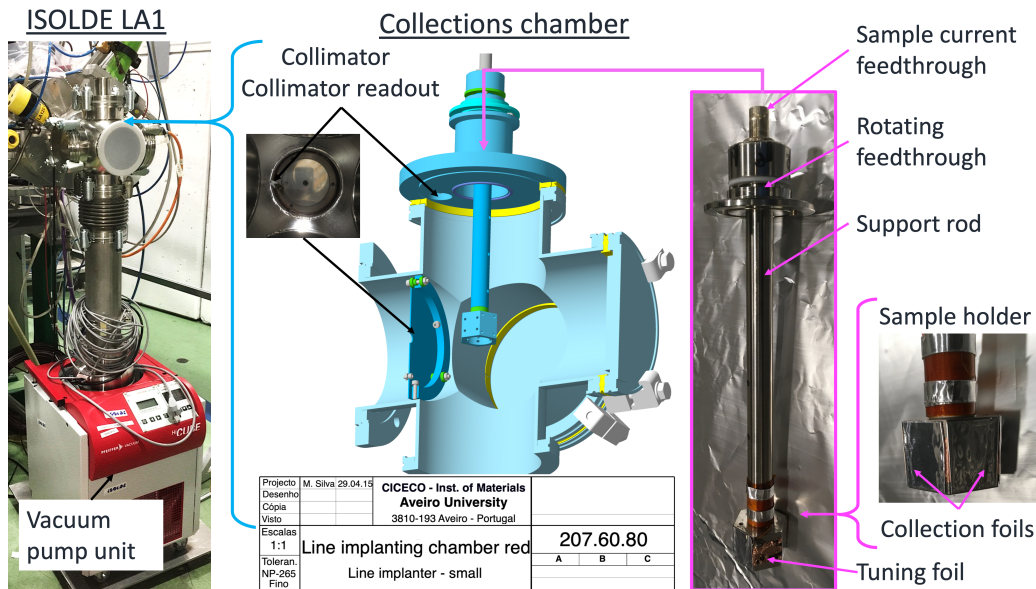


Figure 2.4: The ion implantation assembly showing the vacuum chamber coupled to the LA1 beamline for collections. Insets: the six-sided sample holder used to implant ion beams onto aluminum foils (right) and the collimator plate through which the ion beam is passed (left). Central 3D CAD model courtesy of M. Silva.

aluminum foils at the LA1 beamline at the setup shown in Fig. 2.4.

The samples were measured offline by γ - spectroscopy using a high-purity germanium detector (ORTEC HPGe) and α -spectroscopy (ORTEC Alpha Aria) with a Canberra PIPS detector. The α detector was calibrated using a sample with four α -emitters: ^{148}Gd ($1.167 \text{ kBq} \pm 3.24\%$), ^{239}Pu ($1.057 \text{ kBq} \pm 3.24\%$), ^{241}Am ($1.186 \text{ kBq} \pm 3.24\%$), and ^{244}Cm ($1.190 \text{ kBq} \pm 3.23\%$), measured on November 1, 2007 (2552 days before calibration). The reference sample was used to perform an energy and efficiency calibration of the spectrum in the measurement position. The detection efficiency in the measurement position was evaluated to be $1.65(3)\%$, with typical peak full-width at half-maximum (FWHM) $7.0(7) \text{ keV}$. For species with known energies and intensities of α - and γ - decay, measurement of the characteristic emitted decay radiation allows the identification and quantification of the number of nuclei of a particular species collected.

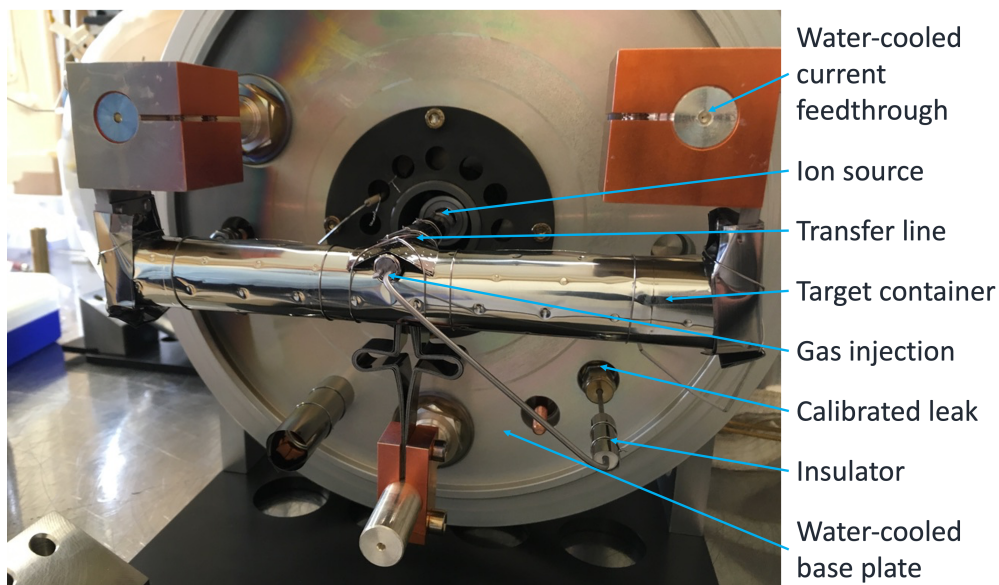


Figure 2.5: The inside of a target vessel, showing a tantalum target container wrapped in heat shields and a feedthrough for injection of reactive gases into the back of the transfer line between the target and the FEBIAD-type ion source.

2.4 Techniques for studies of molecular beams

As refractory species, the majority of the actinide elements are presumably difficult to extract from thick ISOL targets in the form of monatomic gas. Instead, most of the actinides are predicted or known to form fluoride compounds that are more volatile than their atomic counterparts, as shown in Fig. 1.5. In this work, the ISOL method was used to produce actinides in thick targets of UC_x and ThC_x . Reactive gas was added to the target environment through a pressure difference applied across a calibrated leak made of sintered stainless steel, permitting a flow rate of reactive gas into the target and ion source environment on the order of 10^{-3} to 10^{-6} mbar L s^{-1} . A gas mix containing carbon tetrafluoride (CF_4) was injected through a calibrated leak into the transfer line between the target and ion source as shown in Fig. 2.5, providing the source of fluorine for molecular formation. Initially, a mixture of noble gases (He, Ne, Ar, Kr, Xe at 20% each) was used for setup and ion beam tuning. Xe-containing gas is not recommended for production of actinide fluoride molecules since Xe was observed to form Xe_2^+ molecules that are present on the masses of interest. For the remaining studies, the gas mix was therefore a composition of Ar and CF_4 at different partial pressures.

Due to the unknown chemical distribution across the different molecular sidebands in the ion source and in some cases the unknown ionization potentials of the molecules, the FEBIAD-type ion source was used. The electron impact can ionize or alternatively fragment the molecules, resulting in a fragmentation pattern observed in the mass-separated beams. The possibility of molecular dissociation during ionization adds complexity to the identification process, making it difficult to determine even a relative distribution of molecular species formed in the target. With the methods described in this work, the observables are limited to the distribution of molecular and atomic ion beams produced for given target and ion source conditions and operational parameters.

On many masses (e.g. $A = 237$), the mass resolving power required to separate the actinide nuclei is higher than the typical order of $R = 1 \times 10^5$ achievable with an MR-ToF MS. If an element-selective resonance ionization scheme is readily available, the laser ionization adds on top of the ToF mass measurements to enable identification. For molecular species that may not have a molecule-selective ionization scheme available, identification by resonance laser ionization is challenging or impossible. The identification and quantification must be done through the remaining techniques of mass spectrometry and decay spectroscopy.

For fragile molecules, the high-temperature environments in the target and ion source can cause dissociation and breakup. Some ion source designs, such as the photo-cathode concept introduced in Section 1.3, may be capable of providing ion source environments at lower temperatures. Further work is needed to develop and eventually implement the concepts. Instead of forming molecules in the target and ion source unit and ionizing them in the ion source before extraction, the ion traps frequently employed for preparing and studying radioactive ions at RIB facilities offer an alternative route to produce radioactive molecules of interest. RFQcb devices such as ISCOOL, ISOLTRAP RFQcb (ISOLDE), the RFQcb at IGISOL, and the TITAN RFQ at TRIUMF typically use DC and RF potentials to confine ions in a pseudopotential region, where ions are cooled by repeated collisions with lighter buffer gas atoms, often helium. Mechanisms of molecular formation with typical contaminant reactants such as water and oxygen have been studied offline for many molecules, but deliberate molecular formation from radioactive ion beams in gas-filled ion traps is a relatively new technique. Molecular formation has been observed in all of the aforementioned devices for radioactive species including actinides, initiating efforts in several laboratories worldwide to characterize, optimize, and intentionally apply this technique of molecular formation to produce experimentally feasible rates of the molecular species of interest [69].

The use of buffer gas lends itself to deliberate injection of reactive gases for molecular formation with the radioactive species. Injecting trace amounts of reactive gases into ion traps could enable intentional development of species such as polyatomic symmetric-top and chiral molecules. Formation of long-lived RaOH^+ has already been observed in an ion trap environment [81]. In recent years, molecular beam formation has been observed in the actinide elements of thorium, uranium and plutonium at the IGISOL facility [132]. In-trap formation of molecular beams at CERN-ISOLDE is part of this work and is discussed later in Publication II, but this mechanism has yet to be deliberately exploited for subsequent studies of the resulting molecules.

2.5 Experimental requirements

While not typically used for ion identification, other experimental end stations can be sensitive to both stable and radioactive contamination. In addition to the quantity of the isotope of interest extracted from the target and ion source, these experiments have requirements on beam purity and the identification of contaminants.

Mass spectrometry experiments are able to separate and identify contaminants with sufficiently different binding energies for a given mass resolving power. This allows the experiment to detect and identify species independent of half-life or decay mechanism, but also limits the acceptable ratio of contaminant ions to the ion of interest. Contaminants that are too similar in mass to the species of interest can dominate the spectrum and create a challenge for fitting, compromising the information that can be extracted from a mass spectrum.

In contrast, laser spectroscopy experiments are insensitive to the mass difference, but are sensitive to the proximity of both atomic or molecular contaminants that have electronic transitions near the wavelength of the spectroscopic step. The actinides display many electronic levels with similar energies, and some level energies are not yet known (see Ref. [117] for a current overview of actinide levels). Decay spectroscopy experiments are robust against contaminants with similar masses and electronic structures. Except for losses in transmission efficiency that may occur as a result of a large contaminant species in the ion beam, decay spectroscopy experiments are also insensitive to stable or extremely long-lived contaminants. Due to the nature of detecting radioactive decay, decay spectroscopy experiments can become compromised by radioactive contaminants that decay, affecting the number or intensity of peaks in the decay spectrum, or simply contributing to background counts.

With the exception of the ISOLTRAP experiment, most end stations do not incorporate a mass-separation step after the separator magnets of the ISOLDE facility and thus rely on the resolving power of the facility separator magnets. Prior determination of the beam composition, and possible unwanted contamination, is valuable. All experiments have a limit to their achievable sensitivity when studying low ion rates of a species of interest in the presence of a high contaminant ion rate. These experimental requirements necessitate both yield measurements and identification of ion beam composition. This work aims to identify the yield and ion beam composition for actinide atomic and fluoride molecular ion beams through one or more of the techniques discussed in the preceding sections.

Results and Discussion

The actinide mass region	34
Production of actinide atomic ion beams	36
Extraction and production of molecular ion beams containing an actinide nucleus	56
Offline developments for studies of molecular beams	80
Conclusions	87
Outlook	95

This chapter presents results on the production of actinide nuclei as atomic and molecular ion beams from uranium and thorium carbide target materials. The majority of the results and discussion in this chapter are not included in the three publications, but are rather intended to place the publications within the larger context of this work. To avoid duplication, the results that can be found in the publications are referenced as such during the discussion.

In **Publication I**, neptunium and plutonium nuclides are identified and quantified for the first time at ISOLDE. Both elements have more protons than the heaviest easily available target nucleus ^{238}U , prompting a discussion of how far the ISOL method can extend production into the light actinide elements.

In **Publication II**, the formation of molecular ion beams in the actinide region is studied. Techniques and considerations for the formation of molecular ions in the target and ion source unit and in the RFQcb ion trap are discussed. Ion beam compositions in the actinide and actinide molecule mass region are shown to contain high rates of molecular ions formed from thick uranium carbide targets. Molecules formed by injection of reactive gases are ionized with surface ion sources or electron bombardment ion sources. Dissociation behavior of molecular ions after ionization is observed in mass spectra, identifying the metastable molecular ions using the apparent mass of the fragment. Mass-separated atomic or molecular ion beams react with residual gases to form molecular ions during buffer gas cooling. Singly- and doubly-charged-species are observed and reported.

In **Publication III**, ISOLDE's offline 2 mass separator is upgraded for the study of molecular beam formation and molecule-laser interactions with the addition of new gas mixing and injection systems. Barium fluoride molecules are used as a proof-of-principle, characterizing effects of high-power laser light, molecular formation, and ion source operation.

These chapters contain an extended discussion of supporting and additional information on these topics surrounding the three publications. The experiments performed within this work for the production of actinides were conducted online at the ISOLDE facility. The first study [133] proposed the use of a previously-irradiated UC_x target (target number #638), which had been used to deliver beam for an experiment online two years before this work. The remaining long-lived inventory of actinide nuclides [134] was used for investigations of resonantly laser-ionized actinide atomic beams, leading to the results presented in Section 4 as well as in Publications I and II. A following study used a previously-irradiated UC_x target with a surface ion source and reactive gas injection (target number #637) for molecular extraction, discussed in Section 5 and in Publication II. Two UC_x targets (target

numbers #713 and #751) and one ThC_x target (#791) with VD5 ion sources and CF₄ gas injection were used to study the molecular extraction of actinide beams [135]. One of these ion sources (coupled to the first UC_x target) failed during operation through electrical connection of the anode voltage to the ion source ground potential. Results from the surviving UC_x and the ThC_x target and ion source units are discussed in Section 5 and additionally in Publication II. After presentation of the results, combined conclusions from the operation of actinide targets with reactive gas injection are given in Chapter 7.

3. The actinide mass region

Experiments face several challenges other than the refractory properties of the actinides when working in this mass region at an ISOL facility, including contaminants and higher mass resolving power required to separate these comparatively heavy ion beams. Though they are not part of the actinide series, francium and radium ions are present as isobaric ion beam components on many masses of interest in the actinide mass region. With high vapor pressures at 2000 °C, both francium and radium are quickly and efficiently released from thick targets, allowing the extraction of isotopes with half-lives down to the order of tens of ms [44, 136]. Additionally, francium and radium both have relatively low ionization potentials (3.94 and 5.28 eV, respectively), facilitating efficient surface ionization. In the monofluoride sideband, this situation is slightly changed. Francium fluoride, while it may form in the target and ion source unit, would thermodynamically favor dissociation rather than ionization. As a result, the FrF^+ ion is not present on the monofluoride sideband. In contrast, radium monofluoride (RaF^+) is observed strongly, sometimes simply as contamination without deliberately supplying fluorine for molecular formation. Within the actinide mass region, there is a set of isobars where a neutron-rich atomic radium species can be observed while simultaneously observing the neutron-deficient radium isotope on the monofluoride sideband, with a difference of 19 neutrons, e.g., $A = 230$ as shown in Fig. 3.1. This demonstrates the influence of molecular formation on the composition of isobaric ion beams. These species are isobars and are mass-separated by the same m/q , but both ^{211}Ra and ^{230}Ra nuclides are present. Additionally, this effect identifies the potential loss in efficiency that can occur as a result of combining molecular formation and the mass separation into isobars. For the case of radium: the radioactive nuclei are present as the monofluoride species ($^{211}\text{RaF}^+$ in Fig. 3.1). The additional observation of the radium ion ($^{230}\text{Ra}^+$) in the atomic form implies that not all radium nuclei form a molecular ion. Some ^{211}Ra will form the $^{211}\text{RaF}^+$ observed on mass 230, but some may remain atomic and be observed only on $A = 211$ as $^{211}\text{Ra}^+$, while some ^{230}Ra will form the $^{230}\text{RaF}^+$ molecular ion and will be observed on mass $A = 249$. Splitting the population of radioactive nuclides onto multiple masses can cause a loss in efficiency, which should be carefully

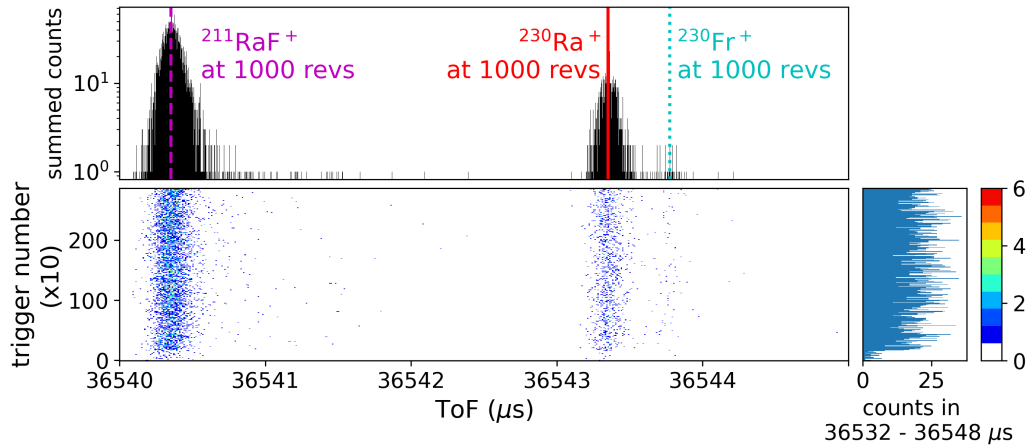


Figure 3.1: ToF spectrum from the ISOLTRAP MR-ToF MS showing ion counts of a mass-separated beam ($A = 230$) from the HRS. The horizontal axis shows the measured time difference between ejection from the ISOLTRAP RFQcb and detection after trapping the ions for 1000 revolutions in the MR-ToF MS. The vertical axis of the top panel shows ion counts within time bins of 100 ns. Predicted ToF from an offline calibration is shown with vertical lines for RaF, Ra, Fr, in purple, red, and cyan, respectively.

evaluated against the benefits for each unique application.

4. Production of actinide atomic ion beams

Outline

4.1	Actinium	36
4.2	Thorium	38
4.3	Protactinium	39
4.4	Uranium	40
4.5	Publication I: Production of neptunium and plutonium nuclides from uranium carbide using 1.4-GeV protons	40

4.1 Actinium

As the first element in the actinide series, all isotopes of actinium are radioactive, with the most stable isotope ^{227}Ac having a half-life of 21.77 years. Short half-lives contribute to the difficulty in studying this element, leaving a remarkable absence of data [137]. Some isotopes of actinium are predicted to exhibit octupole deformation, motivating studies of nuclear structure across the isotopic chain [138]. In addition to its interesting and little-known structural, chemical, and nuclear properties, actinium has gained significant interest for the isotope ^{225}Ac , with a half-life of 9.9 days and four α -decays in its decay chain giving it promising characteristics as a radiopharmaceutical candidate for targeted- α therapy cancer treatment [10, 139].

Actinium melts at 1050 °C and boils at 3250 °C, exhibiting refractory properties. Past experiments have taken advantage of nuclear decay in combination with the volatility of Ra and Fr precursors to produce select actinium isotopes (e.g. ^{225}Ac [140]) through the collection and subsequent β -decay of their isobaric parent Ra and Fr nuclei. Previous work was done at ISOLDE on the direct extraction of actinium atomic ion beams and the characteriza-

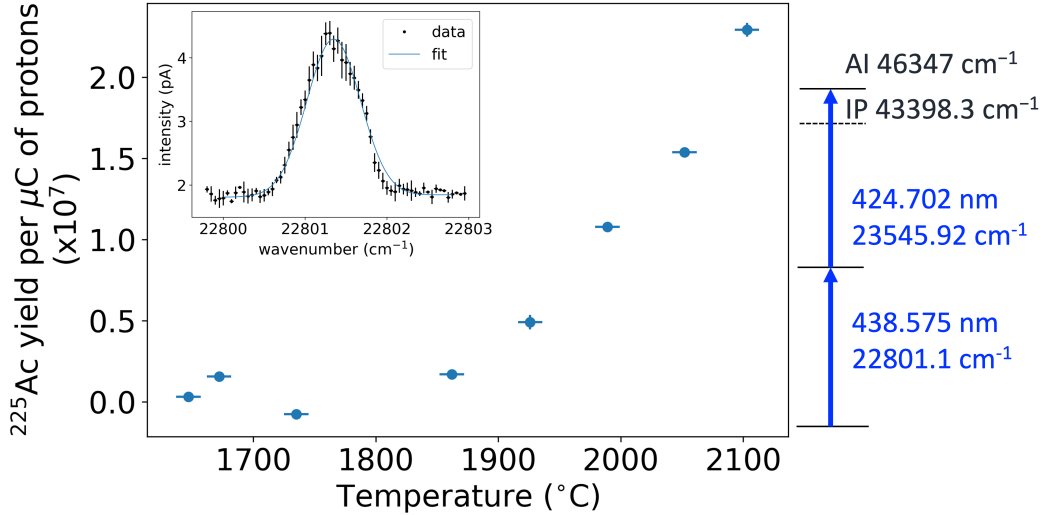


Figure 4.1: Measured rates of resonantly laser-ionized ^{225}Ac produced from UC_x as a function of the target temperature. Inset: ion current measured on a Faraday cup as a function of the wavenumber of the laser providing the first excitation step for resonance ionization of actinium. The laser scheme used [143, 109] is shown on the right.

tion of Ac, Ra and Fr at ISOLDE [141, 142] produced from UC_x targets using RILIS. The same technique was used to study actinium atomic ion beams in this work.

In this work, actinium was produced online and extracted as an ion beam at ISOLDE using UC_x target material and reactions with 1.4-GeV protons. Because of the refractory properties, the target material was heated to temperatures above 2000 $^\circ\text{C}$ to facilitate release. Second harmonic generation of the output of two Ti:Sa lasers was employed to provide a two-step resonance ionization scheme to ionize the Ac, shown in Fig. 4.1.

This work on the production of resonantly laser-ionized actinium was further used to deliver RIBs of actinium isotopes for several experiments. ^{228}Ac was produced and delivered for the study of β -delayed fission in the actinide isotopes [144]. The newly-implemented PI-LIST technique described in Section 1.3 was used to perform high-resolution in-source laser spectroscopy of Ac nuclei [112, 145], showing trends in the nuclear charge radius in the region of octupole-deformed nuclei. The single-ion counting infrastructure implemented in this work (described in Chapter 2) was used to detect the actinium ions. The experiment achieved a resolution of 400 MHz with a

narrow-band laser system combining a Matisse continuous-wave Ti:Sa laser with a seeded ring Ti:Sa cavity for the isotopes $^{224-229}\text{Ac}$, and a resolution of 800 MHz using a dual-etalon Ti:Sa laser for the isotopes $^{230,231}\text{Ac}$, spanning a range of 8 Ac isotopes. Data is under analysis [138, 145].

4.2 Thorium

Thorium is the most refractory of the light actinides. In metallic form, it has a melting point of 1750 °C and a boiling point of 4787 °C, the highest of the actinide elements. It also has a large adsorption enthalpy on tantalum [75, 146], making it very likely to stick to the surfaces of the target container for longer times than experimental time scales. Thorium is also very refractory as a carbide, with melting temperatures of 2500 °C, which is above the typical target material operating temperature.

Thorium is available naturally, dominantly as ^{232}Th , with traces of the isotopes $^{227,230,231,234}\text{Th}$ occurring in decay chains of Th and U. In the context of the actinides, thorium is easy to obtain—it is three times more abundant in Earth’s crust than stable Sn [147]—and is used in alloys, coatings and other applications. These thorium isotopes may be comparatively well-studied among the actinides, but other isotopes of thorium are not so readily available. While studies of thorium ion production have been done e.g. using filament-based dispensers at IGISOL [148], the production of laser-ionized thorium atomic ion beams using the ISOL method was not attempted at ISOLDE in this work. Though the production of thorium is not discussed in the papers included in this thesis, the delivery of specific radioactive thorium isotopes to experiments was accomplished during this work.

The isotope ^{229}Th , which has gained significant interest for applications of its uniquely low-lying isomer, was produced at ISOLDE by delivering the mass-separated beam $A = 229$, containing laser-ionized ^{229}Ac as well as surface-ionized ^{229}Ra and ^{229}Fr . All three species β -decay into ^{229}Th at the experimental end station, enabling experiments to study the radioactive thorium isotope of interest without direct extraction of thorium from the ISOL target [149].

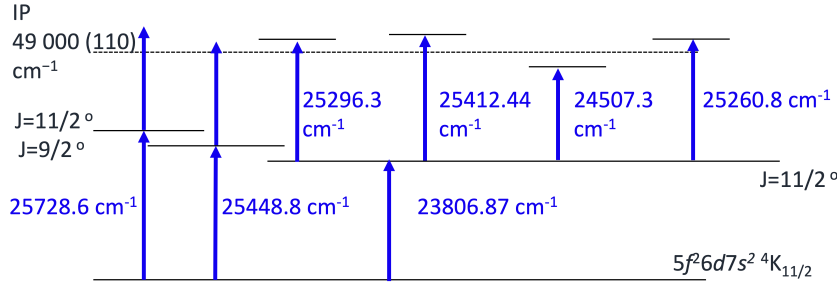


Figure 4.2: Attempted schemes for resonance ionization of protactinium atoms, with level energies and assignments from Ref. [150].

4.3 Protactinium

Protactinium, the third element in the actinide series, is less refractory than thorium and has high predicted cross-sections for in-target production, particularly for isotopes close to the target nucleus. Protactinium also has several isotopes with long half-lives in the context of the ISOL technique. The longest-lived isotope is ^{231}Pa (32,760 years), with other isotopes including ^{233}Pa and ^{230}Pa (26.967 and 17.4 days, respectively) which are long-lived enough to survive slow release times. Despite this, the existing body of evidence suggests that protactinium “may well be the most difficult of all to extract from natural sources” [147], showing high adsorption rates onto a variety of substrates. The extraction of atomic ion beams of Pa from thick ISOL targets was thus predicted to be difficult, despite the promising production rates.

A UC_x target with a rhenium surface ion source was used for the study. Recent work on the ionization potential and the electronic structure of the protactinium atom [150] offered many possible options for resonance laser ionization schemes using Ti:Sa lasers. From the available compilation of resonance schemes and atomic energy levels, the two-step laser schemes shown in Fig. 4.2 were attempted, with no resonance behaviour observed on the ion beam intensity on the masses of the longest-lived isotopes ($^{231,233,230}\text{Pa}$). It was concluded that protactinium is too refractory, adsorbs too strongly onto the materials used for the target material and container, or forms refractory molecules with carbon or oxygen in the target.

4.4 Uranium

Since the discovery of nuclear fission in 1938, research in the field of nuclear energy has characterized uranium and its properties and compounds. Concerted research efforts including the Manhattan Project make uranium and its properties better-understood than the other actinides, with comprehensive information on uranium and its compounds covered in textbooks (e.g. Refs. [147, 151]).

As the target material available with the highest atomic number, uranium is present in bulk quantities and can also appear as a surface-ionized contaminant in the actinide mass region when using uranium targets. Depleted uranium, typically used for ISOL targets, mainly contains the isotope ^{238}U , with the long-lived isotopes $^{235,234}\text{U}$ often present in small quantities (natural abundance values are 0.72 and 0.005 atomic %, respectively [147]). While radiogenic uranium isotopes are likely produced in reactions between ^{238}U targets and high-energy protons, the U atoms are also challenging to extract from a target material that is chemically identical.

A resonance laser ionization scheme was implemented for uranium at the ISOLDE facility (Fig. 4.3), enabling the ionization of uranium atoms and identification of contamination. The two-step single-wavelength scheme developed by Savina et al. [152] requires the use of only a single Ti:Sa laser with second harmonic generation.

An additional laser can be used to resonantly ionize the population from the first thermally excited state as shown in Fig. 4.4. Resonance laser ionization of the target material enables operation and beam tuning in the high-mass region, in addition to monitoring target conditions through the observed quantities of resonantly-ionized target atoms. $^{234,235,238}\text{U}$ were identified by laser response and ToF mass measurements (Publication II) [153].

4.5 Publication I: Production of neptunium and plutonium nuclides from uranium carbide using 1.4-GeV protons

Uranium has the proton number $Z = 92$, and is the fourth element in the actinide series. Producing isotopes of the elements above uranium ($Z > 92$) requires nuclear reactions beyond the fission, fragmentation, and spallation processes typically considered when exploiting the ISOL method.

There are multiple pathways to form transuranium elements. These include neutron-capture processes at reactors, light ion reactions— typically on

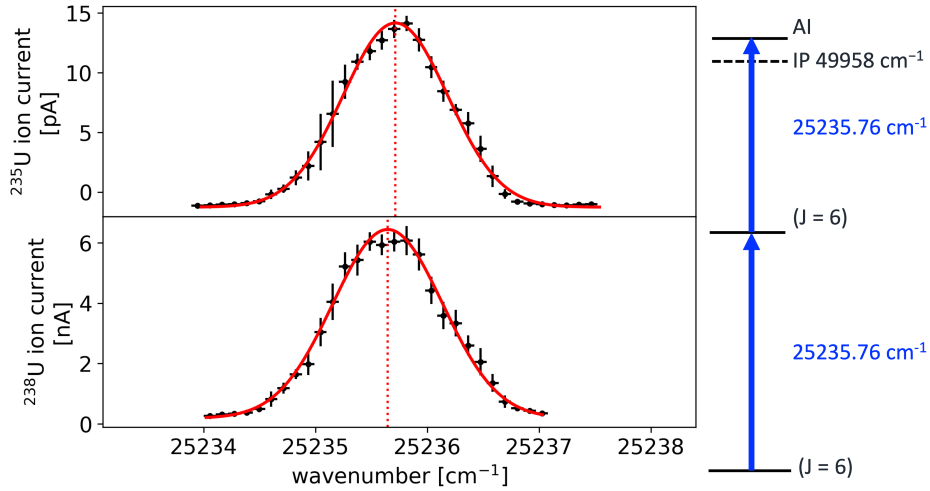


Figure 4.3: Mass separated ion beam from the ISOLDE GPS on mass 235 (top) and 238 (bottom) from a UC_x target with a tungsten surface ion source. Ion intensity on a Faraday cup is shown corresponding to the frequency of the single Ti:Sa laser used to provide the resonance laser ionization scheme shown at right. The shift in centroid (vertical dotted lines) is 2 GHz (0.069 cm^{-1}). Peak FWHM is 33 GHz.

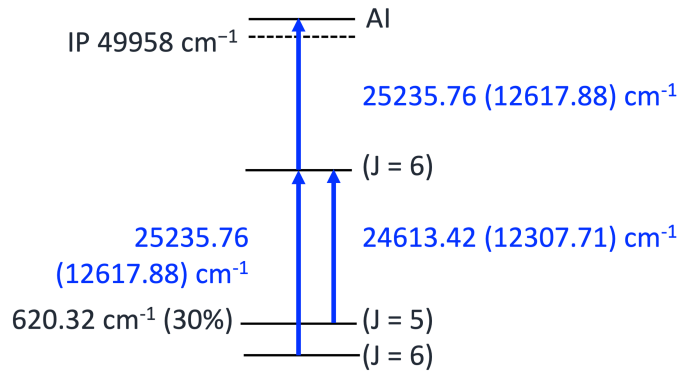


Figure 4.4: Uranium two-step resonance laser ionization scheme showing ionization from the ground state [152] and the first thermally populated excited state with a population of 30% at 2000 °C. Fundamental wavenumbers are shown in brackets.

actinide targets, fusion of heavy ion beams, and reactions including multi-nucleon transfer. Heavy-ion accelerator facilities such as GSI can provide an accelerated projectile nucleus with sufficient energy to overcome the Coulomb barrier and interact with a target nucleus. At a given energy, the two nuclei have some probability of forming a compound nucleus, which can break up to form a fission product which contains more protons than the original target nucleus. The available rates of isotopes produced this way depends on the cross-section of this reaction. Rates can be less than one nucleus per second, necessitating high efficiency and sensitivity for experimental stations (e.g. nobelium produced in fusion-evaporation of ^{48}Ca on a ^{208}Pb target [154]). These reactions allow experiments to probe the full actinide range including even No and Lr, the two heaviest actinides.

The production of transuranium species has barely been investigated at facilities with proton driver beams such as CERN-ISOLDE and TRIUMF-ISAC. Prior to this work, studies at TRIUMF demonstrated the presence of ^{239}Pu produced in a thick uranium ISOL target [155]. Available in bulk quantities as depleted uranium, ^{238}U is frequently used as an ISOL target. It is long-lived (4.5 billion years) but still requires considerations for handling of radioactive material. In this work, the production of transuranium nuclei from ^{238}U using high-energy protons is investigated at CERN-ISOLDE and described here in Publication I [156].

Neptunium is very refractory, limiting extractable quantities from the target. Despite the challenges posed by its chemical properties, Np is an interesting case motivated by a lack of experimental measurements of atomic or nuclear structure beyond the long-lived isotope ^{237}Np [117] and more recently $^{237,239}\text{Np}$ [157]. Information on isotope shifts and electronic states is limited, motivating experimental laser spectroscopy studies of atomic neptunium. One proton number higher than neptunium, plutonium similarly requires nuclear reactions beyond fission, fragmentation and spallation for production at ISOL facilities.

The availability of these two new elements is reported in this publication and has been released to the community. Beyond the work presented in the publication, further laser spectroscopy studies [158] were proposed in this work and have been conducted to test the feasibility of suppressing the surface-ionized uranium contamination using the Laser Ion Source and Trap (LIST) ion source [112, 145] discussed earlier in Section 1.3. Data analysis is in progress.

Bibliographic Information

M. Au, M. Athanasakis-Kaklamanakis, L. Nies, R. Heinke, K. Chrysalidis, U. Köster, P. Kunz, B. Marsh, M. Mougeot, L. Schweikhard, S. Stegemann, Y.N. Vila Gracia, Ch.E. Düllmann, S. Rothe, “Production of neptunium and plutonium nuclides from uranium carbide using 1.4-GeV protons”, *Phys. Rev. C.*, 107, 064604 (2023). doi: 10.1103/PhysRevC.107.064604. arXiv:2303.12226 nucl-ex.

Author contributions










Corresponding author: M. Au

CRedit author statement:

Conceptualization: M. Au, R. Heinke, K. Chrysalidis, B. Marsh, S. Rothe. Investigation: M. Au, M. Athanasakis-Kaklamanakis, L. Nies, R. Heinke, K. Chrysalidis, U. Köster, M. Mougeot, S. Stegemann, Y.N. Vila Gracia. GEANT4 simulations and analysis: P. Kunz, M. Au. Analysis: M. Au. Supervision: K. Chrysalidis, B. Marsh, Ch.E. Düllmann, S. Rothe. M. Au prepared the manuscript. All authors reviewed the manuscript.

Copyright Notice

©2023 American Physical Society. This is an accepted version of this article published in 10.1103/PhysRevC.107.064604 under the terms of the Creative Commons Attribution 4.0 International license. Further distribution of this work must maintain attribution to the author(s) and the published article’s title, journal citation, and DOI.

Production of neptunium and plutonium nuclides from uranium carbide using 1.4-GeV protonsM. Au ^{1,2,*}, M. Athanasakis-Kaklamanakis ^{1,3}, L. Nies ^{1,4}, R. Heinke ¹, K. Chrysalidis ¹, U. Köster,^{1,5} P. Kunz ⁶, B. Marsh,¹ M. Mougeot ^{1,7,†}, L. Schweikhard,⁴ S. Stegemann,¹ Y. Vila Gracia,¹ Ch. E. Düllmann ^{2,8,9} and S. Rothe ¹¹European Organization for Nuclear Research (CERN), Meyrin, 1211 Geneva, Switzerland²Department of Chemistry, Johannes Gutenberg-Universität Mainz, 55099 Mainz, Germany³Katholieke Universiteit Leuven, Instituut voor Kern-en Stralingsfysica, B-3001 Leuven, Belgium⁴Institut für Physik, University of Greifswald, 17489 Greifswald, Germany⁵Institut Laue-Langevin, 38000 Grenoble, France⁶TRIUMF, Vancouver, Canada V6T 2A3⁷Max Planck Institut für Kernphysik, 69117 Heidelberg, Germany⁸GSI Helmholtzzentrum für Schwerionenforschung, 64291 Darmstadt, Germany⁹Helmholtz Institute Mainz, 55099 Mainz, Germany

(Received 11 March 2023; accepted 8 May 2023; published 8 June 2023; corrected 7 August 2023)

Accelerator-based techniques are one of the leading ways to produce radioactive nuclei. In this work, the isotope separation on-line method was employed at the CERN-ISOLDE facility to produce neptunium and plutonium from a uranium carbide target material using 1.4-GeV protons. Neptunium and plutonium were laser-ionized and extracted as 30-keV ion beams. A multireflection time-of-flight mass spectrometer was used for ion identification by means of time-of-flight measurements as well as for isobaric separation. Isotope shifts were investigated for the 395.6-nm ground state transition in ^{236,237,239}Np and the 413.4-nm ground state transition in ^{236,239,240}Pu. Rates of ^{235–241}Np and ^{234–241}Pu ions were measured and compared with predictions of in-target production mechanisms simulated with GEANT4 and FLUKA to elucidate the processes by which these nuclei, which contain more protons than the target nucleus, are formed. ²⁴¹Pu is the heaviest nuclide produced and identified at a proton-accelerator-driven facility to date. We report the availability of neptunium and plutonium as two additional elements at CERN-ISOLDE and discuss the limit of accelerator-based isotope production at high-energy proton accelerator facilities for nuclides in the actinide region.

DOI: [10.1103/PhysRevC.107.064604](https://doi.org/10.1103/PhysRevC.107.064604)**I. INTRODUCTION**

The actinide region of the nuclear chart is a focus of research for topics including the *r*-process and astrophysical isotopic abundances [1], nuclear fission [2,3], nuclear medicine [4,5], environmental monitoring [6], and energy production [7]. Experimental measurements of nuclear masses, β decay, neutron capture, and fission properties are required to benchmark theoretical nuclear structure models, but are missing for many nuclei [8,9]. Laser spectroscopy has the capability to reveal both nuclear and atomic information through techniques such as high-resolution resonance ionization and collinear laser spectroscopy [10–12]. Resonance ionization laser schemes have been developed for many actinide elements [13,14], facilitating the use of laser ionization as a

spectroscopic technique, a tool for efficient and element-selective production of radioactive ion beams, as well as for trace element detection [15].

All actinide nuclides are radioactive. ²³²Th and ^{235,238}U are available naturally in macroscopic quantities, but the majority of the other actinide isotopes must be artificially produced, with production often being one of the most limiting factors in their study and use. Research reactors are the leading method of production for the study of some actinide isotopes, producing a selection of species [16]. Some specific isotopes can also be obtained through generators made from decaying parent nuclides, for example ²²⁷Th (and ²²⁷Ra) produced from ²²⁷Ac [17]. Alternatively, actinides can be produced at accelerator facilities using a projectile on a thin target to induce fusion-evaporation reactions or multinucleon transfer. The reaction products can then be separated in flight as ion beams; long-lived isotopes can be collected for off-line isolation and use [18]. The isotope separation on-line (ISOL) method uses an energetic driver beam that interacts with a thick target, generating reaction products that diffuse through the target material and effuse to the ion source where they are ionized and extracted as an ion beam. The ISOLDE facility at CERN uses 1.4-GeV protons from the CERN Proton Synchrotron Booster to produce and deliver more than 1000 different

*Corresponding author: mia.au@cern.ch

†Present address: University of Jyväskylä, 40014 Jyväskylä, Finland.

Published by the American Physical Society under the terms of the [Creative Commons Attribution 4.0 International](https://creativecommons.org/licenses/by/4.0/) license. Further distribution of this work must maintain attribution to the author(s) and the published article's title, journal citation, and DOI.

nuclide species [19,20]. Uranium carbide (UC_x) from depleted uranium is one of the most commonly used target materials [21,22]. The ISOL method is typically able to provide isotopes lighter than the target nucleus through fission, fragmentation, and spallation reactions. The production of above-target elements (higher proton number Z than the target nucleus) has barely been studied. In the case of the ^{238}U target nucleus, above-target production pathways would reach into the elusive transuranium region.

Beams of ^{238}Np (2019) and ^{239}Pu (2013) were produced at TRIUMF, Canada from the ISOL method with 500-MeV protons from two separate UC_x targets using resonance laser ionization in rhenium hot cavity surface ion sources, and isotopic yields were reported [25,26]. The extraction behavior of actinide beams from the UC_x target matrix still remains largely uncharacterized. Experimental data on availability, intensity, and purity of Np and Pu ion beams will enable experiments on these elements at ISOL facilities. Identifying the high- Z limits of the accelerator-based production technique at proton accelerator facilities gives essential information for the field of actinide research. Theoretical estimates can be provided by models describing the processes occurring in collisions of 1.4-GeV protons with target nuclei like the Monte Carlo code FLUKA [27,28], which is used to describe nuclide production at ISOLDE [20].

II. METHODS

The depleted UC_x target ($UC_2\text{-}C_2$ with 0.25 wt% ^{235}U , 82.95 wt% ^{238}U , 16.8 wt% C, density 3.67 g/cm³) used for the experiment was irradiated using $5(10^{18})$ protons over a time of 313 h (≈ 2 weeks) while actively used for isotope production and extraction during an experiment ending on 12 November 2018. After a 929(1) d (≈ 2.5 yr) cooling period, first investigations were conducted using the remaining long-lived inventory. At 934.0(5) d of cooling time, another irradiation of $8.5(10^{17})$ 1.4-GeV protons was performed on the target unit. Subsequent measurements were taken both with and without direct irradiation over an experimental period ending at 942.4(5) d after the end of the initial irradiation. In this study, measurements were taken under three conditions:

- (i) “Before, off” Before any additional irradiation (after the cooling period).
- (ii) “After, off” After reirradiation, without the proton beam actively hitting the target.
- (iii) “After, on” After reirradiation, with the proton beam actively hitting the target.

The FLUKA model of in-target production was used to predict production of elements up to plutonium for a beam of 1.4-GeV protons, Gaussian full-width at half-maximum (FWHM) 6.35 mm, on a depleted UC_x target [20]. Particle fluence spectra caused by the 1.4-GeV proton beam are modeled along with the inventory of radionuclides produced during irradiation. The simulated fluence was additionally used as input for the ActiWiz software [29] to calculate in-target inventory of long-lived actinides after 734 d (≈ 2 yr) of cooling time [30]. A GEANT4 [31,32] package-based model developed at TRIUMF [33] was adapted to the ISOLDE proton beam

energy and geometry to model reaction pathways. This was used to model 10^9 1.4-GeV primary protons irradiating a UC_x target (83.2 wt% U and 16.8 wt% C) of natural uranium, consisting of ^{234}U (0.005 %), ^{235}U (0.72 %), and ^{238}U (99.275 %). The difference caused by the ^{235}U content is expected to be negligible. Excessive decay time was included in the GEANT4 model to evaluate the largest feasible effect of previous irradiation and cooling time, i.e., all inventory has been allowed to decay, considering a decay time extending to timescales relevant to the scheduling of future experiments [9792 days (≈ 27 yr) after primary impact]. The FLUKA and GEANT4 models were used to compare modeled rates with experimental rates achievable by using a previously irradiated target. Further details of the models can be found in Appendix A.

The experimental setup is shown schematically in Fig. 1. Ions were formed using the resonance ionization laser ion source (RILIS) [23,34] and a rhenium hot cavity surface ion source. Ions were extracted as 30-keV ion beams, which were mass-separated using the general purpose separator (GPS) dipole magnet. The two-step ionization schemes [14] shown in Fig. 1 were chosen, using intracavity second harmonic generation in titanium:sapphire (Ti:Sa) lasers [35,36] for the first excitation step (FES) and second excitation step (SES) of Np and Pu laser ionization schemes. A grating Ti:Sa laser [37] was also used to perform scans of the FES wavelength, with typical laser FWHM of 7 GHz. Simultaneous application of a uranium laser ionization scheme [38] during beam composition studies enabled the identification of potential contaminants such as ^{238}U from the target material. Further details of the ion source are described in Appendix B.

The target and ion source are heated separately by resistive (Joule) heating, such that the ion source could be at 2000°C for surface ionization while keeping the target at temperatures estimated to be 500(200)°C by conduction only. With the ion source heated to facilitate surface ionization of the released species, the target temperature was increased stepwise in 100–300°C increments from 1000°C to a maximum of 2100°C in the “before, off” condition. At nominal target temperature (2000°C), additional heat deposition from the proton beam is expected to contribute less than 10% to the total target heating power. Further details regarding the target temperature are described in Appendix B.

Mass scans with the laser ionization switched on/off were conducted using the ISOLDE GPS separator magnet in the “after, off” condition. Because of the potential increase in surface ionization caused by additional heating from laser power deposition, mass scans with lasers “off” were done with the FES blocked or detuned from resonance, and the SES on resonance. Isotope shifts are on the order of 1–2 GHz per neutron number and were not corrected for during the mass scans. In this work, “MagneToF detector” refers to the detector immediately after the mass-separator magnet, unless “ISOLTRAP MagneToF detector” is explicitly indicated. Rates on the MagneToF detector are reported as the Faraday cup (FC) equivalent absolute ion intensity calculated from the manufacturer-provided gain curve [24].

For analysis of the beam composition using mass spectrometry, the beam from the ISOLDE GPS was cooled and bunched in the ISOLTRAP Radio-Frequency Quadrupole

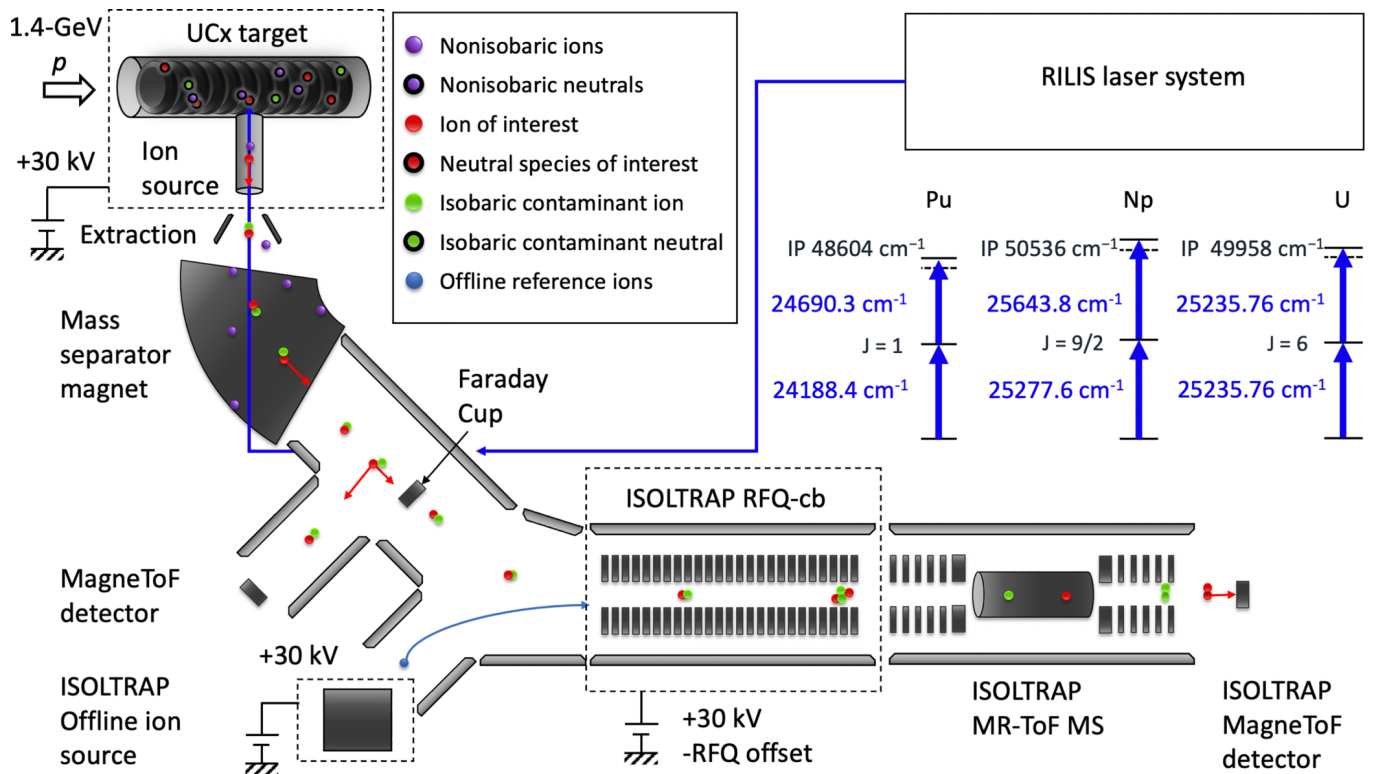


FIG. 1. Schematic of the experimental setup. Isotopes are generated in the UC_x target by 1.4-GeV protons (up to 2 μA) from the CERN Proton Synchrotron Booster. Reaction products diffuse and effuse into the hot cavity ion source where they can be resonantly ionized by lasers from RILIS [23]. Ions are extracted as a beam via the 30-kV extraction electrode and separated by their mass-to-charge ratio in the separator magnet. The mass-separated beam is either sent to a MagneToF detector [24] or through the central beamline to ISOLTRAP, where the ions are cooled and bunched in the RFQ-cb and sent to the MR-ToF MS for isobaric mass separation.

Cooler-Buncher (RFQ-cb) [39] using helium buffer gas. Ion bunches were then injected into the ISOLTRAP multireflection time-of-flight mass spectrometer (MR-ToF MS) [40] and captured between the electrostatic mirror potentials using the in-trap lift method [41]. Further details can be found in Appendix C.

III. RESULTS

A. In-target production models

The production mechanisms extracted from the GEANT4 model predict that some species ($^{239,240}U$, $^{236,238,241}Np$, $^{234-237}Pu$) are entirely or primarily generated by inelastic reactions. Others ($^{237,239}Np$, $^{238,239}Pu$) form primarily through decay of a parent nucleus. The reaction pathways summarized in Table I predict different possibilities for in-target inventory of these species using pre-irradiated targets compared to the situation during direct irradiation.

The isotopes of Np, Pu, and Am observed with at least one event in the GEANT4 model with 10^9 primary proton projectiles are $^{228-244}Np$, $^{234-244}Pu$, and $^{235-244}Am$. Several of these isotopes ($^{228-229,242-244}Np$, $^{242-244}Pu$, and $^{235-240,242-244}Am$) were predicted with event rates less than 100 per 10^9 primaries and are therefore not included in Table I. The GEANT4 model suggests that the production of some isotopes features a large contribution from decay. For example, the dominant mechanism to form ^{239}Pu from the target material is ^{238}U

undergoing neutron capture to ^{239}U , which decays with a half-life of 23.45 min through ^{239}Np (2.3 d) into ^{239}Pu , with 98.2% of the ^{239}U produced from neutron capture reactions, 97.1% of the ^{239}Np produced by ^{239}U decay, and 99.7% of the ^{239}Pu events produced by ^{239}Np decay. This makes ^{239}Pu , and other long-lived isotopes with significant decay feeding, available in measurable quantities without continuous proton irradiation. Other isotopes, such as $^{236,237}Pu$, are predicted to form primarily through reactions rather than decay, particularly in the case of ^{237}Pu since there is no contribution from in-target decay of the long-lived ^{237}Np . With the exceptions of ^{241}Am (162 events, 97.5% from decay of ^{241}Pu), and ^{243}Am , (seven events, five from decay of ^{243}Pu), all Am isotopes were predicted to come entirely from inelastic reactions with protons and heavy ions. These isotopes produced dominantly through direct reactions are thus not expected to be available in off-line operation.

B. Rates from resonance laser-ionization

Pu ion beams were detectable at the lowest target temperatures among the studied actinide beams, with resonant laser response visible on the MagneToF detector at a target temperature of at least 1150°C in the “before, off” condition. Np ion beams were identified only at target temperatures above 2100°C. The laser ionization schemes presented in Fig. 1 for Np and Pu showed resonant enhancement on nominal mass

TABLE I. Production mechanisms in % of total events for selected nuclides of interest calculated using GEANT4 QGSP_INCLXX+ABLA with 10^9 1.4-GeV proton primaries. “Inelastic” and “Decay” columns give the sums over inelastic and radioactive decay processes, respectively. The larger contribution is indicated in bold. Various capture reactions are included in the model but not shown in the table. Some processes with event fractions below 1 % (e.g., photonuclear reactions) are not shown and only the dominant parent nucleus and its corresponding percentage fraction of total events are given. The number of total events is scaled from 10^9 protons to obtain the nuclides per μC equivalent.

isotope	Inelastic:	<i>p</i>	<i>n</i>	<i>d</i>	<i>t</i>	^3He	α	ions	Decay:	parent	nuclides/ μC	
^{234}U	36.4	28.4	7.2	0.4	-	-	-	-	63.6	^{234}Pa	59.4	6.7×10^9
$^{236}\text{U}^a$	65.5	52.2	11.8	0.8	-	-	-	-	34.3	^{236}Pa	34.3	1.3×10^{10}
^{237}U	70.5	61.7	7.4	0.9	0.1	-	-	-	29.0	^{237}Pa	29.0	1.9×10^{10}
$^{239}\text{U}^a$	1.9	-	-	1.3	0.5	-	0.1	-	-	-	-	2.2×10^9
^{240}U	100.0	-	-	-	85.7	-	11.9	2.4	-	-	-	2.1×10^6
^{231}Np	99.0	93.1	-	3.5	0.5	-	-	-	1.0	^{231}Pu	1.0	1.3×10^6
^{232}Np	100.0	92.3	0.3	5.4	0.3	0.1	-	-	-	-	-	1.3×10^7
^{233}Np	99.8	91.1	0.2	6.1	0.5	0.1	-	-	0.2	^{233}Pu	0.2	3.6×10^7
^{234}Np	100.0	89.9	0.2	7.7	0.7	0.1	-	-	-	-	-	2.0×10^8
^{235}Np	99.8	88.4	0.2	8.9	1.0	0.2	-	-	0.2	^{235}Pu	0.2	3.8×10^8
^{236}Np	100.0	86.2	0.1	11.1	1.4	0.2	-	-	-	-	-	8.7×10^8
^{237}Np	3.7	3.0	-	0.6	0.1	-	-	-	96.3	^{237}U	96.3	2.0×10^{10}
^{238}Np	100.0	61.0	-	27.4	8.8	1.1	0.4	-	-	-	-	3.9×10^8
^{239}Np	3.0	-	-	2.2	0.6	0.2	0.1	-	97.0	^{239}U	97.0	2.2×10^9
^{240}Np	73.0	-	-	-	47.8	5.2	18.8	1.3	27.0	^{240}U	27.0	7.8×10^6
^{241}Np	100.0	-	-	-	-	-	96.3	3.7	-	-	-	6.8×10^5
^{235}Pu	99.2	62.5	-	-	-	18.8	10.9	-	0.8	^{235}Am	0.8	8.0×10^5
^{236}Pu	97.1	67.8	-	-	-	13.5	12.5	-	2.9	^{236}Np	1.9	1.3×10^6
^{237}Pu	99.5	39.7	-	-	-	15.5	39.7	0.3	0.5	-	-	2.3×10^6
^{238}Pu	0.9	0.1	-	-	-	0.1	0.7	-	99.1	^{238}Np	99.1	4.0×10^8
^{239}Pu	0.3	-	-	-	-	-	0.3	-	99.7	^{239}Np	99.7	2.2×10^9
^{240}Pu	24.0	-	-	-	-	2.5	20.9	0.6	76.0	^{240}Np	75.5	1.0×10^7
^{241}Pu	53.9	-	-	-	-	-	51.7	2.2	46.1	^{241}Np	46.1	1.4×10^6

^a $^{236,239}\text{U}$ are 0.2 % and 98.1 % produced by neutron capture reactions, respectively.

^{237}Np (Fig. 2) and ^{239}Pu (Fig. 3) beams, respectively, corresponding to the isotopes ^{237}Np and ^{239}Pu , which were predicted to have the largest in-target inventory for the elements Np and Pu (Table I). After irradiating the target with additional proton beam and heating to 1990°C, a mass scan of the GPS separator magnet on the MagneToF detector showed a laser effect for Pu on the masses 236, 239, and 240 (Fig. 4). The laser wavelengths were optimized on ^{239}Pu . Fitting the difference

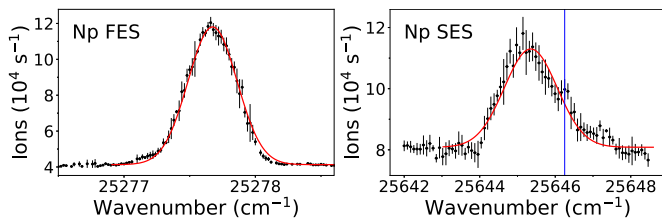


FIG. 2. Np laser ionization resonance on mass 237 at a target temperature of 2110°C and the “after, off” condition. Rates from the GLM MagneToF detector. Left: FES scan using 25645 cm^{-1} for the SES. The Gaussian fit shown gives a peak width of 6.3 GHz. Right: SES scan using 25277.8 cm^{-1} for the FES. The Gaussian fit shown gives a peak width of 27.57 GHz which is typical for autoionizing states. Blue line: a shoulder at 25646.25 cm^{-1} which could come from another atomic or molecular ion with the same mass-to-charge ratio.

between the mass spectra with lasers on and lasers off with a sum model of seven Gaussian peaks fixed at the masses of $^{234-240}\text{Pu}$ (Fig. 4) gives peaks corresponding to the laser response on each mass. For ^{237}Pu , only an upper limit can be extracted.

For Np, a very small laser enhancement effect was visible in a mass spectrum at a target temperature of 2110°C (Fig. 5). ^{237}Np , the longest-lived Np isotope, can be seen as a shoulder on the large ^{238}U peak. The difference was modeled with Gaussian peaks fixed at the masses of $^{235-239}\text{Np}$.

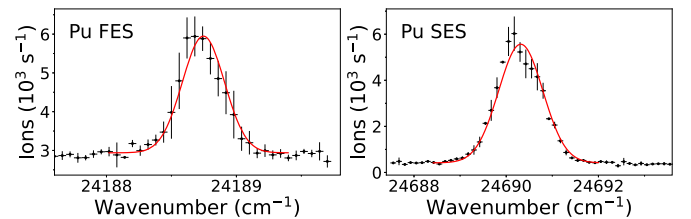


FIG. 3. Pu laser ionization resonance on mass 239 at a target temperature of 1990°C and the “after, off” condition. Rates from the MagneToF detector. Left: FES scan using 24690.4 cm^{-1} for the SES. Gaussian fit gives a peak width of 5.7 GHz. Right: SES scan using 24188.4 cm^{-1} for the FES. Gaussian fit gives a peak width of 33.8 GHz.

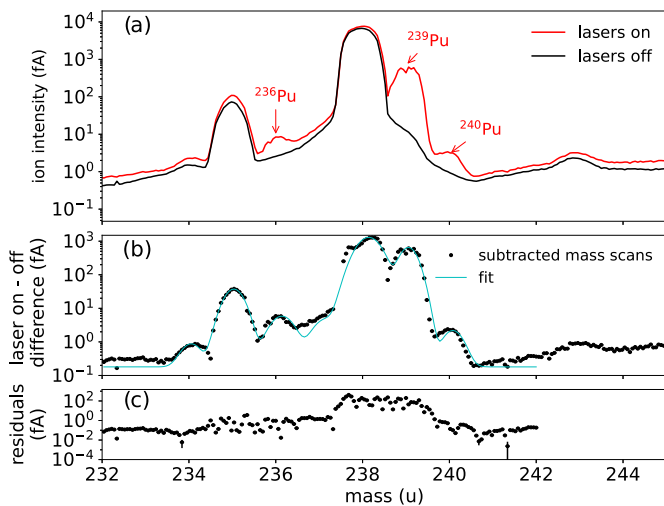


FIG. 4. (a) Signal on the MagneToF detector during a mass scan of the ISOLDE GPS in the “after, off” condition. The mass spectrum taken with the laser scheme for resonant ionization of Pu (Fig. 1) is shown in red. The mass spectrum with the FES laser off resonance is shown in black. (b) The difference between “lasers on” and “lasers off” mass scans in (a) fitted with a model of combined Gaussians. (c) Difference between the experimental data and the fit shown in (b).

C. Time-of-flight identification

Time of flight (ToF) spectra from the MR-ToF MS were used for beam composition identification. Nonisobaric contamination in an isobaric ToF spectrum can be matched with the corresponding mass on a given number of revolutions by using the ToF calibration (e.g., Fig. 6). In cases where a laser scheme was available for the contaminant (e.g., $^{235,238}\text{U}$ from

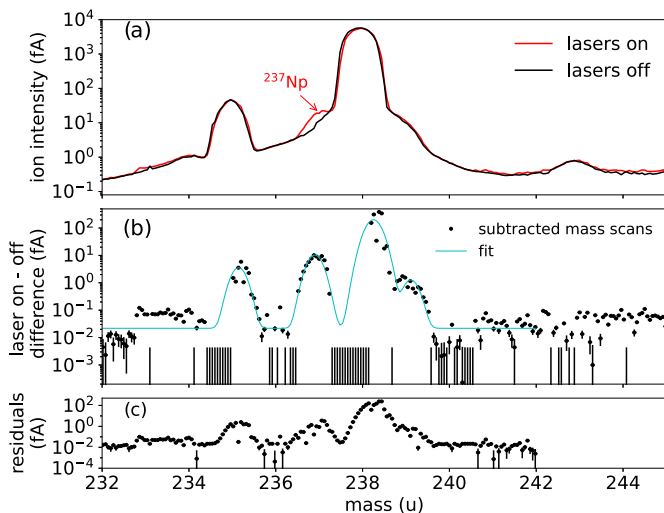


FIG. 5. (a) Signal on the MagneToF detector during a mass scan of the ISOLDE GPS in the “after, off” condition. The mass spectrum taken with the laser scheme for resonant ionization of Np (Fig. 1) is shown in red. The mass spectrum with the FES laser off resonance is shown in black. (b) The difference between “lasers on” and “lasers off” mass scans in (a) fitted with a model of combined Gaussians. (c) Difference between the experimental data and the fit shown in (b).

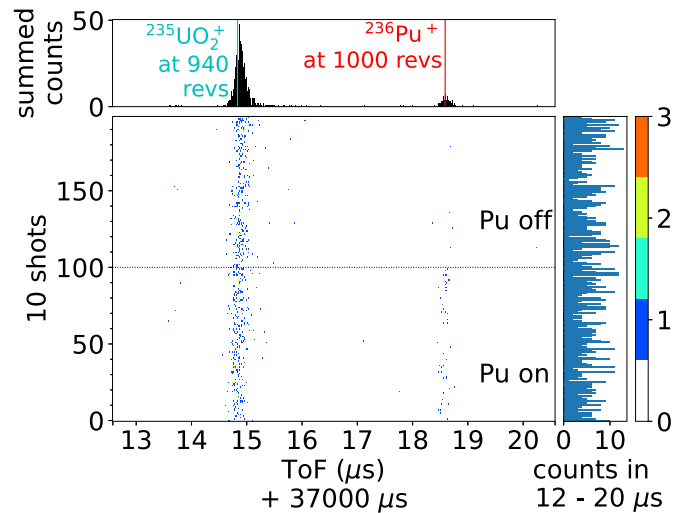


FIG. 6. ToF spectrum of mass 236 separated by the GPS with the Pu ionization scheme in the ion source. Trapping the ions for 1000 revs in the ISOLTRAP MR-ToF MS gives two visible ion ToF traces in the ToF range of interest for ^{236}Pu (red). The Pu FES was blocked around 1000 shots, which led to a significant reduction in intensity of the trace around $37018.5\ \mu\text{s}$.

the target material), the laser effect on the contaminant was used for additional identification (see Fig. 7).

On nominal mass 236, ^{236}Pu was identified in the MR-ToF MS after trapping for 1000 revolutions using laser response. It was present in the ToF spectrum along with a nonisobaric contaminant that showed no change in intensity with the Pu FES. The contaminant arrived $3.7\ \mu\text{s}$ earlier than the ^{236}Pu . This corresponds within 60 ns to the expected time-of-flight of $^{235}\text{U}^{16}\text{O}_2$ on 940 revolutions (Fig. 6). Since the mass resolving power of the GPS would have prevented simultaneous injection of Pu and UO_2 into the ISOLTRAP RFQ-cb, some surface-ionized ^{235}U appears to have formed $^{235}\text{U}^{16}\text{O}_2$ in the RFQ-cb. ^{235}U is also known to be present in the target material and is an expected contaminant that would not be fully suppressed by the separator magnet.

On nominal mass 239, ^{239}Pu was identified with the ISOLTRAP MR-ToF MS along with contaminants. At 1000 revolutions, the ToF centroid of the contaminant was earlier than the ^{239}Pu as shown in Fig. 7. The contaminant at 1000 revolutions responded to the Pu laser scheme and matched the predicted time of flight for $^{239}\text{Pu}^{16}\text{O}$ at a lower number of revolutions. Laser-ionized ^{239}Pu appears to have formed $^{239}\text{Pu}^{16}\text{O}$ in the RFQ-cb. With trapping time corresponding to 992 and 990 revolutions of ^{239}Pu , the ^{239}PuO was not visible, confirming that it is nonisobaric. ^{238}U from the target material was identified as another contaminant. The ToF trace matched the expected ToF of ^{238}U and responded to the U laser ionization scheme, but not the Pu laser scheme. On 800 revolutions another contaminant was identified, matching the expected ToF of $^{238}\text{U}^{16}\text{O}$.

On nominal mass 240, ^{240}Pu was identified in the MR-ToF MS with only one trace visible at 1000 revolutions. On 990 revolutions, a contaminant was present $4.86\ \mu\text{s}$ later than ^{240}Pu , which matched with the expected ToF of

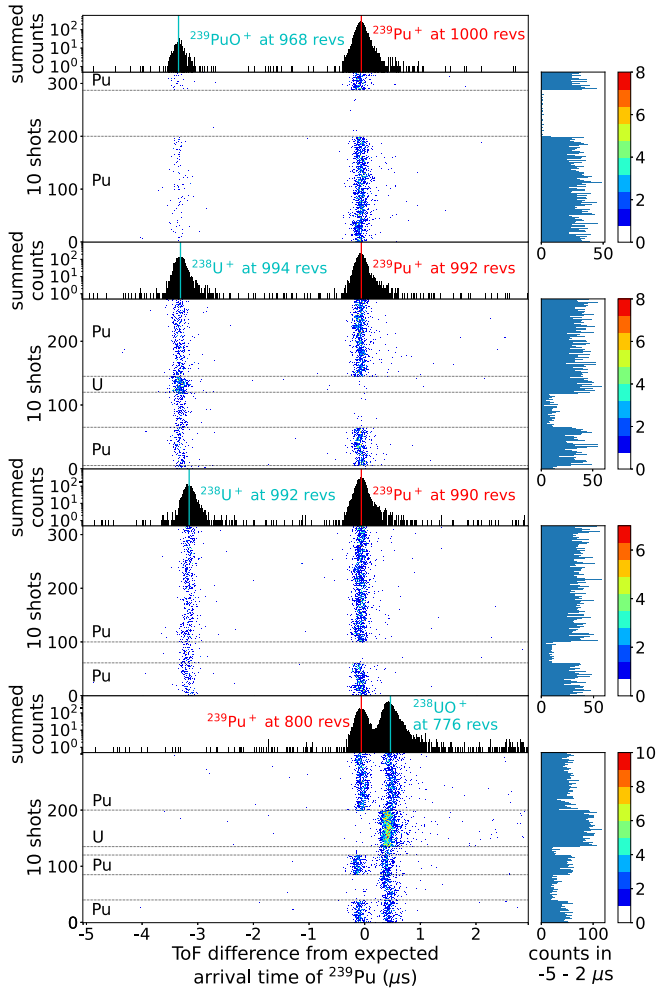


FIG. 7. ToF spectrum of mass 239 separated by the GPS, trapped for 1000, 992, 990, and 800 revolutions in the ISOLTRAP MR-ToF MS. Vertical axes show the summed counts and counts per ten cycles (shots) for each number of revolutions. The color scale indicates the number of counts in a 10 ns time bin. Horizontal axes show ToF since bunch ejection from the RFQ-cb with respect to the predicted ToF for ^{239}Pu . Horizontal dotted lines indicate a change in the laser configuration; laser scheme(s) applied (U, Pu) are indicated on the left.

$^{240}\text{Pu}^{16}\text{O}_2$ on 930 revolutions (Fig. 8). Both traces dropped noticeably in count rate when the Pu FES was blocked. No count rates above background were observed on this mass with the U laser in the ion source and the Pu FES blocked.

D. Isotope shifts

The 395.6-nm transition in Np and the 413.4-nm transition in Pu were scanned for three isotopes each (Figs. 9 and 10) using the grating Ti:Sa laser. The Gaussian fit gave a FWHM of approximately 5 GHz. From the three isotopes, the linear best fits found for the isotope shifts with respect to nuclide mass were: $y_{\text{Np}} = 0.320(63)m - 76(15) \text{ cm}^{-1}$ and $y_{\text{Pu}} = -0.0514(7)m + 12.29(0.16) \text{ cm}^{-1}$. For Np, deviations from linearity are larger than experimental uncertainty,

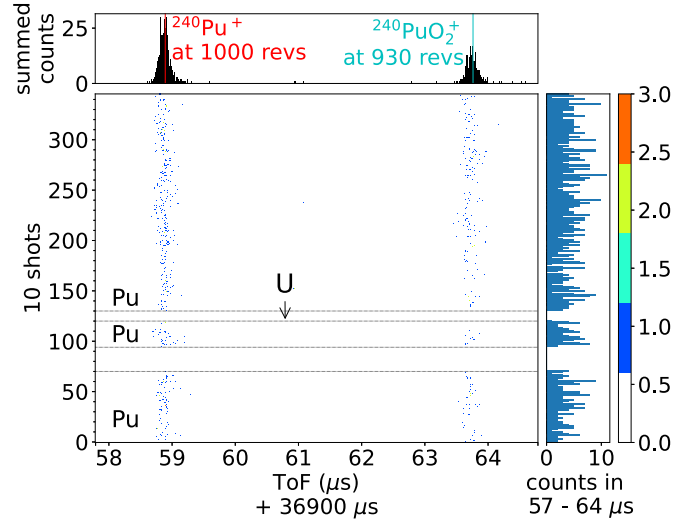


FIG. 8. ToF spectrum of mass 240 separated by the GPS and trapping for 990 revolutions in the ISOLTRAP MR-ToF MS. Red and blue show the expected ToFs for ^{240}Pu and $^{240}\text{Pu}^{16}\text{O}_2$ at 990 and 930 revolutions, respectively. Horizontal dotted lines indicate a change in the laser configuration; laser scheme(s) applied (U, Pu) are indicated.

suggesting that the isotope shifts are not linear. ^{236}Np , with an odd neutron number, appears to exhibit a smaller isotope shift than the extrapolation of the data points $^{237,239}\text{Np}$, which both have even numbers of neutrons. For Pu, deviations from linearity are within the absolute uncertainty of the wave meter (0.03 cm^{-1}) and the uncertainty given by the linear best fit.

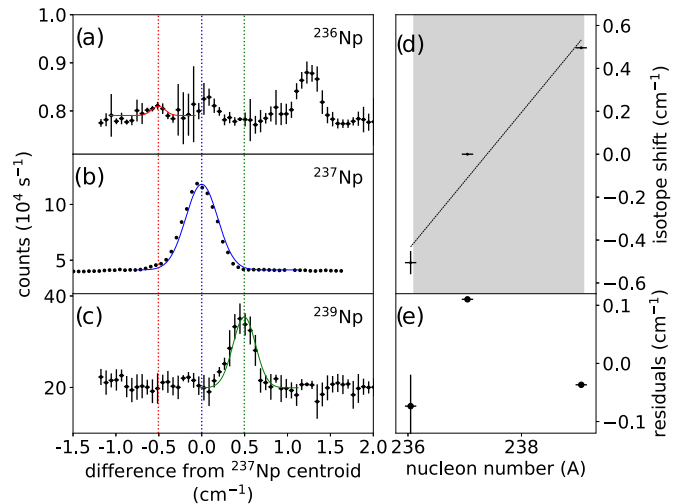


FIG. 9. Intensity on the MagneToF detector vs. the laser wave number of the Np FES for mass-separated ion beams: (a) $A = 236$, (b) $A = 237$, (c) $A = 239$ from the GPS. Wave numbers are with respect to the centroid of the FES resonance of ^{237}Np , shown as the dotted blue line in (b). (d) Plot of isotope shift with respect to ^{237}Np and linear best fit (black dashed line). The fit's large 95% confidence interval indicated in grey extends beyond the plot range. (e) Residuals shown as the difference between the measured isotope shift and the best fit shown in (d).

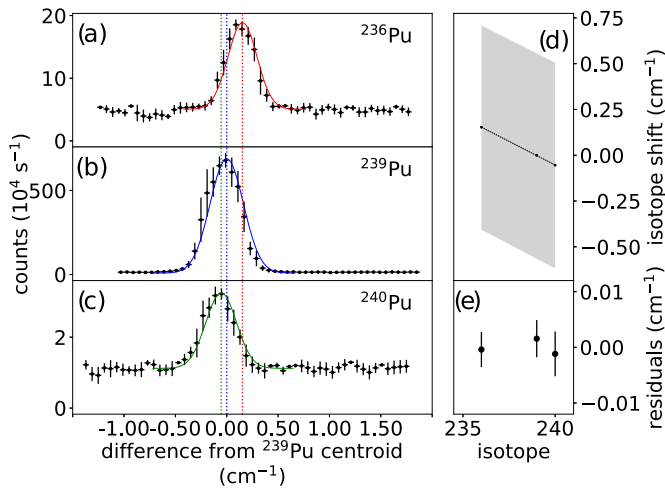


FIG. 10. Intensity on the GLM MagneToF detector vs. the wave number of doubled Ti:Sa light of the Pu FES for mass-separated ion beams: (a) $A = 236$, (b) $A = 239$, (c) $A = 240$ from the GPS. Wave numbers in (a), (b), (c) are with respect to the centroid of the FES resonance of ^{239}Pu , shown as the dotted blue line in (b). (d) Plot of isotope shift with respect to ^{239}Pu and linear best fit (black dashed line) with its 95% confidence interval indicated in grey. (e) residuals shown as the difference between the measured isotope shift and the best fit shown in (d).

E. Release properties

The time structure of isotope release from thick targets exhibits an element-dependent behavior that limits extraction of short-lived isotopes using the ISOL technique [21,42]. Isotopes with half-lives less than 10 ms can be extracted for quickly released species such as alkali metals, while short-lived isotopes of slowly released species will decay before being released [20]. For ^{239}Pu , the release time was evaluated by recording the response to stopping direct proton irradiation (Fig. 11) after irradiation with a proton intensity of 1 μA with a constant ion current indicating steady-state conditions of production and release. For Pu, steady-state conditions were achieved after irradiation times on the order of 600 s. The signal on an FC for ^{239}Pu was recorded immediately after stopping irradiation. An exponential of the form $A \exp\left(-\frac{t}{\tau}\right) + C$ was used to fit the data. Here, C represents the constant background on the FC. The amplitude A of the exponentially falling signal indicates the rate of isotopes generated by protons on target. The exponential decrease captures the combined release following many individual pulses, and therefore sets an upper limit for the time required to extract a Pu isotope from the UC_x target. At a target temperature of 1990(50) $^\circ\text{C}$, this upper limit of the extraction time constant τ was evaluated to be 430(34) s. For the 24110-yr half-life of the ^{239}Pu used in this experiment, the contribution of radioactive decay to the decrease of signal during the 500 s measurement is 6.6×10^{-10} of the initial amount and is therefore negligible in the determination of the release time. For neptunium, an upper limit of the release time was not successfully extracted.

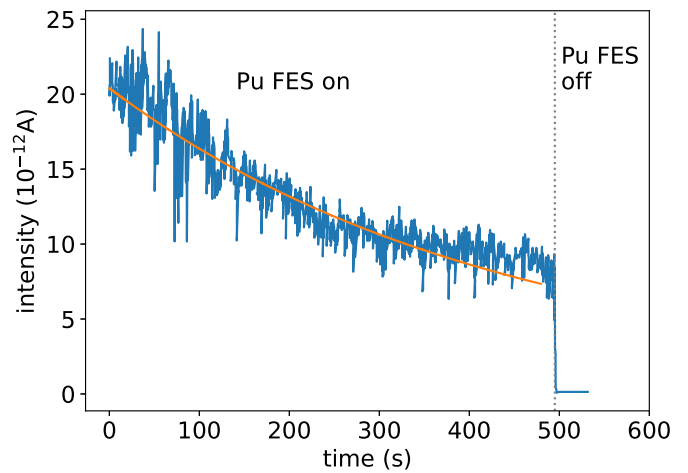


FIG. 11. Release response of ^{239}Pu at 1990 $^\circ\text{C}$ target temperature after the target was irradiated with an integrated current of 1 μA of protons. Data are shown in blue and the best fit using an exponential decay is shown in orange. Time 0 indicates the stop of irradiation. The grey vertical line indicates the blocking of the Pu FES from the ion source and the resulting surface-ionized background.

F. Comparison of measured and simulated rates

The modeled inventory generated by 1 μC of proton primaries using GEANT4 and FLUKA is compared against the measured values in Fig. 12. Resonance signal height on each

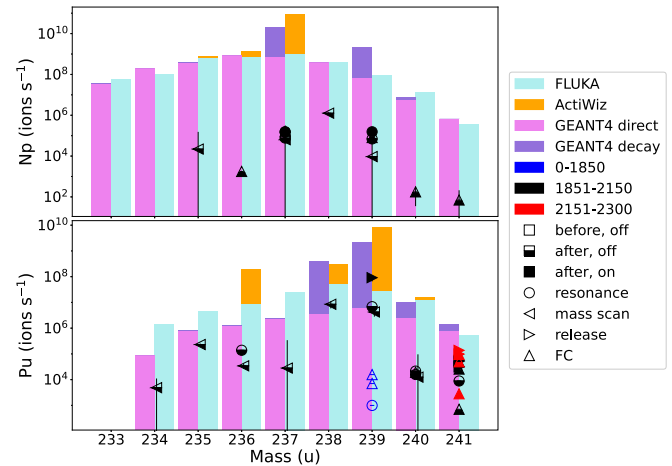


FIG. 12. Combined rates of laser-ionized Np (top) and Pu (bottom) beams from laser resonances (circles), mass scans (left arrows), protons on/off measurements (right arrows), and FC measurements (up arrows) shown with predicted total in-target production rates from the FLUKA and GEANT4 models as bars. The rates from direct reactions are shown in light blue and pink for FLUKA and GEANT4 respectively. The fractions from decay reactions are shown using orange and purple bars for ActiWiz and GEANT4 respectively. Marker colors indicate the target temperature in $^\circ\text{C}$ during the measurement (blue: below nominal, black: nominal, red: above nominal) and the marker fill indicates the irradiation state during the measurement (empty: offline measurement before re-irradiation, half-filled: measurement taken after re-irradiation with the proton beam “off”, filled: online measurement during irradiation).

TABLE II. Maximum rates reported for Np and Pu ions at target temperatures between 1850 and 2150°C. Measurements where uncertainties are larger than the measured value are not included.

mass (u)	Np (ions/s)	Pu (ions/s)
235	$2(1) \times 10^4$	$2.3(2) \times 10^5$
236	$1.76(14) \times 10^3$	$1.38(2) \times 10^5$
237	$1.56(51) \times 10^5$	$<2.8 \times 10^4$
238	$1.3(1) \times 10^6$	$8.5(2.6) \times 10^6$
239	$1.55(4) \times 10^4$	$6.82(9) \times 10^6$
240	$1.7(14) \times 10^2$	$2.14(4) \times 10^4$
241	$7.1(4) \times 10^1$	$2.6(7) \times 10^4$

mass and peak heights from the sum of the Gaussian fits gives a rate of the laser-ionized species without considering the surface-ionized species or surface-ionized contaminants. ToF compositions indicate negligible contributions from surface ionization of Pu compared to the laser-ionized Pu ions. From evaluation of the isotope shifts and the laser linewidth of approximately 5 GHz, the effect in intensity of the different isotopes can be estimated (Figs. 9 and 10).

IV. DISCUSSION

Isotope shifts are connected to the changes in nuclear charge radii and are therefore not necessarily expected to be linear with neutron number [43], especially in the actinide region of the nuclear chart [12]. The $^{236,239,240}\text{Pu}$ isotope shifts agree with linearity, but the $^{236,237,239}\text{Np}$ isotope shifts are not well described by a linear fit. The offsets could suggest odd-even staggering or the presence of a kink in the nuclear charge radius. These preliminary measurements motivate future campaigns to extract further information about the nuclear charge radii of Np.

From laser resonances, laser on/off mass scans and proton on/off measurements, ion beam rates are reported for $^{235-241}\text{Pu}$ (Fig. 12). These rates are achievable with the use of pre-irradiated uranium carbide targets combined with production of isotopes through inelastic reactions during irradiation and can be achieved at nominal (1850–2150°C) UC_x target temperatures. In contrast, rates of Np isotopes are below 10^6 ions s^{-1} even with protons on target and target temperatures above 2100°C, indicating poor release efficiency as follows from a comparison with simulated production rates. Maximum rates observed experimentally in this work are reported in Table II. Further developments may be required to enhance extraction from the target or improve the efficiency of resonance ionization laser schemes.

Mass scans and ToF measurements of ion beams mass-separated by the separator magnets show considerable rates of surface-ionized $^{235,238}\text{U}$ on the nearby masses of interest. The mass-separated actinide beams from ISOLDE formed molecules in the ISOLTRAP RFQ-cb, creating contaminants several mass units away from the species of interest, particularly for U and Pu. These contaminants account for non-isobaric contaminants in the ToF spectra. In many cases the ToF could be matched with a laser effect and corresponding number of revolutions to identify a likely contaminant

(Fig. 7). The rate of molecular formation increases with storage time [44] and may result in fewer ions through the formation of neutral species. The molecular formation decreased the effective efficiency of the species of interest, therefore ion rates from the MR-ToF MS measurements are not reported.

The GEANT4 model (Table I) predicts trends in production mechanisms for these above-target isotopes. The light Np isotopes $^{228-236}\text{Np}$ are produced to more than 99% through inelastic reactions, with direct irradiation contributing more than 85% to the total production for all of these isotopes. $^{237,239,240}\text{Np}$ show large production fractions through decay, with 96.3%, 97.0%, and 27.0%, respectively. $^{240,241}\text{Np}$ were mostly produced through inelastic reactions with ^{240}Np mainly from tritons (47.8%) and α particles (18.8%), and ^{241}Np dominantly from α particles (96.3%) and heavier ions (3.7%). Heavier isotopes $^{242-244}\text{Np}$ were modeled with less than five events each, entirely from heavy ions. For Pu, inelastic reactions with protons and α particles contributed dominantly to the modeled production of the lighter isotopes $^{234-237}\text{Pu}$, while the heavier isotopes $^{238-244}\text{Pu}$ result largely from the β decay of Np isotopes and, for isotopes above ^{240}Pu , also from heavy ion inelastic reactions. For $^{237,239}\text{Np}$ and $^{238,239}\text{Pu}$, decay contributions are described in both models. The FLUKA model and the direct reaction contribution from the GEANT4 model agree well for Np but show slightly different behavior in the case of Pu. Differences in the predictions of decay contributions given by the ActiWiz model and the GEANT4 model could be attributed to the difference in the modeled cooling time.

Events of $^{235-240,242-244}\text{Am}$ were modeled to be between 1 and 100 events per 10^9 primary protons. 162 events of ^{241}Am were modeled dominantly from ^{241}Pu decay. Two of the Am isotopes seen in the model, $^{242,244}\text{Am}$, have short half-lives (16 h and 10 h, respectively) and β decay into $^{242,244}\text{Cm}$. Neither ^{242}Cm nor ^{244}Cm decay into the next element, Bk, marking the Z limit of elements available for experiments at high-energy proton-accelerator-based thick target facilities. To reach usable rates of nuclides with higher proton numbers, these facilities could employ heavier target nuclei, improve extraction efficiency by several orders of magnitude, or improve experimental sensitivity and increase duration. There are limited practical options for targets of bulk material with nuclei heavier than ^{238}U , where decreasing half-lives and available quantities of actinide targets come with increased costs and radioactivity handling considerations. These results demonstrate the availability of two new transuranium beams from UC_x targets at the ISOLDE facility with rates typically required for current experimental sensitivity. Additionally, comparisons of production pathways with measured rates suggest the potential availability of a select few Am isotopes for experiments with state-of-the-art sensitivity.

V. CONCLUSIONS

From 1.4-GeV proton irradiations of a UC_x target, above-target nuclides of neptunium and plutonium have been produced, released from the hot target, resonantly laser-ionized and identified as ion beams at the ISOLDE facility. Production mechanisms modeled by GEANT4 predict

production-pathway-specific yields. On the neutron-deficient side of stability, Np and Pu isotopes are formed through inelastic reactions, mostly induced by protons. Decay contributions from β -decaying U precursors are significant for $^{237,239,240}\text{Np}$ and $^{238-244}\text{Pu}$, with the β decay of Np contributing to the Pu inventory. The use of previously irradiated targets with long cooling times thus contributes to the in-target inventory especially of Pu isotopes, while neutron-deficient isotopes are produced dominantly from direct irradiation.

Two-step ionization schemes using intra-cavity doubled Ti:Sa lasers were applied to resonantly ionize both Np and Pu. Isotope shifts were investigated for the 395.6-nm ground state transition in $^{236,237,239}\text{Np}$ and the 413.4-nm ground state transition in $^{236,239,240}\text{Pu}$. To our knowledge, there are no data available in literature for the charge radius of Np nuclei. With two odd-odd nuclei and odd-even ^{236}Np , Np isotope shifts did not follow a linear trend. Further measurements are required to extract information about the nuclear charge radii. In the case of Pu, isotope shifts are linear with nucleon number in the investigated range and can be extrapolated for use over a wider range of isotopes.

Ion production rates were measured for $^{235-240}\text{Np}$ and $^{234-240}\text{Pu}$ (Fig. 12). ToF MS spectra show surface-ionized contamination on the masses of interest, originating from the uranium carbide target material. Oxide formation is observed in a gas-filled RFQ-cb. Comparing the observed rates with predicted in-target inventory gives an estimation for the extraction efficiency of Np on the order of 0.001% and Pu on the order of 0.1%. Target temperatures required for observable rates of Np were above 2100°C, while target temperatures required for Pu were above 1150°C. Pu is released within 400–500 s at nominal target temperatures. The difference in extraction efficiency and observed temperature may be attributed to the more refractory properties of Np; it exhibits a higher enthalpy of formation of the gaseous monatomic element and also a higher adsorption enthalpy on tantalum, the target container material [45].

The demonstrated availability of Np and Pu beams at ISOLDE brings two new actinide elements into reach for experiments at ISOL facilities with useful intensities of specific isotopes as functions of different experimental parameters such as decay time. Information on laser ionization schemes, magnitudes of isotope shifts, and release temperatures informs future experiments requesting beams of these elements.

^{241}Pu is the heaviest nuclide identified at a proton-accelerator-driven ISOL facility to date. While extremely sensitive experiments may be capable of extending studies one element higher to specific isotopes of Am discussed here, the investigation of production mechanisms suggests that plutonium is the high- Z limit of heavy nuclide production from 1.4-GeV protons on a ^{238}U target with typical rates required for current experimental sensitivity.

ACKNOWLEDGMENTS

The authors gratefully acknowledge technical support from E. Barbero, M. Bovigny, B. Crepieux, J. Cruikshank, and the ISOLDE operations staff. This project has received funding from the European Union's Horizon 2020 Research and

Innovation Program (Grant No. 861198 project LISA MSCA ITN). The authors acknowledge support from the German Federal Ministry of Education and Research (BMBF) for ISOLTRAP (Grants No. 05P18HGCI A and No. 05P21HGCI I). L.N. acknowledges support from the Wolfgang Gentner Program of the German Federal Ministry of Education and Research (Grant No. 13E18CHA).

APPENDIX A: IN-TARGET PRODUCTION MODELS

The FLUKA Monte Carlo model of in-target production is a standard tool available for users of the CERN-ISOLDE facility, with a database of modeled values [20]. This model uses the ABLA description of nuclear de-excitation through particle evaporation and fission for the decay pathways of nuclear systems [46]. The FLUKA model incorporates no cooling time for radioactive decay. Instead, the FLUKA model of particle fluence spectra in the target was used as input to the ActiWiz Creator software version 3.4 [29]. ActiWiz is based on 100 CPU years of FLUKA calculations modeling interactions of protons, charged pions, photons, and neutrons above 20 MeV with the evaluated libraries JEFF 3.3, ENDF VIII.0, and EAF2010 for neutrons below 20 MeV. The ActiWiz model was used to extend the FLUKA model to include the inventory of radionuclides produced during the cooling period and is detailed in Ref. [30].

GEANT4 (version GEANT4-11) was used with physics list QGSP_INCLXX_HP_ABLA, an experimental physics list using the Liège intranuclear cascade model for nucleon-nucleus interactions below 3 GeV, with neutronHP (high precision neutron package) for neutron cross sections below 20 MeV and de-excitation modeled using ABLA with data sets for neutron, proton, and pion cross sections for elastic, inelastic, capture, and fission reactions as described in [32].

Predictions from the INCLXX and ABLA models show good agreement for a selection of lighter isotopic chains measured at ISOLDE [47].

APPENDIX B: TARGET AND RESONANCE IONIZATION LASER ION SOURCE

The measured temperature was calibrated against the target and ion source heating current and required power using an optical pyrometer up to 2000°C. The calibration data were extrapolated to estimate the target and ion source temperatures during the experiment with an uncertainty estimated to be 100°C. The calibration was performed before the loading of the target material and the first irradiation of the target.

Three diode pumped solid-state (DPSS) Nd:YAG lasers were used to pump a total of four titanium:sapphire (Ti:Sa) lasers based on wavelength selection by grating tuning [35] or a combination of a Lyot filter and Fabry-Perot etalon [36] with a repetition rate of 10 kHz. One intracavity second-harmonic generation (IC-doubled) grating Ti:Sa laser [37] was used to provide the first excitation step (FES) for either Pu or Np, with typical output power up to 400 mW. The other three IC-doubled Ti:Sa lasers were used to provide the second excitation step (SES) of Pu, the identical wavelength of the FES and SES of U, and the SES of Np, each with up to 2.5 W

of output power. The Pu resonance ionization scheme was developed by Kneip *et al.* [14] and uses a FES from the ground state to the $5f^56d^27s J = 1$ state followed by a SES to an autoionizing state located above the ionization potential. The U scheme was developed by Savina *et al.* [38] and features a two-step, single wavelength ionization from the ground state to an autoionizing state. Several schemes were investigated for Np using a FES of 25277.6 cm^{-1} from the ground state to a $J = 9/2$ state.

To switch between ionizing Pu or Np, the grating Ti:Sa was changed between the Pu FES and the Np FES. Wavelength scans of the FES were done by changing the diffraction grating angle. Small-range wavelength scans of the second step were done manually by changing the etalon angle. The frequency of the Ti:Sa lasers was measured using a High Finesse WS7 wave meter (uncertainty 20% of the laser linewidth) to sample the fundamental, non-frequency-doubled mode. Atomic transitions in the ion source are expected to be Doppler-broadened, with the FWHM given by $\Delta\nu_D$, where

$$\Delta\nu_D = \nu_0 \sqrt{\frac{8k_B T \ln 2}{mc^2}}, \quad (\text{B1})$$

where T is the absolute temperature, k_B is the Boltzmann constant, m is the mass of the atom, ν_0 is the nominal laser frequency, and c is the speed of light in vacuum. For the employed transitions around 400 nm, the Doppler broadening at 2000°C thus corresponds to Gaussian peak shapes with FWHM above 1.6 GHz for a mass of 238 u. Laser linewidth and power-broadening may increase the experimentally observed peak widths further [23].

APPENDIX C: ION BEAM ANALYSIS

The ion beams mass-separated by the GPS separator magnet were injected into the ISOLTRAP RFQ-cb, where they were collisionally cooled with the He buffer gas at pressures up to 10^{-5} mbar measured within 1 m of the injection. The amount of injected beam was controlled using a collection time, such that longer collection times were used for beams with lower intensity. Storage time in the RFQ-cb was thus

larger for beams of lower intensity and ranged between 1 ms and 2 s in this experiment. After ejection from the RFQ-cb, the ion bunch energy was reduced to 3.2 keV using a pulsed drift tube. Ion bunches were then injected into the ISOLTRAP MR-ToF MS [40] and trapped between the electrostatic mirror potentials using the in-trap lift method [41] for typically 1000 revolutions before release and detection of the ions' ToF. The difference in ToF allows components with different mass-over-charge ratios m/q to be separated in time t with a mass resolving power R given by

$$R = \frac{m}{\Delta m} = \frac{t}{2\Delta t}, \quad (\text{C1})$$

where t is the absolute time of flight and Δt is the FWHM of the ToF distribution. After trapping times of up to 40 ms, the ions were ejected onto the ISOLTRAP MagneToF detector. Ion arrival times were measured from the time of ejection from the RFQ-cb and recorded with 100 ps resolution. Mass resolving powers R in excess of 10^5 were achieved for the investigated mass range.

Additionally, nonisobaric beam components formed in the trapping and cooling process from the mass-separated beam can be identified. These components can appear in the same ToF spectrum when traveling through the in-trap lift cavity of the MR-ToF MS with the isobaric beam component on a different number of revolutions during bunch ejection. Non-isobaric components were identified by varying the trapping time of the isobaric beam bunch in the MR-ToF MS. This leads to different absolute ejection times, which increases the chance that the non-isobaric component is separated from the isobaric beam bunch. The ISOLTRAP MR-ToF MS was calibrated using $^{85,87}\text{Rb}$ and ^{133}Cs from the ISOLTRAP offline ion source and using ^{238}U from the ISOLDE GPS target and ion source. The reference measurements were used to create a calibration to relate known masses to an expected ToF in the form

$$t_{\text{calibration}}(m) = a\sqrt{m/q} + b, \quad (\text{C2})$$

where a and b are the calibrated parameters.

-
- [1] E. M. Holmbeck, R. Surman, A. Frebel, G. C. McLaughlin, M. R. Mumpower, T. M. Sprouse, T. Kawano, N. Vassh, and T. C. Beers, Characterizing r-process sites through actinide production, *J. Phys. Conf. Ser.* **1668**, 012020 (2020).
- [2] M. R. Mumpower, T. Kawano, T. M. Sprouse, N. Vassh, E. M. Holmbeck, R. Surman, and P. Möller, β -delayed fission in r-process nucleosynthesis, *Astrophys. J.* **869**, 14 (2018).
- [3] A. N. Andreyev, K. Nishio, and K.-H. Schmidt, Nuclear fission: A review of experimental advances and phenomenology, *Rep. Prog. Phys.* **81**, 016301 (2018).
- [4] E. R. Birnbaum, M. E. Fassbender, M. G. Ferrier, K. D. John, and T. Mastren, Actinides in Medicine, *Encyclopedia of Inorganic and Bioinorganic Chemistry* (John Wiley and Sons, Ltd, New York, 2018), pp. 1–21.
- [5] A. K. H. Robertson, C. F. Ramogida, P. Schaffer, and V. Radchenko, Development of ^{225}Ac radiopharmaceuticals: TRIUMF perspectives and experiences, *Current Radiopharmaceuticals* **11**, 156 (2018).
- [6] A. Kudo, *Radioactivity in the Environment* (Elsevier Science, New York, 2001).
- [7] J. Lee, *Nuclear Reactor Physics and Engineering* (John Wiley and Sons, Inc., New York, 2020).
- [8] T. Kajino and G. J. Mathews, Impact of new data for neutron-rich heavy nuclei on theoretical models for r-process nucleosynthesis, *Rep. Prog. Phys.* **80**, 084901 (2017).
- [9] K.-H. Schmidt and B. Jurado, Review on the progress in nuclear fission experimental methods and theoretical descriptions, *Rep. Prog. Phys.* **81**, 106301 (2018).
- [10] V. Sonnenschein, Laser developments and high resolution resonance ionization spectroscopy of actinide elements, Ph.D. thesis, University of Jyväskylä (2015).

- [11] A. Voss, V. Sonnenschein, P. Campbell, B. Cheal, T. Kron, I. D. Moore, I. Pohjalainen, S. Raeder, N. Trautmann, and K. Wendt, High-resolution laser spectroscopy of long-lived plutonium isotopes, *Phys. Rev. A* **95**, 032506 (2017).
- [12] M. Block, M. Laatiaoui, and S. Raeder, Recent progress in laser spectroscopy of the actinides, *Prog. Part. Nucl. Phys.* **116**, 103834 (2021).
- [13] P. Kunz, G. Huber, G. Passler, and N. Trautmann, Efficient three-step, two-color ionization of plutonium using a resonance enhanced 2-photon transition into an autoionizing state, *Eur. Phys. J. D* **29**, 183 (2004).
- [14] N. Kneip, Ch. E. Düllmann, V. Gadelshin, R. Heinke, C. Mokry, S. Raeder, J. Runke, D. Studer, N. Trautmann, F. Weber, and K. Wendt, Highly selective two-step laser ionization schemes for the analysis of actinide mixtures, *Hyperfine Interact.* **241**, 45 (2020).
- [15] S. Raeder, N. Kneip, T. Reich, D. Studer, N. Trautmann, and K. Wendt, Recent developments in resonance ionization mass spectrometry for ultra-trace analysis of actinide elements, *Radiochim. Acta* **107**, 645 (2019).
- [16] J. Roberto, C. Alexander, R. Boll, J. Burns, J. Ezold, L. Felker, S. Hogle, and K. Rykaczewski, Actinide targets for the synthesis of super-heavy elements, *Nucl. Phys. A* **944**, 99 (2015).
- [17] D. McAlister and E. Horwitz, Chromatographic generator systems for the actinides and natural decay series elements, *Radiochim. Acta* **99**, 151 (2011).
- [18] Y. Blumenfeld, T. Nilsson, and P. V. Duppen, Facilities and methods for radioactive ion beam production, *Phys. Scr.* **2013**, 014023 (2013).
- [19] R. Catherall, W. Andreatza, M. Breitenfeldt, A. Dorsival, G. J. Focker, T. P. Gharsa, T. J. Giles, J. L. Grenard, F. Locci, P. Martins, S. Marzari, J. Schipper, A. Shornikov, and T. Stora, The ISOLDE facility, *J. Phys. G: Nucl. Part. Phys.* **44**, 094002 (2017).
- [20] J. Ballof, J. Ramos, A. Molander, K. Johnston, S. Rothe, T. Stora, and Ch. E. Düllmann, The upgraded ISOLDE yield database - A new tool to predict beam intensities, *Nucl. Instrum. Methods Phys. Res. B* **463**, 211 (2020).
- [21] J. Ramos, Thick solid targets for the production and online release of radioisotopes: The importance of the material characteristics, a review, *Nucl. Instrum. Methods Phys. Res. B* **463**, 201 (2020).
- [22] A. Gottberg, Target materials for exotic ISOL beams, *Nucl. Instrum. Methods Phys. Res. B* **376**, 8 (2016).
- [23] V. Fedosseev, K. Chrysalidis, T. D. Goodacre, B. Marsh, S. Rothe, C. Seiffert, and K. Wendt, Ion beam production and study of radioactive isotopes with the laser ion source at ISOLDE, *J. Phys. G: Nucl. Part. Phys.* **44**, 084006 (2017).
- [24] D. Stresau, K. Hunter, W. Sheils, P. Raffin, and Y. Benari, A new class of robust sub-nanosecond ToF detectors with high dynamic range, 54th ASMS Conference on Mass Spectrometry, Seattle, Washington (2006).
- [25] P. Kunz, TRIUMF yield database (2022).
- [26] P. Kunz, J. Lassen, C. Andreoiu, and F. H. Garcia, Transuranium isotopes at ISAC/TRIUMF, *Nucl. Instrum. Methods Phys. Res. B* **534**, 90 (2023).
- [27] C. Ahdida, D. Bozzato, D. Calzolari, F. Cerutti, N. Charitonidis, A. Cimmino, A. Coronetti, G. L. D'Alessandro, A. D. Servelle, L. S. Esposito, R. Froeschl, R. G. Alía, A. Gerbershagen, S. Gilardoni, D. Horváth, G. Hugo, A. Infantino, V. Kouskoura, A. Lechner, B. Lefebvre *et al.*, New capabilities of the FLUKA multi-purpose code, *Front. Phys.* **9**, 788253 (2022).
- [28] G. Battistoni, T. Boehlen, F. Cerutti, P. Chin, L. Esposito, A. Fassò, A. Ferrari, A. Lechner, A. Empl, A. Mairani, A. Mereghetti, P. G. Ortega, J. Ranft, S. Roesler, P. Sala, V. Vlachoudis, and G. Smirnov, Overview of the FLUKA code, *Ann. Nucl. Energy* **82**, 10 (2015).
- [29] H. Vincke and C. Theis, ActiWiz optimizing your nuclide inventory at proton accelerators with a computer code, *Prog. Nucl. Sci. Tech.* **4**, 228 (2014).
- [30] C. Duchemin, T. Cocolios, M. Fedosseev, B. Marsh, S. Rothe, and T. Stora, EDMS No. 2379738, Technical Report, CERN, European Organization for Nuclear Research, 2020.
- [31] J. Allison, K. Amako, J. Apostolakis, P. Arce, M. Asai, T. Aso, E. Bagli, A. Bagulya, S. Banerjee, G. Barrand, B. Beck, A. Bogdanov, D. Brandt, J. Brown, H. Burkhardt, P. Canal, D. Cano-Ott, S. Chauvie, K. Cho, G. Cirrone *et al.*, Recent developments in GEANT4, *Nucl. Instrum. Methods Phys. Res. A* **835**, 186 (2016).
- [32] GEANT4 user documentation, Technical Report, CERN, 2022.
- [33] F. H. Garcia, C. Andreoiu, and P. Kunz, Calculation of in-target production rates for isotope beam production at TRIUMF, *Nucl. Instrum. Methods Phys. Res. B* **412**, 174 (2017).
- [34] S. Rothe, T. Day Goodacre, D. V. Fedorov, V. N. Fedosseev, B. A. Marsh, P. L. Molkanov, R. E. Rossel, M. D. Seliverstov, M. Veinhard, and K. D. Wendt, Laser ion beam production at CERN-ISOLDE: New features - More possibilities, *Nucl. Instrum. Methods Phys. Res. B* **376**, 91 (2016).
- [35] V. Sonnenschein, I. D. Moore, I. Pohjalainen, M. Reponen, S. Rothe, and K. Wendt, Intracavity Frequency Doubling and Difference Frequency Mixing for Pulsed ns Ti:Sapphire Laser Systems at On-Line Radioactive Ion Beam Facilities, *Proceedings of the Conference on Advances in Radioactive Isotope Science (ARIS2014)*, JPS Conference Proceedings 6, 2015, Vol. 030126, pp. 1–6.
- [36] S. Rothe, B. A. Marsh, C. Mattolat, V. N. Fedosseev, and K. Wendt, A complementary laser system for ISOLDE RILIS, *J. Phys.: Conf. Ser.* **312**, 052020 (2011).
- [37] A. Teigelhöfer, P. Bricault, O. Chachkova, M. Gillner, J. Lassen, J. P. Lavoie, R. Li, J. Meißner, W. Neu, and K. D. Wendt, Grating tuned Ti:Sa laser for in-source spectroscopy of Rydberg and autoionizing states, *Hyperfine Interact.* **196**, 161 (2010).
- [38] M. R. Savina, B. H. Isselhardt, A. Kucher, R. Trappitsch, B. V. King, D. Ruddle, R. Gopal, and I. Hutcheon, High useful yield and isotopic analysis of uranium by resonance ionization mass spectrometry, *Anal. Chem.* **89**, 6224 (2017).
- [39] F. Herfurth *et al.*, A linear radiofrequency ion trap for accumulation, bunching, and emittance improvement of radioactive ion beams, *Nucl. Instrum. Methods Phys. Res. A* **469**, 254 (2001).
- [40] R. N. Wolf, F. Wienholtz, D. Atanasov, D. Beck, K. Blaum, C. Borgmann, F. Herfurth, M. Kowalska, S. Kreim, Y. A. Litvinov, D. Lunney, V. Manea, D. Neidherr, M. Rosenbusch, L. Schweikhard, J. Stanja, and K. Zuber, ISOLTRAP's multi-reflection time-of-flight mass separator/spectrometer, *Int. J. Mass Spectrom.* **349–350**, 123 (2013).
- [41] F. Wienholtz, D. Beck, K. Blaum, C. Borgmann, M. Breitenfeldt, R. B. Cakirli, S. George, F. Herfurth, J. D. Holt, M. Kowalska, S. Kreim, D. Lunney, V. Manea, J. Menéndez, D. Neidherr, M. Rosenbusch, L. Schweikhard, A. Schwenk, J.

- Simonis, J. Stanja *et al.*, Masses of exotic calcium isotopes pin down nuclear forces, *Nature (London)* **498**, 346 (2013).
- [42] J. P. Ramos, A. Gottberg, R. S. Augusto, T. M. Mendonca, K. Riisager, C. Seiffert, P. Bowen, A. M. Senos, and T. Stora, Target nanomaterials at CERN-ISOLDE: Synthesis and release data, *Nucl. Instrum. Methods Phys. Res. B* **376**, 81 (2016).
- [43] X. F. Yang, S. J. Wang, S. G. Wilkins, and R. F. Ruiz, Laser spectroscopy for the study of exotic nuclei, *Prog. Part. Nucl. Phys.* **129**, 104005 (2023).
- [44] M. Au, M. Athanasakis-Kaklamanakis, L. Nies, J. Ballof, R. Berger, K. Chrysalidis, P. Fischer, R. Heinke, J. Johnson, U. Köster, D. Leimbach, B. Marsh, M. Mougeot, J. Reilly, E. Reis, M. Schlaich, C. Schweiger, L. Schweikhard, S. Stegemann, J. Wessolek *et al.*, In-source and in-trap formation of molecular ions in the actinide mass range at CERN-ISOLDE, [arXiv:2303.12215](https://arxiv.org/abs/2303.12215) [physics.ins-det].
- [45] J. Ballof, Radioactive Molecular Beams at CERN-ISOLDE, Ph.D. thesis, Johannes Gutenberg-University Mainz, Mainz, Germany, CERN CDS: CERN-THESIS-2021-226 (2021), <https://cds.cern.ch/record/2797475>.
- [46] A. Kelic, M. V. Ricciardi, and K.-H. Schmidt, ABLA07 - Towards a complete description of the decay channels of a nuclear system from spontaneous fission to multifragmentation, [arXiv:0906.4193](https://arxiv.org/abs/0906.4193).
- [47] S. Lukić, F. Gevaert, A. Kelić, M. V. Ricciardi, K. H. Schmidt, and O. Yordanov, Systematic comparison of ISOLDE-SC yields with calculated in-target production rates, *Nucl. Instrum. Methods Phys. Res. A* **565**, 784 (2006).

Correction: An error in wording was introduced during the production process in the first paragraph of Sec. II, item (iii), and has been fixed.

5. Extraction and production of molecular ion beams containing an actinide nucleus

Outline

5.1	Publication II: In-source and in-trap formation of molecular ions in the actinide mass range at CERN-ISOLDE	57
5.2	Publication in preparation: Actinium fluorides	64
5.3	Thorium molecular ions	72
5.4	Protactinium molecular ions	72
5.5	Uranium molecular ions	73
5.6	Transuranium molecular ions	74

Radioactive molecules have gained recognition for their potential in both fundamental and applied science [70, 97, 159] since recent advances at ISOLDE have shown the possibility of extracting information from experimental observables using laser spectroscopy [78]. Many candidate molecules have been proposed to search for physics beyond the standard model, particularly actinide molecules [82]. Studies of such molecules have the potential to become a complementary approach to high-energy particle physics, but most molecules with sensitivity to fundamental effects are unavailable due to limited production. A recent worldwide effort has been initiated to produce and study these radioactive molecules [69, 71]. The production and spectroscopy of RaF [78] and AcF [160] at ISOLDE are pioneering developments in this rapidly-growing field.

At the heart of RIB facilities such as ISOLDE, the target and ion source are responsible for the production, extraction, ionization, and delivery of the ion beam [64]. A natural application of the ISOL method towards the production of radioactive molecules is to simply form the species of interest in the target and ion source unit, followed by ionization and extraction as

an ion beam as routinely done for atomic ion beams of interest. Unfortunately, this method does not apply to all molecules of interest, particularly fragile configurations that are not stable in high-temperature environments. To create these molecules at ISOL facilities, other techniques that provide lower-temperature environments for molecular formation are needed, with the requirement that these techniques must keep the ability to integrate with the radioactive species produced in the target through accelerator-driven nuclear reactions.

5.1 Publication II: In-source and in-trap formation of molecular ions in the actinide mass range at CERN-ISOLDE

In the publication, considerations for the production of radioactive molecules both in the target and ion source unit and in gas-filled ion traps are presented. Uranium carbide targets are used to provide ion beams demonstrating several molecular formation techniques. The results can be used to perform further systematic studies of the parameters identified for the different formation methods and as an online proof-of-concept to motivate detailed studies in an offline environment. For studies in the actinide mass region, characterization of ion beam compositions on several masses of interest is reported, providing information towards future experiments in the actinide and actinide molecule mass region on possible molecular contaminants on several masses of interest.

Bibliographic Information

M. Au, M. Athanasakis-Kaklamanakis, L. Nies, J. Ballof, R. Berger, K. Chrysalidis, P. Fischer, R. Heinke, J. Johnson, U. Köster, D. Leimbach, B. Marsh, M. Mougeot, J. Reilly, E. Reis, M. Schlaich, Ch. Schweiger, L. Schweikhard, S. Stegemann, J. Wessolek, F. Wienholtz, S. G. Wilkins, W. Wojtaczka, Ch. E. Düllmann, S. Rothe, “In-source and in-trap formation of molecular ions in the actinide mass range at CERN-ISOLDE” (2023) *Nucl. Instrum. and Methods B.*, 541 (pp. 375-379). *Proc. EMIS XIX at RAON, 2022*. doi: 10.1016/j.nimb.2023.05.015. arXiv:2303.12215, physics.inst-det.

Author contributions

Corresponding author: M. Au
CRediT author statement:

Conceptualization: M. Au, M. Athanasakis-Kaklamanakis, K. Chrysalidis, R. Heinke, B. Marsh, S.G. Wilkins, Ch.E. Düllmann, S. Rothe. Investigation: M. Au, M. Athanasakis-Kaklamanakis, L. Nies, J. Ballof, R. Berger, P. Fischer, J. Johnson, U. Köster, D. Leimbach, M. Mougeot, B. Reich, J. Reilly, E. Reis, M. Schlaich, Ch. Schweiger, S. Stegemann, J. Wessolek, F. Wienholtz, S.G. Wilkins, W. Wojtaczka. Analysis: M. Au. Supervision: K. Chrysalidis, R. Heinke, B. Marsh, Ch.E. Düllmann, S. Rothe. M. Au prepared the manuscript. All authors reviewed the manuscript.

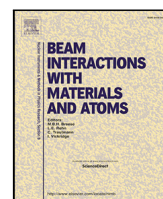
Copyright Notice

©2023 The Authors. Published by Elsevier B.V. This is an accepted version of this article published in 10.1016/j.nimb.2023.05.015. This is an open access article under the CC BY license.



Contents lists available at ScienceDirect

Nuclear Inst. and Methods in Physics Research, B

journal homepage: www.elsevier.com/locate/nimb

In-source and in-trap formation of molecular ions in the actinide mass range at CERN-ISOLDE

M. Au^{a,b,*}, M. Athanasakis-Kaklamanakis^{a,c}, L. Nies^{a,d}, J. Ballof^{a,e}, R. Berger^{a,f}, K. Chrysalidis^a, P. Fischer^d, R. Heinke^a, J. Johnson^c, U. Köster^{a,g}, D. Leimbach^{a,1}, B. Marsh^a, M. Mougeot^{a,h,2}, B. Reich^a, J. Reillyⁱ, E. Reis^a, M. Schlaich^j, Ch. Schweiger^{a,h}, L. Schweikhard^d, S. Stegemann^a, J. Wessolek^{a,i}, F. Wienholtz^j, S.G. Wilkins^{a,k}, W. Wojtaczka^c, Ch.E. Düllmann^{b,l,m}, S. Rothe^a

^a CERN, Geneva, Switzerland^b Johannes Gutenberg-Universität Mainz, Mainz, Germany^c KU Leuven, Leuven, Belgium^d Universität Greifswald, Greifswald, Germany^e FRIB, Michigan State University, East Lansing, MI, United States of America^f Philipps-Universität Marburg, Marburg, Germany^g Institut Laue-Langevin, Grenoble, France^h Max Planck Institut für Kernphysik, Heidelberg, Germanyⁱ The University of Manchester, Manchester, United Kingdom^j Technische Universität Darmstadt, Darmstadt, Germany^k Massachusetts Institute of Technology, Cambridge, United States of America^l GSI Helmholtzzentrum für Schwerionenforschung, Darmstadt, Germany^m Helmholtz Institute Mainz, Mainz, Germany

ARTICLE INFO

Keywords:

Radioactive molecules

Molecular ion beams

Isotope Separation On Line

Actinides

Mass spectrometry

ABSTRACT

The use of radioactive molecules for fundamental physics research is a developing interdisciplinary field limited dominantly by their scarce availability. In this work, radioactive molecular ion beams containing actinide nuclei extracted from uranium carbide targets are produced via the Isotope Separation On-Line technique at the CERN-ISOLDE facility. Two methods of molecular beam production are studied: extraction of molecular ion beams from the ion source, and formation of molecular ions from the mass-separated ion beam in a gas-filled radio-frequency quadrupole ion trap. Ion currents of U^+ , UO_{1-3}^+ , UC_{1-3}^+ , UF_{1-4}^+ , $UF_{1,2}O_{1,2}^+$ are reported. Metastable tantalum and uranium fluoride molecular ions are identified. Formation of UO_{1-3}^+ , $U(OH)_{1-3}^+$, UC_{1-3}^+ , $UF_{1,2}O_{1,2}^+$ from mass-separated beams of U^+ , $UF_{1,2}^+$ with residual gas is observed in the ion trap. The effect of trapping time on molecular formation is presented.

1. Introduction

There is interdisciplinary interest in radioactive molecules bridging fields of molecular physics, atomic physics and nuclear physics, as well as physics beyond the standard model [1]. Experimental research possibilities with many radioactive molecules are currently constrained by their limited production. This is particularly the case for radioactive molecules containing an actinide element. Only actinides in the decay chains of primordial ^{232}Th and $^{235,238}\text{U}$ are available in macroscopic quantities in nature. All others must be produced artificially.

The Isotope Separation On-Line (ISOL) method allows production of a wide range of radioactive nuclides across the nuclear chart through reactions induced by the impact of an accelerated particle beam hitting a thick target. The ISOLDE facility at CERN [2] uses 1.4-GeV protons accelerated by CERN's Proton Synchrotron Booster (PSB) and can employ a variety of target and ion source systems. Once created, the reaction products must diffuse out of the target material and effuse to the ion source, where they are ionized and extracted as a beam of charged particles. For refractory species, forming volatile compounds has been employed as a technique to improve extraction from the target

* Corresponding author at: CERN, Geneva, Switzerland.

E-mail address: mia.au@cern.ch (M. Au).¹ Present address: University of Gothenburg, Sweden.² Present address: University of Jyväskylä, Finland.<https://doi.org/10.1016/j.nimb.2023.05.015>

Received 15 February 2023; Received in revised form 3 May 2023; Accepted 3 May 2023

0168-583X/© 2023 The Author(s). Published by Elsevier B.V. This is an open access article under the CC BY license (<http://creativecommons.org/licenses/by/4.0/>).

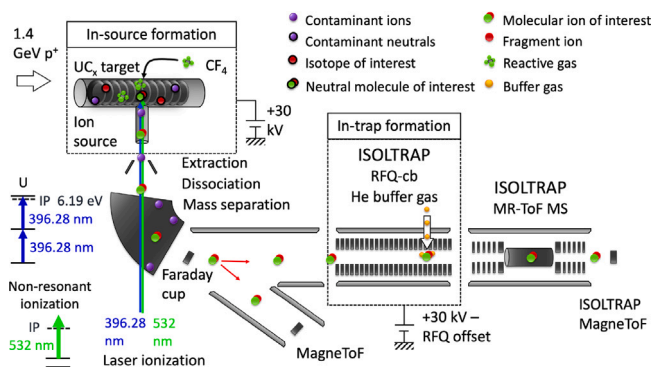


Fig. 1. Schematic of the experimental setup. Molecules are generated in the UC_x target or from the mass-separated ion beam in the ISOLTRAP RFQ-cb. The mass-separated beam is sent to a MagnetoF detector or bunched and sent to the MR-ToF MS for identification. The uranium resonant ionization scheme shown uses a single titanium:sapphire laser [14].

by delivering the isotopes of interest as molecular ion beams [3–6]. In specific cases, the formation of molecules can reduce the isobaric contamination remaining after mass separation. The production of actinide molecules could address the scarcity and purity problems limiting many experiments on actinide isotopes. In addition, they present promising cases themselves [1,7–9].

2. Method

The ISOLDE facility was used to study actinide species produced from four porous micro-structured uranium carbide (UC_x) target units: a previously-irradiated target coupled to a rhenium surface ion source; a previously-irradiated target coupled to a tungsten surface ion source; and two new targets coupled to Forced Electron Beam Induced Arc Discharge (FEBIAD) ion sources [10]. The ISOLDE Resonance Ionization Laser Ion Source (RILIS [11]) was used to resonantly ionize atomic U with the ionization scheme shown in Fig. 1. Ion beams were extracted from the ion source using a 30-kV potential difference and separated by their mass-to-charge ratio in the separator magnet. Mass-separated ion beams were either sent to a MagnetoF detector or cooled and bunched in the ISOLTRAP Radio-Frequency Quadrupole cooler-buncher (RFQ-cb) [12]. The bunched beam was sent to the Multi-Reflection Time-of-Flight Mass Spectrometer (MR-ToF MS) [13], where ions were separated based on their mass-to-charge ratios, including isobars, which were identified through ToF mass measurements. The experimental setup is shown schematically in Fig. 1.

3. In-source molecular formation

The target units with the tungsten surface ion source and the two FEBIAD type ion sources were equipped with calibrated leaks (1.3×10^{-4} , 3×10^{-4} and 5.7×10^{-5} mbar $L s^{-1}$) through which carbon tetrafluoride (carbon tetrafluoromethane, CF_4) gas was injected as a reagent for fluoride molecule formation. Using the two different types of ion sources, surface-, electron-impact-, and non-resonantly laser-ionized-molecules were observed. Nominal operating temperatures for a UC_x target and the different ion sources are near 2000 °C. Some measurements were performed with different experimental parameters where indicated such as in the captions of Figs. 2 and 3.

Uranium molecules from the target material and tantalum molecules from the target container were identified using mass scans performed with the ISOLDE mass separator magnets (Fig. 2) and verified using the ISOLTRAP MR-ToF MS. $^{235,238}U$ are present in the target as well as trace amounts of ^{234}U as a product of ^{238}U decay. These formed UO^+ and UO_2^+ with $^{16,18}O$ present from residual gas or oxide residues in the target. Depending on the degree of oxidation, the molecular oxide

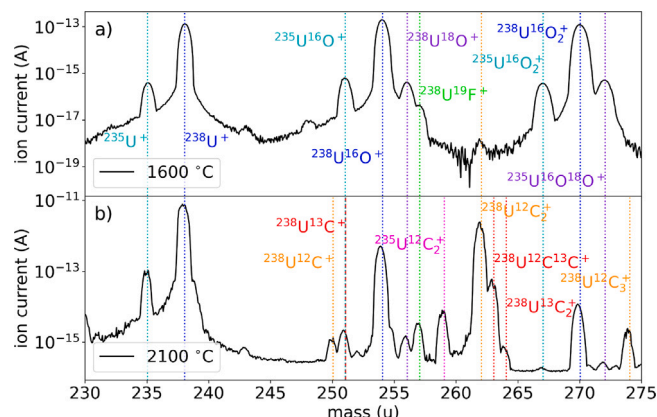


Fig. 2. Ion beam current recorded on the MagnetoF detector during a scan of the GPS mass separator magnet showing the surface-ionized molecules from a rhenium ion source coupled to a previously irradiated UC_x target at a target temperature of (a) 1600 °C and (b) 2100 °C. Note the logarithmic scale.

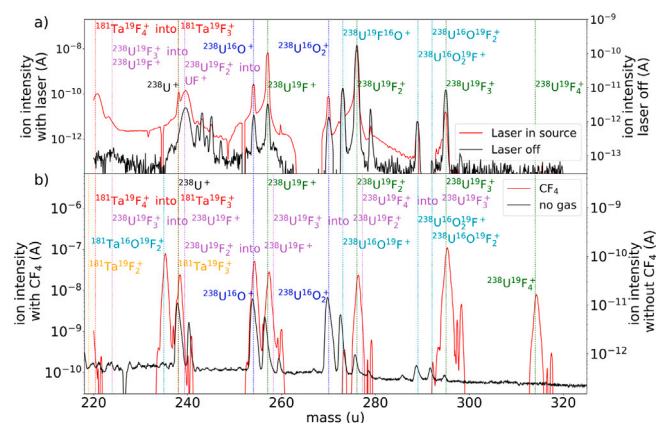


Fig. 3. Mass spectra of ion beams from UC_x targets using the GPS mass separator magnet. (a) a tungsten surface ion source with CF_4 gas injection through a calibrated leak for an ion source internal pressure of approximately 1.6×10^{-4} mbar without (black) and with 38 W of 532-nm laser light at a repetition rate of 10 kHz (red). Target at 1650 °C and ion source at 1370 °C. (b) a FEBIAD ion source before (black) and after injection of CF_4 through a calibrated leak for an ion source internal pressure of approximately 7.5×10^{-5} mbar (red). Target at 1200 °C and ion source at 1830 °C.

ion intensity decreased with time and target heating in the presence of excess carbon from the UC_x target. At higher temperatures, uranium carbides (UC^+ and UC_2^+) were observed, formed from both $^{12,13}C$ (Fig. 2). With the addition of CF_4 , $UF_{1,2,3}^+$ and UFO^+ dominated the total surface- or plasma-ionized beam. Details of experimental parameters are given in Fig. 3.

3.1. Non-resonant laser and plasma ionization

UO^+ and UO_2^+ dominate the ion beam for oxidized targets. With first ionization potentials of 6.0313(6) eV and 6.128(3) eV for UO and UO_2 , respectively [15], these species are observed with both surface and FEBIAD ion sources. With CF_4 injection, tungsten surface ionization, and 30 W of 532-nm laser light, UF^+ and UF_2^+ are the most intense uranium molecular ion beams. Surface-ionized UF_3^+ is detectable with a Faraday Cup; UF_4^+ is not observed (Fig. 3 (a)). Using a FEBIAD ion source, the UF_3^+ sideband is dominant and UF_4^+ is observed. Higher rates of U^+ likely result from the breakup of uranium molecules in the FEBIAD ion source before extraction as an ion beam. Sideband ratios depend strongly on the concentration of CF_4 , favoring $UF_{2,3}^+$ with higher leak rates of CF_4 . Bond dissociation energies of UO (7.856(135) eV),

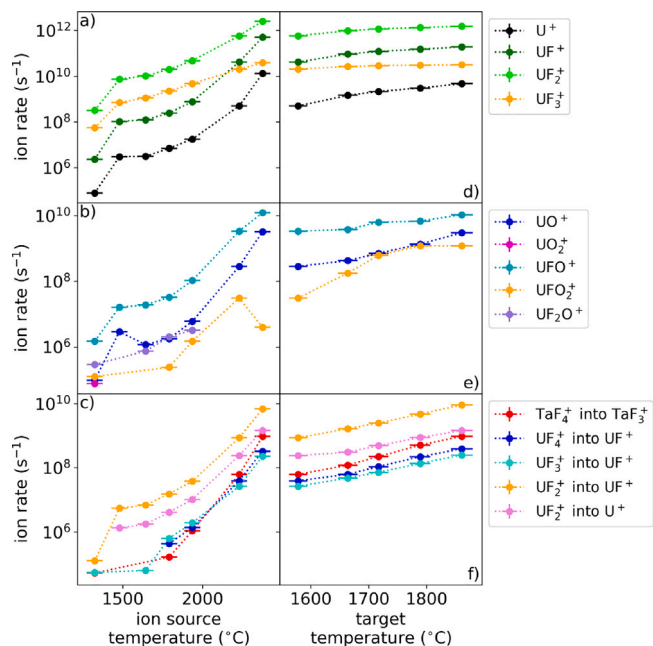


Fig. 4. Rates of ion beams from a tungsten surface ion source recorded on a Faraday Cup after mass separation from the ISOLDE separator magnets shown in logarithmic scale. (a), (b), (c): as a function of ion-source temperature for a target temperature of 1578 °C. (d) (e) (f): rates as a function of target temperature for an ion source temperature of 2230 °C. (c) and (f): rates of fragment ions measured on the apparent mass corresponding to the indicated dissociation of metastable molecular ions.

UO_2 (7.773(145) eV) [15] suggest that some dissociation of neutral and singly-charged oxides should occur within the FEBIAD ion source.

3.2. Metastable molecular ions

In mass spectrometry, the term ‘metastable’ is used to describe molecular ions possessing sufficient excess energy to fragment in the field-free region after leaving the ion source [16]. Upon fragmentation, the fragment ions retain a fraction of the kinetic energy of the extracted precursor ion. This causes fragment ions to pass through the mass separator magnetic field with an apparent mass m^* corresponding to [16]

$$m^* = \frac{m_f^2}{m_p} \quad (1)$$

where m_f represents the mass of the fragment ion and m_p represents the mass of the precursor metastable molecular ion. Fragment ions and their precursors were identified from the apparent mass and studied as a function of the target and surface ion source temperatures (Fig. 4). Increasing the ion source temperature significantly increased the fragment ion intensity, suggesting that at high temperatures, the molecules are more likely to have sufficient excess energy to reach the metastable states that fragment after extraction. Fragment molecules are indicated where observed in Fig. 3. Rates of U^+ , $\text{UF}_{1,2,3}^+$ and UF_xO_y^+ also increase with ion source temperature as surface ionization efficiency increases. This increase could also partially result from increased molecular fragmentation into ionic species occurring in the ion source.

4. In-trap molecular formation

To study in-trap molecular formation, the ISOLTRAP RFQ-cb was employed with a buffer gas (here He at up to 10^{-5} mbar measured within 1 m of the injection) to cool and bunch the ions. Mass-separated beams ionized using each of the studied ion sources were sent to the RFQ-cb for cooling and bunching. For studies of beam composition and in-trap molecular formation, a sample of the continuous ion beam was

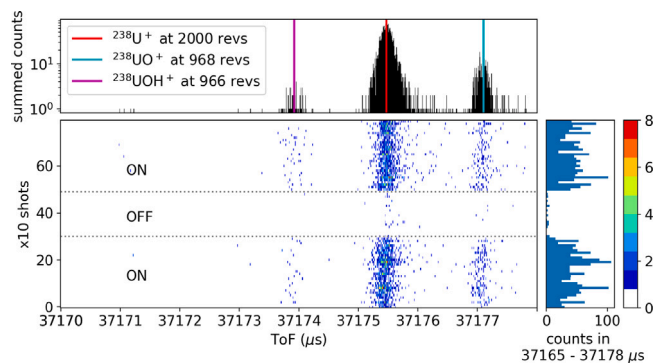


Fig. 5. ToF spectrum of $A = 238$ mass-separated ion beams after cooling and bunching in the ISOLTRAP RFQ-cb, then trapping for 2000 revolutions in the MR-ToF MS as calculated for ^{238}U . The status of the U resonant laser (on or off) is indicated. Vertical lines shown in the top panel indicate ToFs expected from offline calibrations. See text for further details.

taken into the RFQ-cb. Ions were confined in the RFQ-cb for a trapping time during which interaction occurred between the ions, the buffer gas and residual gas contamination. The ion bunch was then ejected from the RFQ-cb and the arrival times of ions in each shot were measured with respect to the ejection time. Identification was performed with the MR-ToF MS using expected ToF values extracted from a calibration using $^{85,87}\text{Rb}^+$, $^{133}\text{Cs}^+$ from the ISOLTRAP offline ion source [17], and online $^{238}\text{U}^+$ from ISOLDE. ToF spectra were accumulated over a number of shots as seen in Figs. 5, 6, and 7.

The atomic uranium resonant laser ionization scheme in the ion source affected the count rates of uranium molecules (e.g. UO^+ and UOH^+ in Fig. 5) observed from the RFQ-cb ion trap. Combined with the mass-separation step of the separator magnets, this indicates that the molecules are formed from ions in the mass-separated U^+ beam rather than in the target or ion source. For U and Ta, ratios depend on the trapping time as shown in Figs. 6 and 7. In addition to atomic ions forming molecules, molecular ions mass-separated by ISOLDE (including UF^+ , UF_2^+ , TaF^+ , TaF_2^+) reacted with the residual gas or buffer-gas contaminants to form molecules by pickup of C, O, H and OH (Figs. 7,8) and in some cases (UF^+ , UF_2^+) were observed with higher charge states (UF^{2+} , UF_2^{2+}). To avoid detector saturation, attenuators were used to reduce the intensity of the ion beam injected into the RFQ-cb. This reduced absolute rates of in-trap formation and the formation efficiency relative to the ion beam intensity extracted from the ion source. Rates of molecular formation in the ion-trap represent ratios in the regime below space-charge limitations.

Notably, the in-trap UO_x formation showed an identical response to the storage time in the RFQ-cb before and after the addition of a liquid nitrogen cold trap to the buffer gas line, indicating that reaction products enter the ion trap through diffusion into the vacuum chamber rather than buffer gas injection.

5. Conclusions

For previously irradiated or oxidized targets, UO^+ and UO_2^+ sidebands are on the order of 10^5 ions s^{-1} at target temperatures above 1600 °C. Without further addition of oxygen, the intensity of these contaminants will decrease over time, with the UO_2^+ sideband depleting first, followed by the UO^+ sideband. At nominal target temperatures (2000 °C) and above, UC^+ , UC_2^+ can similarly reach rates of 10^4 ions s^{-1} or more. Fragments formed from the dissociation of metastable U and Ta fluorides arrive as additional non-isobaric contaminants in mass-separated beams. Fragment ions and their precursor ions can be identified using their apparent mass (Eq. (1)) and anticipated for a given mass-to-charge ratio with the rates presented here. We present some representative rates of molecular ions extracted from different ion

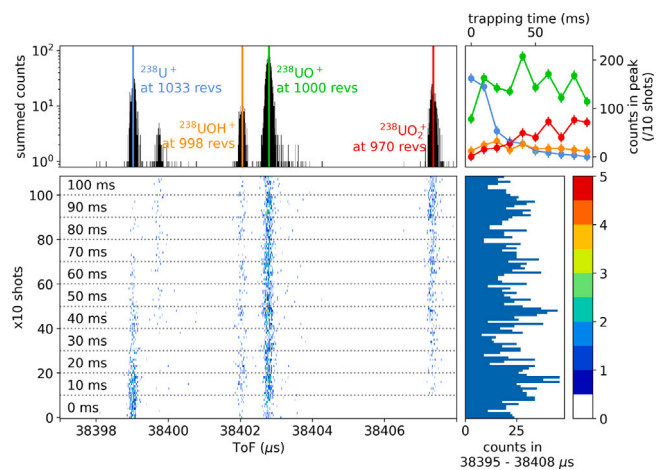


Fig. 6. ToF spectra for various storage times (indicated on the left) of A = 238 mass-separated ion beams from the tungsten surface ion source with RILIS for U after cooling and bunching in the ISOLTRAP RFQ-cb, then trapping for 2000 revolutions in the MR-ToF MS as calculated for $^{238}\text{UO}^+$. Summed counts in each of the identified peaks are shown as a function of trapping time. See text for further details.

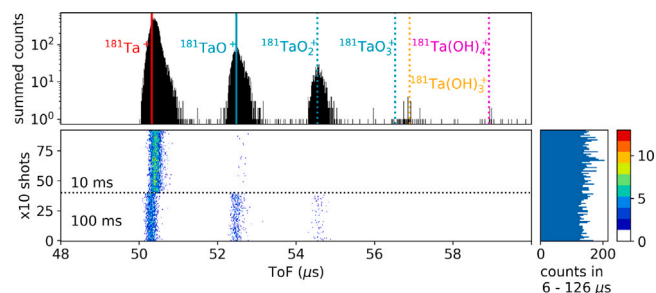


Fig. 7. ToF spectrum of A = 181 mass-separated ion beams from the FEBIAD ion source after bunching in the ISOLTRAP RFQ-cb. Cooling time is indicated. Vertical lines in the top panel show ToFs expected from the offline calibration for single-pass operation of the MR-ToF MS.

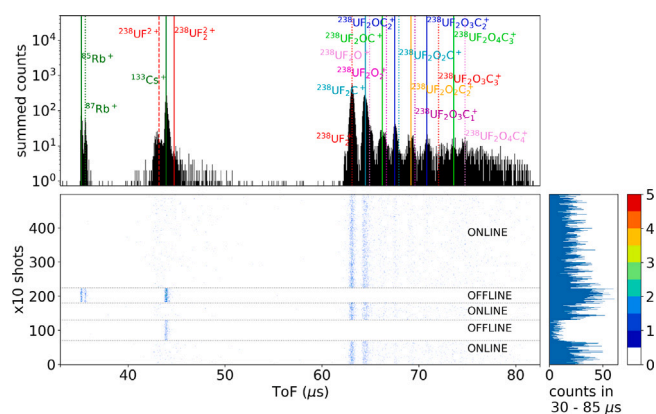


Fig. 8. ToF spectra of A = 276 mass-separated ion beams from a W surface source with CF_4 injection in single-pass operation of the MR-ToF MS with trapping time 200 ms. Horizontal lines show switching between offline reference beam ($^{85,87}\text{Rb}^+$, $^{133}\text{Cs}^+$). Vertical lines show identified non-isobaric actinide molecules from molecular formation and charge exchange in the ISOLTRAP RFQ-cb.

sources with oxidation, CF_4 , and target temperatures noted in Fig. 4 and Table 1 as well as some representative rates for formation of molecular ions in the RFQ-cb with trapping times noted in Table 2. Rates from the ion source depend very strongly on target and ion source temperature and CF_4 injection rate. Rates from the RFQ-cb depend on trapping time.

Table 1

Some observed rates of uranium ion beams from a rhenium surface source and from an electron impact ion source with injected CF_4 , recorded on a Faraday cup after mass separation from the ISOLDE mass separator magnet.

Ion source	Target temperature (°C)	Species	Rate (ions s ⁻¹)
Re surface previously irradiated	1600	$^{238}\text{U}^+$	$2.5(1) \times 10^3$
	1600	$^{238}\text{U}^+$	$8.9(6) \times 10^5$
	1600	$^{238}\text{U}^{16}\text{O}^+$	$4.0(6) \times 10^3$
	1600	$^{238}\text{U}^{16}\text{O}^+$	$1.4(2) \times 10^6$
	1600	$^{238}\text{U}^{18}\text{O}^+$	$2.5(9) \times 10^3$
	1600	$^{238}\text{U}^{16}\text{O}_2^+$	$2.4(1) \times 10^3$
	1600	$^{238}\text{U}^{16}\text{O}_2^+$	$7.9(5) \times 10^5$
Re surface previously irradiated	1600	$^{238}\text{U}^{16}\text{O}^{18}\text{O}^+$	$3.5(5) \times 10^3$
	2100	$^{235}\text{U}^+$	$6.3(1) \times 10^5$
	2100	$^{238}\text{U}^+$	$5(1) \times 10^7$
	2100	$^{235}\text{U}^{12}\text{C}^+$	$7(1) \times 10^3$
	2100	$^{238}\text{U}^{16}\text{O}^+$	$1.24(6) \times 10^4$
	2100	$^{238}\text{U}^{16}\text{O}^+$	$3.3(2) \times 10^6$
	2100	$^{238}\text{U}^{18}\text{O}^+$	$8(1) \times 10^3$
FEBIAD with CF_4	1818	$^{235}\text{U}^{12}\text{C}_2^+$	$4.5(7) \times 10^4$
	2100	$^{238}\text{U}^{12}\text{C}_2^+$	$1.3(2) \times 10^7$
	2100	$^{238}\text{U}^{12}\text{C}^{13}\text{C}_2^+$	$3(2) \times 10^5$
	2100	$^{238}\text{U}^{16}\text{O}_2^+$	$7.3(3) \times 10^4$
	2100	$^{238}\text{U}^{16}\text{O}^{18}\text{O}^+$	$7.4(8) \times 10^2$
	2100	$^{238}\text{U}^{12}\text{C}_3^+$	$1.3(4) \times 10^4$
	1818	$^{238}\text{U}^{16}\text{O}_2^+$	$2.8(5) \times 10^7$
	1818	$^{238}\text{U}^{16}\text{F}_2^+$	$6(1) \times 10^8$
	1818	$^{238}\text{U}^+$	$1.5(1) \times 10^{11}$
	1818	$^{238}\text{U}^{16}\text{O}^+$	$3.2(2) \times 10^{11}$
	1818	$^{238}\text{U}^{19}\text{F}^+$	$1.7(1) \times 10^{11}$
	1818	$^{238}\text{U}^{19}\text{F}^{16}\text{O}^+$	$1.3(1) \times 10^{10}$
	1818	$^{238}\text{U}^{19}\text{F}_2^+$	$1.4(1) \times 10^{11}$
1818	$^{238}\text{U}^{19}\text{F}^{16}\text{O}_2^+$	$3.0(7) \times 10^7$	
1818	$^{238}\text{U}^{19}\text{F}^{16}\text{O}^+$	$3.5(5) \times 10^9$	
1818	$^{238}\text{U}^{19}\text{F}_3^+$	$6.8(5) \times 10^{11}$	
1818	$^{238}\text{U}^{19}\text{F}_4^+$	$4.9(4) \times 10^{10}$	

Table 2

Observed rates of ions formed inside the RFQ-cb from initial mass-separated ion beams extracted from a tungsten surface ion source. Counts per seconds of initial beam sampling time were recorded on the ISOLTRAP MagneToF detector after mass separation in the MR-ToF MS. See text for more details.

Trapping time (ms)	Initial ion beam	Species	Rate (ions s ⁻¹ of injection time)
5	$^{234}\text{U}^+$	$^{234}\text{U}^+$	$8.0(8) \times 10^{-2}$
5	$^{234}\text{U}^+$	$^{234}\text{UO}_2\text{H}^+$	$9(1) \times 10^{-2}$
5	$^{235}\text{U}^+$	$^{235}\text{U}^+$	$1.64(5) \times 10^0$
5	$^{235}\text{U}^+$	$^{235}\text{UO}_2^+$	$5(1) \times 10^{-2}$
5	$^{238}\text{U}^+$	$^{238}\text{U}^+$	$4.40(7) \times 10^4$
5	$^{238}\text{U}^+$	$^{238}\text{UO}^+$	$5.6(2) \times 10^2$
5	$^{238}\text{U}^+$	$^{238}\text{UOH}^+$	$1.5(1) \times 10^2$
5	$^{235}\text{UF}^+$	$^{235}\text{UF}^+$	$1.39(3) \times 10^4$
5	$^{235}\text{UF}^+$	$^{235}\text{UFO}^+$	$3.6(3) \times 10^3$
5	$^{235}\text{UF}^+$	$^{235}\text{UFOH}^+$	$7(1) \times 10^1$
100	$^{235}\text{UF}^+$	$^{235}\text{UFO}^+$	$1.16(6) \times 10^4$
100	$^{235}\text{UF}^+$	$^{235}\text{UFOH}^+$	$5.2(9) \times 10^2$
100	$^{238}\text{UF}^+$	$^{238}\text{UF}^+$	$1.39(8) \times 10^5$
100	$^{238}\text{UF}_2^+$	$^{238}\text{UF}_2^+$	$1.69(3) \times 10^4$
100	$^{238}\text{UF}_2^+$	$^{238}\text{UF}_2\text{O}^+$	$7(1) \times 10^1$
100	$^{238}\text{UF}_2^+$	$^{238}\text{UFO}_2\text{H}^+$	$1.6(6) \times 10^1$
200	$^{238}\text{UF}_2^+$	$^{238}\text{UF}_2^+$	$1.17(2) \times 10^4$
200	$^{238}\text{UF}_2^+$	$^{238}\text{UF}_2\text{O}^+$	$3.4(3) \times 10^2$
200	$^{238}\text{UF}_2^+$	$^{238}\text{UFO}_2\text{H}^+$	$9.2(1.4) \times 10^1$
200	$^{238}\text{UF}_2^+$	$^{238}\text{UF}_2^{2+}$	$8.2(9) \times 10^1$
200	$^{238}\text{UF}_2^+$	$^{238}\text{UF}_2^{2+}$	$2.9(5) \times 10^1$

Production of fluoride molecular ions from the ion source is achieved by adding CF_4 . Since many actinide fluorides are stable at temperatures above 1000 °C, in-source formation is a promising approach that can use parameters including target and ion source temperatures and fluorine partial pressure to control formation rates.

To form molecules that may not be stable at high temperatures, molecular formation in the RFQ ion trap is presented as a possible approach. Formation of oxides, carbides, and hydroxides from the mass-separated atomic and molecular ion beams occurs in the ISOLTRAP RFQ-cb in the presence of residual gases. Trapping time is shown to be a parameter influencing the formation of molecules in the ion trap. The molecular formation reported here in the ISOLTRAP RFQ-cb may have implications for other RFQ-cb ion traps used in beam preparation (e.g. the ISOLDE cooler ISCOOL [2]) which require further investigations.

These studies combined characterize the composition of beams heavier than the target material and provide information on the process of creating molecular actinide beams in targets and in ion traps.

Declaration of competing interest

The authors declare that they have no known competing financial interests or personal relationships that could have appeared to influence the work reported in this paper.

Acknowledgments

The authors gratefully acknowledge support from the ISOLDE operations team, the ISOLDE targets and ion sources team, and Simone Gilardoni. This project has received funding from the European Union's Horizon 2020 Research and Innovation Program (grant No. 861198 project 'LISA' MSC ITN). The authors acknowledge support from the German Federal Ministry of Education and Research (BMBF) for ISOLTRAP (grant No. 05P18HGCI A and 05P21HGCI I). L.N. acknowledges support from the Wolfgang Gentner Program (grant No. 13E18CHA).

References

- [1] G. Arrowsmith-Kron, M. Athanasakis-Kaklamanakis, M. Au, J. Ballof, R. Berger, A. Borschevsky, A.A. Breier, F. Buchinger, D. Budker, L. Caldwell, C. Charles, N. Dattani, R.P. de Groote, D. DeMille, T. Dickel, J. Dobaczewski, C.E. Düllmann, E. Eliav, J. Engel, M. Fan, V. Flambaum, K.T. Flanagan, A. Gaiser, R.G. Ruiz, K. Gaul, T.F. Giesen, J. Ginges, A. Gottberg, G. Gwinner, R. Heinke, S. Hoekstra, J.D. Holt, N.R. Hutzler, A. Jayich, J. Kartheim, K.G. Leach, K. Madison, S. Malbrunot-Ettenauer, T. Miyagi, I.D. Moore, S. Moroch, P. Navrátil, W. Nazarewicz, G. Neyens, E. Norrgard, N. Nussgart, L.F. Pašteka, A.N. Petrov, W. Plass, R.A. Ready, M.P. Reiter, M. Reponen, S. Rothe, M. Safronova, C. Scheidenberger, A. Shindler, J.T. Singh, L.V. Skripnikov, A.V. Titov, S.-M. Udrescu, S.G. Wilkins, X. Yang, Opportunities for fundamental physics research with radioactive molecules, 2023, <http://dx.doi.org/10.48550/ARXIV.2302.02165>, arXiv, URL <https://arxiv.org/abs/2302.02165>.
- [2] R. Catherall, W. Andreatza, M. Breitenfeldt, A. Dorsival, G.J. Focker, T.P. Gharsa, T.J. Giles, J.L. Grenard, F. Locci, P. Martins, S. Marzari, J. Schipper, A. Shornikov, T. Stora, The ISOLDE facility, *J. Phys. G: Nucl. Part. Phys.* 44 (9) (2017) <http://dx.doi.org/10.1088/1361-6471/aa7eba>.
- [3] J. Ballof, C. Seiffert, B. Crepieux, C.E. Düllmann, M. Delonca, M. Gai, A. Gottberg, T. Kröll, R. Lica, M. Madurga Flores, Y. Martinez Palenzuela, T.M. Mendonca, M. Owen, J.P. Ramos, S. Rothe, T. Stora, O. Tengblad, F. Wienholtz, Radioactive boron beams produced by isotope online mass separation at CERN-ISOLDE, *Eur. Phys. J. A* 55 (5) (2019) <http://dx.doi.org/10.1140/epja/i2019-12719-1>.
- [4] U. Köster, O. Arndt, E. Bouquerel, V.N. Fedoseyev, H. Fränberg, A. Joinet, C. Jost, I.S. Kerkines, R. Kirchner, Progress in ISOL target-ion source systems, *Nucl. Instrum. Methods Phys. Res. B* 266 (19–20) (2008) 4229–4239, <http://dx.doi.org/10.1016/J.NIMB.2008.05.152>.
- [5] U. Köster, P. Carbonez, A. Dorsival, J. Dvorak, R. Eichler, S. Fernandes, H. Fränberg, J. Neuhausen, Z. Novackova, R. Wilfinger, A. Yakushev, (IM-)possible ISOL beams, *Eur. Phys. J.: Special Topics* 150 (2007) 285–291, <http://dx.doi.org/10.1140/epjst/e2007-00326-1>.
- [6] R. Eder, H. Grawe, E. Hagebø, P. Hoff, E. Kugler, H.L. Ravn, K. Steffensen, The production yields of radioactive ion-beams from fluorinated targets at the ISOLDE on-line mass separator, *Nuclear Inst. Methods Phys. Res. B* 62 (4) (1992) 535–540, [http://dx.doi.org/10.1016/0168-583X\(92\)95387-7](http://dx.doi.org/10.1016/0168-583X(92)95387-7).
- [7] L.V. Skripnikov, N.S. Mosyagin, A.V. Titov, V.V. Flambaum, Actinide and lanthanide molecules to search for strong CP-violation, *Phys. Chem. Chem. Phys.* 22 (33) (2020) 18374–18380, <http://dx.doi.org/10.1039/d0cp01989e>, arXiv: 2003.10885.
- [8] M.S. Safronova, D. Budker, D. Demille, D.F. Kimball, A. Derevianko, C.W. Clark, Search for new physics with atoms and molecules, *Rev. Modern Phys.* 90 (2) (2018) <http://dx.doi.org/10.1103/RevModPhys.90.025008>, arXiv:1710.01833.
- [9] T.A. Isaev, S. Hoekstra, R. Berger, Laser-cooled RaF as a promising candidate to measure molecular parity violation, *Phys. Rev. A* 82 (2010) 052521, <http://dx.doi.org/10.1103/PhysRevA.82.052521>, URL <https://link.aps.org/doi/10.1103/PhysRevA.82.052521>.
- [10] L. Penescu, R. Catherall, J. Lettry, T. Stora, Development of high efficiency Versatile Arc Discharge Ion Source at CERN ISOLDE, *Rev. Sci. Instrum.* 81 (2) (2010) 1–5, <http://dx.doi.org/10.1063/1.3271245>.
- [11] V. Fedosseev, K. Chrysalidis, T.D. Goodacre, B. Marsh, S. Rothe, C. Seiffert, K. Wendt, Ion beam production and study of radioactive isotopes with the laser ion source at ISOLDE, *J. Phys. G: Nucl. Part. Phys.* 44 (8) (2017) <http://dx.doi.org/10.1088/1361-6471/aa78e0>.
- [12] F. Herfurth, J. Dilling, A. Kellerbauer, G. Bollen, S. Henry, H.-J. Kluge, E. Lamour, D. Lunney, R. Moore, C. Scheidenberger, S. Schwarz, G. Sikler, J. Szerypo, A linear radiofrequency ion trap for accumulation, bunching, and emittance improvement of radioactive ion beams, *Nucl. Instrum. Methods Phys. Res. A* 469 (2) (2001) 254–275, [http://dx.doi.org/10.1016/S0168-9002\(01\)00168-1](http://dx.doi.org/10.1016/S0168-9002(01)00168-1), URL <https://www.sciencedirect.com/science/article/pii/S0168900201001681>.
- [13] R.N. Wolf, F. Wienholtz, D. Atanasov, D. Beck, K. Blaum, C. Borgmann, F. Herfurth, M. Kowalska, S. Kreim, Y.A. Litvinov, D. Lunney, V. Manea, D. Neidherr, M. Rosenbusch, L. Schweikhard, J. Stanja, K. Zuber, ISOLTRAP's multi-reflection time-of-flight mass separator/spectrometer, *Int. J. Mass Spectrom.* 349–350 (1) (2013) 123–133, <http://dx.doi.org/10.1016/j.ijms.2013.03.020>.
- [14] M.R. Savina, B.H. Isselhardt, R. Trappitsch, Simultaneous isotopic analysis of U, Pu, and Am in spent nuclear fuel by resonance ionization mass spectrometry, *Anal. Chem.* 93 (27) (2021) 9505–9512, <http://dx.doi.org/10.1021/acs.analchem.1c01360>.
- [15] L.R. Morss, N. Edelstein, J. Fuger, J.J. Katz, *Chemistry of Actinide and Transactinide Elements, fourth ed.*, Springer, 2010.
- [16] R.A.W. Johnstone, M.E. Rose, *Mass Spectrometry for Chemists and Biochemists*, Cambridge University Press, 2012, pp. 232–288, <http://dx.doi.org/10.1017/cbo9781139166522.009>.
- [17] F. Wienholtz, D. Beck, K. Blaum, C. Borgmann, M. Breitenfeldt, R.B. Cakirli, S. George, F. Herfurth, J.D. Holt, M. Kowalska, S. Kreim, D. Lunney, V. Manea, J. Menéndez, D. Neidherr, M. Rosenbusch, L. Schweikhard, A. Schwenk, J. Simonis, J. Stanja, R.N. Wolf, K. Zuber, Masses of exotic calcium isotopes pin down nuclear forces, *Nature* 498 (7454) (2013) 346–349, <http://dx.doi.org/10.1038/nature12226>.

5.2 Publication in preparation: Actinium fluorides

In Section 4, the manifold reasons for the interest in actinium nuclides (such as studies of nuclear charge radii, octupole deformation and the use of ^{225}Ac for targeted- α therapy) were discussed in the context of producing actinium as an atomic ion. The worldwide production of actinium (particularly ^{225}Ac) is extremely limited, further motivating any developments for increasing production capabilities of existing infrastructure. While molecules are interesting for production and extraction purposes, specific molecules containing actinium (e.g. the diatomic molecule AcF) are of particular interest as promising candidates to search for P, T -violating symmetries. Computational studies indicate that AcF has a large sensitivity to the nuclear Schiff moment of the Ac nucleus [82], which is remarkably large for the nuclides ^{227}Ac and ^{225}Ac . To proceed in the campaign to measure a Schiff moment, characterization of the molecular structure and development of a resonance laser excitation scheme are required. This work focuses on two objectives: using actinium fluoride molecules to aid extraction of actinium nuclides through molecular sideband extraction, and deliberately producing the AcF molecule to deliver ion beams of AcF^+ for the laser spectroscopy experiment proposed in Ref. [160].

In preparation for the experimental campaign on laser spectroscopy of AcF , relativistic coupled-cluster calculations were completed for the ionization potential, dissociation energy, and excited low-lying electronic states below $35\,000\text{ cm}^{-1}$, resulting in a calculated first ionization potential of $48\,866\text{ cm}^{-1}$ ($\approx 6.06\text{ eV}$) and a calculated dissociation energy of $57\,214\text{ cm}^{-1}$ for the channel AcF into Ac [161]. The calculations presented in Ref. [161] suggest that a surface ion source would be capable of ionizing neutral AcF , albeit with rather low efficiency, and that the diatomic molecule would favor ionization over dissociation into Ac (or Ac^+ , which was calculated to be $15\,962\text{ cm}^{-1}$ higher). Since actinium can appear in the oxidation state $3+$, it is highly possible that the actinium effuses through a fluorinated target in a difluoride or trifluoride molecule. The first ionization potentials and dissociation energies of AcF_2 and AcF_3 were not known or calculated at the time of this work. The FEBIAD-type ion source was therefore used in this work for three reasons: to efficiently ionize AcF , to dissociate $\text{AcF}_{2,3}$ into AcF^+ , and to efficiently ionize AcF_2 (and potentially AcF_3) for comparison of the distribution across molecular sidebands.

Actinium was successfully extracted as a molecular ion beam using the injection of CF_4 gas to UC_x and ThC_x targets as described in Section 2.4.

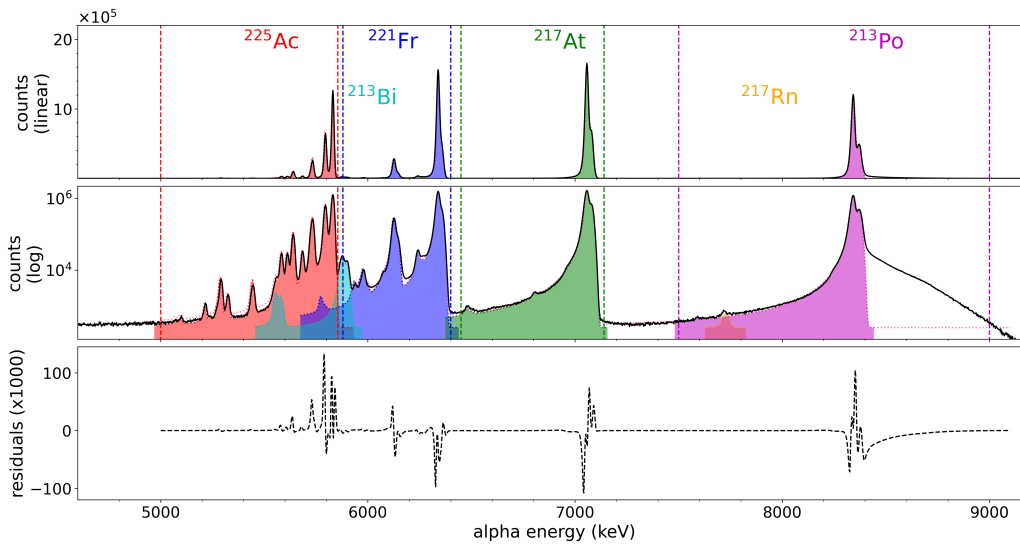


Figure 5.1: α -decay spectrum of an ion-implanted sample collected on mass 263 ($^{225}\text{Ac}^{19}\text{F}_2^+$), measured for 21.75 days throughout a 74 day-long measurement campaign. The characteristic α -decays of ^{225}Ac , and its decay products ^{221}Fr , ^{217}At , ^{217}Rn , ^{213}Po and ^{213}Bi are described by a sum model of Crystal Ball functions [162] and shown in shaded colours (red, dark blue, green, orange, pink, and light blue, respectively). Dashed lines show regions used for counting. Residuals between the model spectrum and the data are shown in the bottom panel.

Actinium was observed on atomic, monofluoride, and difluoride sidebands and identified using ion implantations and α -decay spectroscopy to observe characteristic α -decay energies and branching ratios (see Fig. 5.1). Additional confirmation was completed using the MR-ToF MS for identification by ToF mass measurements. Yields were measured using samples of the ion beam implanted onto foils and studied using α -spectroscopy as well as online γ -decay spectroscopy at the ISOLDE FTS (described in Section 2.3).

A sample of ion beam collected on the mass of $^{225}\text{AcF}_2^+$ shows a measured α -decay spectrum for ^{225}Ac and its decay products, signifying the production of the difluoride molecular ion. The ranges used for counting α -decays of each species are indicated with dashed lines. The observed spectrum is described by an analytical function for peaks in α -particle spectra from Si detectors presented by the Crystal Ball collaboration [162]. Satellite peak structures from the implantation of recoil nuclei in the detector are observed for the daughter nuclei, resulting in a second peak structure for ^{221}Fr , ^{217}At , ^{213}Po and ^{213}Bi shifted to higher energies by the energy of the recoiling nucleus [163]. The high-energy tailing observed on the ^{213}Po peak is due to energy summing of α -particles and electrons emitted within the dead time of the detector due to the short half life of ^{213}Po . This effect was not accounted for in the model. Recoil nuclei in a decay chain have an additional factor in geometrical efficiency resulting from implantation in the walls of the measurement chamber. The measured α -energies and heights correspond well to the branching ratios available in literature ([164, 165, 166, 167]). The spectrum matches with a total of 45 peaks and resolves α -decays with branching ratios as low as 0.003%, unambiguously confirming the presence of ^{225}Ac on the mass of $^{225}\text{Ac}^{19}\text{F}_2^+$ and completing the identification by α -decay spectroscopy.

The presence of $^{225}\text{Ac}^{19}\text{F}_2^+$, confirmed by α -decay spectroscopy, does not give information about contaminants without an emitted α -particle. Confirmation by ToF mass measurements using the ISOLTRAP MR-ToF MS adds additional confidence towards the identification and quantification of the actinium fluorides, e.g. $^{225}\text{AcF}_2^+$ in Fig. 5.2, as well as information about ion beam purity. As seen in Fig. 5.2, the ToF spectrum confirms the presence of $^{225}\text{AcF}_2^+$ and shows no other notable components in the ion beam that may have been overlooked using only α -decay spectroscopy. Due to the high mass resolving power required to separate $^{225}\text{AcF}_2^+$ from $^{225}\text{RaF}_2^+$, the presence of $^{225}\text{RaF}_2^+$ cannot fully be ruled out using ToF mass measurements alone.

Ratios of the molecular sidebands were assessed using the neighboring isotope ^{226}Ac for two reasons: firstly, due to the high mass resolving power required to separate ^{225}Ac from ^{225}Ra ($R = 589217.3$), ratios on the mass $A = 225$ could not be obtained from a ToF spectrum (Fig. 5.2), while separating ^{226}Ac from ^{226}Ra was challenging but possible ($R = 328137.8$) as

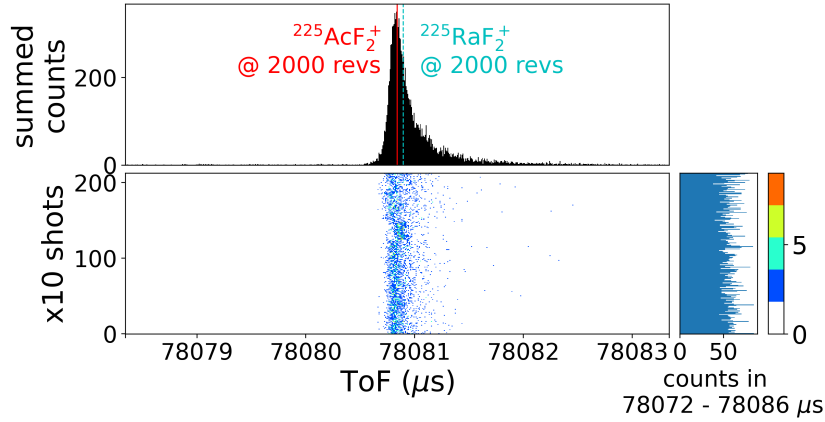


Figure 5.2: ToF spectrum of the mass-separated beam of $^{225}\text{Ac}^{19}\text{F}_2^+$ after 2000 revolutions in the MR-ToF MS. Expected ToF from the calibration is indicated for $^{225}\text{AcF}_2^+$ and $^{225}\text{RaF}_2^+$ with a vertical line (red and light blue respectively) and agrees well with the observed ToF distribution.

shown in Fig. 5.3. Secondly, ^{225}Ra does not reach secular equilibrium with the decay product ^{225}Ac within the duration of the experiment, causing the ratios of actinium and radium to change on the time scale of the measurement. On mass 226, the long half-life of ^{226}Ra prevents the ratio of Ra to Ac from changing. Therefore, ion beams of $^{226}\text{Ac}^+$, $^{226}\text{AcF}^+$, and $^{226}\text{AcF}_2^+$ were used to evaluate the ratio of actinium nuclides present on each mass. The expected in-target production cross-sections are comparable; the ratio of ^{225}Ac to ^{225}Ra is 8, while the ratio of ^{226}Ac to ^{226}Ra is 6.3 based on FLUKA calculations [44, 168, 169]. Molecular formation is expected to depend on electronic configuration. For isotopes of the same element, the effect of different neutron numbers on the electronic configuration (the isotope shift) is expected to have a small influence on the ratio of observed molecules compared to the effects of fragmentation from the hot cathode FEBIAD-type ion source. Table 5.1 shows the purity and ion beam compositions, with the corresponding time-of-flight spectra shown in Fig. 5.3. On the mono-fluoride sideband, actinium and radium monofluoride were both observed. On the difluoride sideband, actinium was identified. Though actinium is known to take oxidation states up to 3, AcF_3^+ was not observed.

With identification completed by the combination of α -decay spectroscopy and by ToF mass measurements, the yield was calculated as a rate per number of protons incident on the target by measuring the number of actinium nuclides collected during a collection time corresponding to a number of pro-

Table 5.1: Ion beam purity of ^{226}Ac measured using ToF mass measurements (Fig. 5.3) to separate isobaric contaminants on the atomic, mono-, and di-fluoride ion beam. Fr (indicated in brackets) was not conclusively confirmed but may be present on the atomic mass in low quantities.

Mass A	Sideband	Purity (%)	Contaminant(s)
226	$^{226}\text{Ac}^+$	44.9(5)	$^{226}\text{Ra}^+$ ($^{226}\text{Fr}^+$)
245	$^{226}\text{AcF}^+$	36.3(5)	$^{226}\text{RaF}^+$
264	$^{226}\text{AcF}_2^+$	100	-

tons incident on the target. The Bateman equations:

$$N_n(t) = N_0(0) \times \left(\prod_{i=0}^{n-1} \lambda_i \right) \times \sum_{i=0}^n \frac{e^{-\lambda_i t}}{\prod_{j=0, j \neq i}^n (\lambda_j - \lambda_i)} \quad (5.1)$$

where $n = 0, 1, 2, 3$ are used to describe the activities using known half-lives of the four nuclei in the decay chain. N_i is the number of atoms and λ_i is the decay constant $\ln 2/t_{1/2}$ with $i = 0, 1, 2, 3$ indicating ^{225}Ac , ^{221}Fr , ^{217}At , and ^{213}Po , respectively. Multiple measurements of the same sample were conducted over time as shown in Fig. 5.4. Initial amounts of the daughter nuclei caused by decay of ^{225}Ac during the 288 s collection are negligible with respect to the 9.92-day half-life of ^{225}Ac . The measured specific activity of each isotope was fitted using the corresponding Bateman equation with the initial quantity of the ^{225}Ac parent as the single free parameter to calculate the number of nuclei present on the foil at the end of the collection. All recoil products follow the expected exponential decay for the decay chain as seen in Fig. 5.4, where the ingrowth of the daughter nuclei is observed when the sample is placed in front of the detector. The observed offset in the detected counts is caused by the slightly higher geometrical efficiency for the recoil nuclei, evaluated to be 0.5%, 0.6%, and 0.4% for the first, second, and third decay product, respectively, in addition to the 1.65(3) % detection efficiency from the sample position (discussed previously in section 2.3). Using the primary decay of ^{225}Ac and correcting the calculated number of nuclei per μC of proton beam incident on the target during the collection gives yields of ^{225}Ac per intensity of primary proton shown in Table 5.2 for a UC_x target with a FEBIAD-type ion source and a calibrated leak with a rate of $5.7 \times 10^{-5} \text{ mbar L s}^{-1}$. Three gas compositions were tested for the formation of actinium fluorides: 10% CF_4 with 90% Ar, 20% CF_4 with 80% Ar, 40% CF_4 with 60% Ar, with a fill pressure of 500 mbar on the calibrated leak.

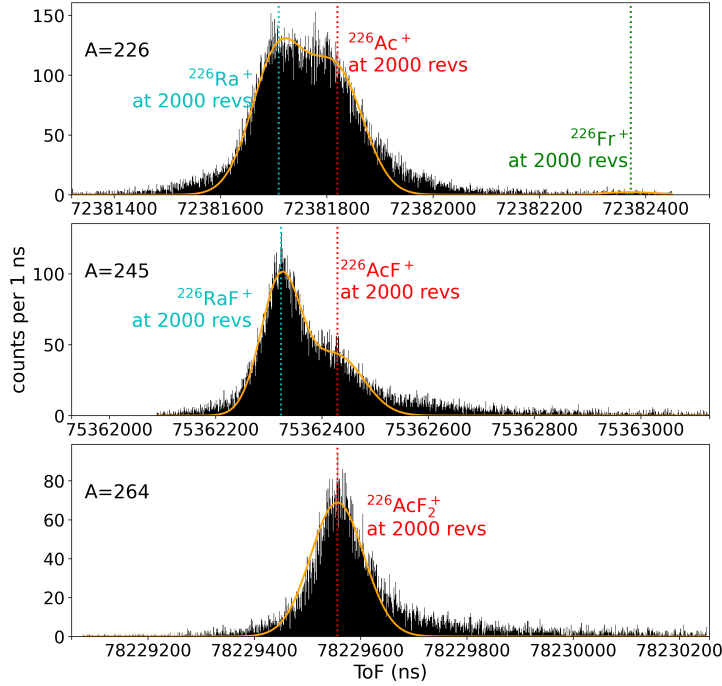


Figure 5.3: ToF spectra of mass-separated beams with nominal masses $^{226}\text{Ac}^+$, $^{226}\text{Ac}^{19}\text{F}^+$, and $^{226}\text{Ac}^{19}\text{F}_2^+$ at 2000 revolutions in the MR-ToF MS. Expected ToFs from the calibration are indicated with vertical lines. A fit of Gaussian peaks corresponding to each species is shown as a solid orange line.

The target material was heated to temperatures in the range of 1900 °C to 2100 °C.

The combination of time-of-flight mass measurements and α -decay spectroscopy shows unambiguously that the ^{225}Ac is delivered in the form $^{225}\text{Ac}^{19}\text{F}_2^+$. The ion beam composition on the atomic, mono- and di-fluoride sidebands offers different possibilities for collections of ^{225}Ac by including or excluding ^{225}Ra or ^{225}Fr . A collection can be made containing all three elements Ac, Ra and Fr on the atomic sideband, with the longest contribution to the sample's half-life coming from ^{225}Ra (14.9 days). Alternatively, a difluoride sample collected on mass 263 would be pure $^{225}\text{AcF}_2^+$, without any contribution from Ra or Fr. Simultaneous collection of ion beams on all three masses would increase the final amount of extracted ^{225}Ac . The efficiency reported here is given for collection on the difluoride mass, with respect to the calculated in-target production rate. The transport efficiency measured using Faraday cup ion current readings after mass separation and before the

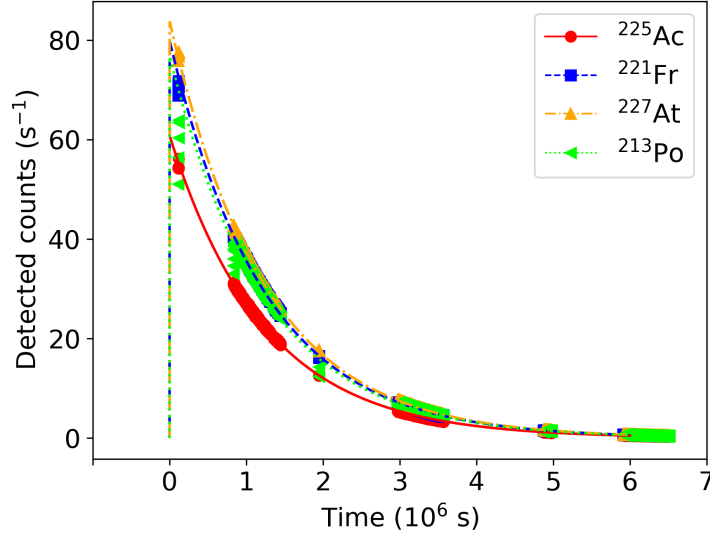


Figure 5.4: Measured counts per second of α -decays for ^{225}Ac and daughter nuclei of a sample collected for 288 s with the mass separator magnet on nominal mass $A = 263$ ($^{225}\text{AcF}_2$). Counts shown are before correction for geometrical detection efficiency and branching ratios. Fits from the corresponding Bateman equation are shown with dotted lines. See text for more details.

Table 5.2: Yield of $^{225}\text{Ac}^{19}\text{F}_2^+$ from collected samples of implanted ions measured using α -decay spectroscopy. The efficiency is given with respect to the predicted in-target production rate of ^{225}Ac [44] from FLUKA Monte-Carlo simulations calculated per μC of 1.4-GeV protons incident on uranium carbide.

Sample No.	$\text{CF}_4:\text{Ar}$ ratio	Target temperature ($^\circ\text{C}$)	Yield (ions μC^{-1})	Total efficiency (%)
1	10:90	2028(50)	$3.74(2) \times 10^5$	0.049(2)
11	20:80	2028(50)	$9.27(4) \times 10^5$	0.120(5)
21	40:60	2067(50)	$3.99(8) \times 10^7$	5.2(1)
22	40:60	2067(50)	$3.79(2) \times 10^7$	4.9(2)

implantation setup was 39 %, with the most significant losses occurring in the gas-filled ISCOOL. At a beam energy of 30 keV, the ions are expected to be implanted at a distance of 18.6 nm below the foil surface according to SRIM simulations [170]. Energy loss for the α -decays of Fr and Po resulting from the ion implantation depth is expected to be less than 4 keV, resulting in a small shift in observed peak centres with respect to the calibration α -source [171].

The target temperature during the experiment did not exceed 2100 °C. This suggests that with the molecular extraction technique, ion beams of actinium can be extracted at nominal operation conditions for a UC_x ISOL target. The first two collections, performed at the same target temperature with the same heating current applied to the target, show a difference in total efficiency that corresponds approximately linearly to the percentage of CF₄ in the gas mixture. The yield increase observed after the increase of CF₄ gas content in the gas mixture suggests that at nominal temperatures, the extraction of actinium was improved by molecular formation. The last two collections were performed with slightly higher temperature; an additional 20 A of target heating was applied, corresponding to approximately 100 W of additional heating power. The increase in yield is drastic, suggesting a strong dependence on temperature for release of the ²²⁵Ac from the target material, as expected from the Arrhenius effect of temperature on diffusion. The yields reported here are achieved at commonly used target temperatures for UC_x, and higher yields could very likely be observed with operation at higher target temperatures [172].

²²⁷Ac is a radiotoxic contaminant that is inseparable from ²²⁵Ac through chemical separation. No signature α -decay was observed above background in the energy region of the α -decay of ²²⁷Ac (4953.26(14) and 4940.7(8) keV with 0.658(14) and 0.546(17) % branching ratios, respectively [173]), giving a maximum fraction of ²²⁷Ac to ²²⁵Ac of $4(2) \times 10^{-12}$. Since ²²⁵Ac also has α -decay energies in the range of the ²²⁷Ac α -branch, the measurement of the upper limit of ²²⁷Ac contamination was evaluated 1.5×10^7 s after the end of the collection to allow for the decay of ²²⁵Ac (17.5 half-lives). The α -decay of the daughter ²¹⁵Po (7386.1 keV with branching ratio 99.999770% [174]) was also used to set an upper limit for the possible ²²⁷Ac fraction. There were no counts above background in the region of the ²¹⁵Po α -decay (7365 to 7405 keV), giving a maximum fraction of ²²⁷Ac to ²²⁵Ac of $4.5(37) \times 10^{-15}$. The mass-separating power of the ISOLDE HRS mass separator dipole magnet ($m/\Delta m = 6000$ [17]) was sufficient to suppress the long-lived ²²⁷Ac. Only an upper limit of the ratio ²²⁷Ac : ²²⁵Ac could be measured as $4.5(37) \times 10^{-15}$.

Resulting from the successful production of the AcF molecule and the delivery of AcF⁺ to experimental end stations, the campaign proposed in

Ref. [160] was successfully conducted to perform the first laser spectroscopy of actinium monofluoride at the CRIS experiment at ISOLDE. Data is presently under analysis.

5.3 Thorium molecular ions

Thorium is predicted to form fluoride molecules, taking valence states up to 4. The boiling temperature of ThF_4 is 1680°C , significantly lower than that of atomic thorium (4787°C). While not all properties of thorium fluoride are known under the conditions in the target and ion source environment, the fluoride molecule has the potential to be more easily extracted.

In this work, radiogenic thorium was observed as ThF_3^+ from a ThC_x target with CF_4 injection, limited to one or two neutron numbers away from the target nucleus ^{232}Th . No thorium was observed from the UC_x targets used in this work. It is likely that the properties of thorium, refractory even in the context of the actinides, prevent the release of radiogenic thorium nuclei from the uranium carbide matrix. In the case of the thorium carbide target, any attempt to extract the thorium will also apply to volatilization of the target material itself. In the case of the uranium carbide target, either the atomic thorium or the thorium compound formed in the target matrix seem to be more refractory than the target matrix.

5.4 Protactinium molecular ions

The chemical properties of protactinium and its fluorides are not well-known, even in the context of the other elements in the actinide series.

Protactinium displays similar chemistry to the transition metals, forming a pentavalent oxidation state. If the trend in volatility can be extrapolated from the behavior of the transition metals, the protactinium fluorides may similarly be more volatile. Additionally, protactinium has been reported to be well-volatilized at high temperatures ($>800^\circ\text{C}$) by the addition of fluorine as F_2 , HF , or SF_6 gases to samples of protactinium formed through thermal neutron activation of thorium, reporting observations of protactinium in valence states up to 5 and initial measurements of some thermodynamic properties for $\text{PaF}_{4,5}$ in the gas phase [175].

In this work, the production of protactinium and extraction as protactinium fluoride was investigated from both uranium carbide and thorium carbide target matrices. From ion implantations, decay spectroscopy and mass spectrometry, no conclusive evidence of large rates of protactinium produc-

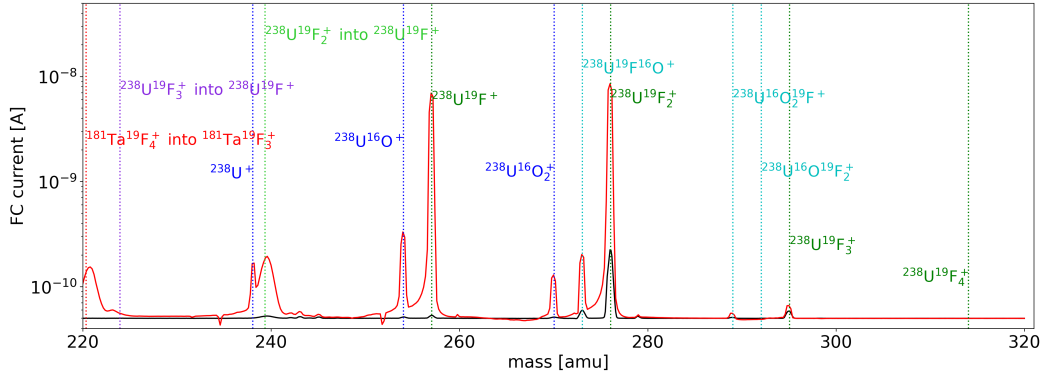


Figure 5.5: Ion beam intensity recorded on a Faraday cup during an offline scan of the GPS mass separator magnet showing the surface-ionized molecules formed from a previously irradiated UC_x target at a temperature of 1600°C without (black) and with 30 W of 532-nm laser light in the ion source (red). Metastable molecules are indicated by a vertical line corresponding to the in-flight breakup of their respective parent “into” a fragment ion [153].

tion was observed, despite the proximity of the protactinium nucleus to both the target U or Th nucleus and high predicted in-target production rates.

5.5 Uranium molecular ions

The fluoride compounds of uranium are used industrially as molecules that are more volatile than atomic uranium, particularly the hexafluoride (UF_6), which is used as a feed for isotope enrichment plants. The historical and industrial uses provide the scientific community with detailed information on these compounds, which can be found in textbooks such as Refs. [147, 151].

In this work, uranium molecules from the target material were observed and identified using mass scans performed with the ISOLDE mass separator magnets GPS and HRS. Without any added reactant, the isotopes of uranium ($^{234,235,238}\text{U}$) present in the target were observed to undergo in-target molecular formation. Mono and dioxides (UO^+ and UO_2^+) were observed with both isotopes $^{16,18}\text{O}$ (Fig. 5.5). At higher temperatures, uranium carbides (UC^+ and UC_2^+) were observed, formed from both $^{12,13}\text{C}$. With the addition of CF_4 (g) for the formation of volatile molecules, uranium fluorides $\text{UF}_{1,2,3,4}^+$ and UFO^+ were observed in large quantities, discussed further in Publication II.

The RILIS, discussed in Section 1.3, is the most frequently used ion source at the ISOLDE facility. Many resonance ionization laser schemes have been

prepared [109] and are regularly employed for delivery of atomic ion beams. The effects of laser light on molecules is studied in this work online within Publication II for molecules in the actinide region, and offline within Publication III, using stable compounds for systematic studies. The effect of 532-nm laser light was significant on both U^+ , $UO_{1,2}^+$, and $UF_{1,2,3}^+$ as shown in Fig. 5.5. A significant effect of the hot cavity ion source temperature on the intensity of metastable uranium molecules and uranium oxides and fluorides was observed, as discussed previously in Publication II. The effect of the nonresonant laser could be attributed to the added power deposited in the ion source, resulting in a higher temperature and thus higher surface ionization efficiency, or to increased molecular breakup in the source. UF_4^+ (IP 9.51 eV [176]) was observed from the FEBIAD ion sources but not the hot cavity ion sources.

For many masses (e.g., $A = 273$ with $^{235}UF_2^+$ and $^{238}UFO^+$) multiple long-lived molecules from the target material or target and ion source construction materials may be present. The mass resolving power of the separator magnet is not sufficient to unambiguously identify isobaric species. ToF mass measurements using the ISOLTRAP MR-ToF MS achieve higher mass resolving power and allow identification as shown in Fig. 5.6.

In addition to in-target formation of uranium molecules, in-trap formation of uranium oxides, carbides, and hydroxides was observed in the ISOLTRAP RFQcb. The molecules were identified using both laser response and time-of-flight. The trapping time had an observable effect on the in-trap molecular formation, as seen in Fig. 5.7. The dissociation of uranium molecular ions after ionization and extraction but before mass-separation was additionally observed by mass separation using the facility mass separator magnets. These mechanisms of molecular formation are discussed further in Publication II.

5.6 Transuranium molecular ions

In Publication I, the production of atomic ion beams of neptunium and plutonium was achieved from UC_x targets using resonance laser ionization. In this work, reactive gas was injected to a UC_x target with a FEBIAD ion source, resulting in the simultaneous extraction of both of the previously observed transuranium elements neptunium and plutonium as fluoride molecular ions.

Neptunium

Neptunium exhibits refractory properties, and as discussed in Publication I, the efficiencies measured for extraction of atomic Np ions were on the order

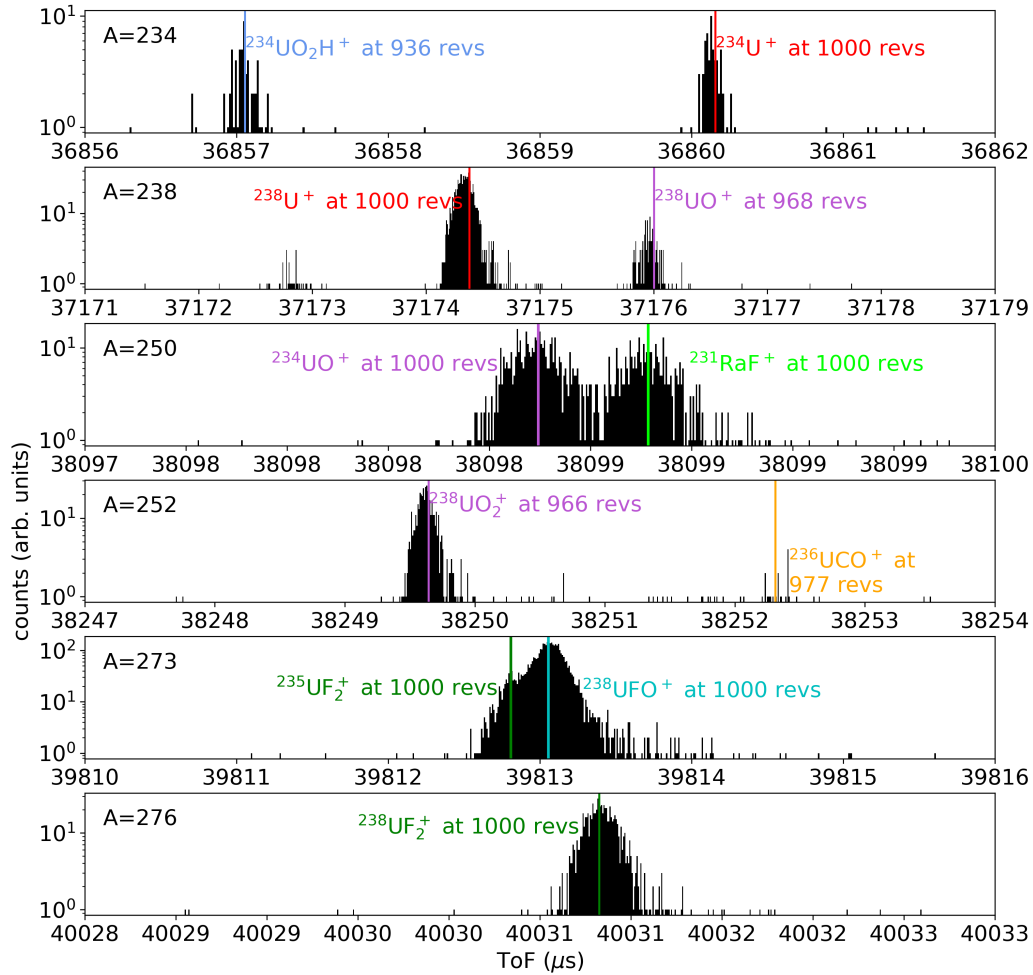


Figure 5.6: ToF spectra of ion beams from a UC_x target and a tungsten surface ion source with CF_4 injection, trapped for 1000 revolutions in the MR-ToF MS. Uranium molecules are observed as well as the formation of non-isobaric molecules in the ISOLTRAP RFQcb. The mass number A of the mass-separated beam delivered from the GPS to the ISOLTRAP experiment is indicated on the left. All labeled species are singly-charged ions. Vertical lines indicate the expected ToF of each species as calculated from the calibration, using reference masses.

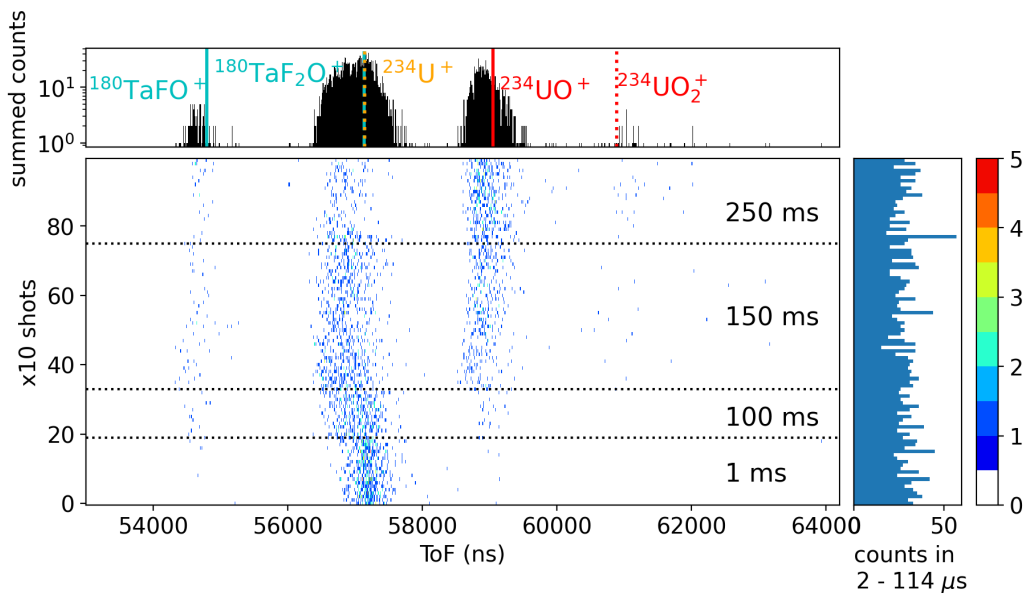


Figure 5.7: ToF distribution of a beam of $A = 234$ with no trapping revolutions in the MR-ToF MS, showing molecular formation in the ISOLTRAP RFQcb at four different cooling times indicated at the right. TaF_2O^+ dissociates into TaFO^+ (dotted and solid vertical cyan lines, respectively), while U^+ (dotted orange) forms UO^+ and UO_2^+ (solid and dotted red lines, respectively) with longer cooling times. With the experimental configuration used for this study, changing the cooling time results in a slight systematic shift in ToF, observed most strongly on the species at $A = 234$ between data taken with cooling times of 1 and 100 ms.

Table 5.3: Yield of neptunium fluorides from collected samples of implanted ions from a UC_x target with a FEBIAD ion source and a calibrated leak (5.7×10^{-5} mbar L s⁻¹, fill pressure 500 mbar) measured using γ -decay spectroscopy. Efficiency is given with respect to the predicted in-target production rate of the Np isotope [44] from FLUKA Monte-Carlo simulations calculated per μC of 1.4-GeV protons incident on uranium carbide.

Sample	CF ₄ :Ar ratio	Target temperature (°C)	Yield (ions μC^{-1})	Total efficiency (%)
²³⁸ NpF ₂ ⁺	20:80	2050(50)	$1.60(2) \times 10^3$	0.039(5)
²³⁴ Np ⁺	20:80	2050(50)	< 3.5	-
²³⁴ NpF ⁺	40:60	2100(50)	1.4×10^2	0.00013
²³⁴ NpF ₂ ⁺	20:80	2100(50)	$3.8(1) \times 10^2$	0.037 (10)
²³⁴ NpF ₃ ⁺	40:60	2100(50)	$< 1.2 \times 10^2$	< 0.0001

of 10^{-3} %, prohibitively low for most radioactive ion beam experiments. The boiling point of Np is 3902 °C, while the neptunium fluorides have boiling points of 2223 °C, 1480 °C, and 55.2 °C, for the compounds NpF₃, NpF₄, and NpF₆, respectively [177]. Though properties such as adsorption enthalpies on tantalum may not be known for all fluoride species, the neptunium fluorides have the potential to be comparatively more volatile than the atomic neptunium, similarly to the behavior of other hexafluoride compounds [178].

Samples of the radioactive ion beam were collected onto aluminum foils, which were measured offline using γ -ray spectroscopy. From the characteristic γ -lines, the number of atoms collected on the foil was obtained and used to calculate the yield. Additionally, a minimum-detectable activity analysis was used to estimate the upper limit at which activity of an isotope would have been observed and identified. Results are displayed in Table 5.3. ²³⁸Np was identified in the form of NpF₂⁺. The ion beam on this mass was heavily contaminated by ²³⁸UF₂⁺, but γ lines of ²³⁸Np (984.45 keV and 1028.53 keV with intensities of 25.2 % and 18.23 %) were observed from a sample collected on mass 276. ²³⁵Np was the most neutron-deficient Np isotope observed with atomic ion beams. With molecular extraction, ²³⁴Np was observed as ²³⁴NpF⁺ and ²³⁴NpF₂⁺, suggesting the possibility to extract a wider range of isotopes using molecular extraction. Further studies are required to characterize the systematics of Np extraction as a fluoride molecular ion.

Plutonium

With one proton more than neptunium, the element plutonium is well known for the properties of the isotope ^{239}Pu . This fissile nuclide gives plutonium its unique place featuring applications in nuclear explosives and in some nuclear reactor designs. Information about the properties of plutonium and its compounds has become declassified in the past decades [179], resulting in the availability of data on plutonium oxides and fluorides [147, 180]. Plutonium is known to form volatile halides, taking valence states up to 6 [181]. Information and experimental observations exist for oxidation states including $\text{PuF}_{3,4}$ [182].

In this work, PuF_x^+ ions were observed in addition to NpF_x^+ in the ToF spectra, shown for $A = 239$ in Fig. 5.8. In Publication I, plutonium was successfully extracted as an atomic ion beam using laser ionization. While molecular extraction may potentially offer an avenue towards delivering higher absolute rates of plutonium nuclides to experiments when compared to the rates measured using laser ionization and atomic ion beams, these higher rates may correspondingly come with higher contaminant rates, such as those presented earlier in Publication II.

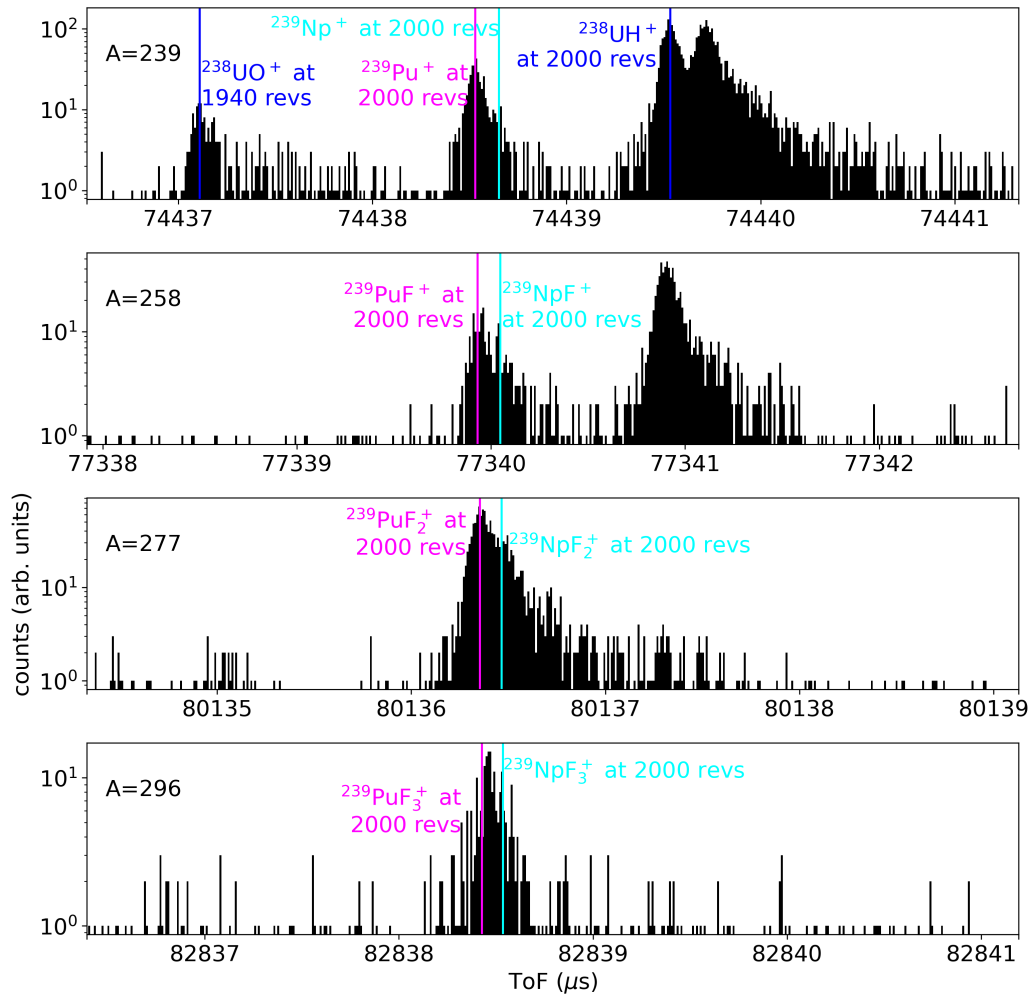


Figure 5.8: ToF spectra of ion beams from a UC_x target and a FEBIAD ion source with CF_4 injection through a calibrated leak ($5.7 \times 10^{-5} \text{ mbar L s}^{-1}$, fill pressure of 500 mbar), trapped for 1000 revolutions in the MR-ToF MS. Neptunium and plutonium fluoride ions are observed as well as contaminants and the formation of non-isobaric molecules in the ISOLTRAP RFQcb. The expected ToF from the calibration is shown for Np and Pu sidebands with vertical lines in cyan and magenta, respectively. Some contaminant ions arrive at a ToF corresponding to a possible contaminant species (dark blue) but are unconfirmed. Others remain fully unidentified. The mass number A of the mass-separated beam delivered from the HRS to the ISOLTRAP experiment is indicated on the left.

6. Offline developments for studies of molecular beams

Outline

6.1	Introduction	80
6.2	Publication III: Developments at CERN-ISOLDE's OFFLINE 2 mass separator facility for studies of molecular ion beams . .	81

6.1 Introduction

The interest in molecular species for both extraction and study, discussed in Section 1.2, has expanded beyond the familiar range of operations at ISOLDE, necessitating further development and systematic studies. Time at an online accelerator-driven facility is a precious commodity and reserved for cases that require radioactive ion beam. To develop new techniques and conduct these systematic studies, offline facilities offer more availability, fewer time constraints, and experimental flexibility in assembly or reconfiguration of hardware. While offline facilities often have constraints on handling limits of radioactivity, they offer many opportunities for the optimization of processes and techniques using stable isotopes or homologues.

ISOLDE's Offline 2 mass separator facility [183, 184, 185] is a laboratory perfectly suited to the offline systematic development of techniques that can later be implemented online at ISOLDE. With a front-end compatible to ISOLDE target and ion source designs, modifications within the target and ion source unit can be integrated and tested. The Offline 2 laser laboratory, with access to the ion source, allows development of laser schemes and studies of laser-related effects. The existing RFQcb allows studies of bunched beams and offline developments for the ion beam preparation process.

The in-trap technique for molecular formation introduced in Publica-

tion II confirms that molecules can be formed in buffer-gas-filled RFQcb ion traps from mass-separated primary beam [153]. By injecting a gas into the helium buffer gas used at the RFQ, species of interest can be additionally introduced into the trapping region for molecular formation, a technique which has yet to be systematically studied offline.

6.2 Publication III: Developments at CERN-ISOLDE's OFFLINE 2 mass separator facility for studies of molecular ion beams

As an existing offline facility for the development of ISOL techniques, Publication III presents the upgrade of Offline 2 for forming and studying molecular beams. With the addition of the infrastructure implemented in this work, new methods for the creation of molecules in the target can be tested, from new ion sources, to new forms of reactant, to the mixing and injection of gases for molecular formation. Development of laser-related techniques such as resonant or non-resonant ionization, or photodissociation of molecules, can be studied systematically. The existing RFQcb can be used to optimize the formation of molecules from mass-separated ion beams in preparation for the production of low-temperature radioactive molecular beams. In Publication III, the new upgrades are used to conduct a proof-of-concept systematic study on the production of barium fluoride molecules as an offline homologue to the radium fluoride molecules produced [77, 78] and studied non-systematically online at ISOLDE. Publication III demonstrates the formation and study of molecular ion beams directly from the ion source, and shows a preliminary set up for the investigation of molecules prepared in the RFQcb ion trap.

Future upgrades beyond Publication III are in progress and were initiated during this work. The addition of a mass-separation stage and beam identification capabilities after the Offline 2 RFQcb were proposed [186] as an upgrade of the ToF drift section presented in Publication III. The proposal to add mass spectrometry infrastructure after the RFQ such as a Wien filter, a deceleration stage coupled to a ToF device, or an MR-ToF was funded. Design and procurement of components for the next upgrade are underway as described in Ref. [184]. The upgraded mass-separation step after the RFQcb would allow the Offline 2 facility to separate and identify masses of interest in the resulting cooled and bunched beams after the RFQ. The effects of in-trap molecular formation and dissociation can then be systematically studied at the offline mass separator before moving this technology to ISOLDE for use

with radioactive ion beams in the formation and preparation of molecular beams for studies of fundamental physics.

Bibliographic Information

M. Au, C. Bernerd, Y. N. Vila Gracia, M. Athanasakis-Kaklamanakis, J. Ballof, M. Bissell, K. Chrysalidis, R. Heinke, L. Le, R. Mancheva, B. Marsh, J. Rolewska, M. Schuett, T. Venenciano, S.G. Wilkins, Ch. E. Düllmann, S. Rothe, “Developments at CERN-ISOLDE’s OFFLINE 2 mass separator facility for studies of molecular ion beams”, (2023) *Nucl. Instrum. and Methods B*. 541 (pp. 144-147). *Proc. EMIS XIX at RAON, 2022*. doi: 10.1016/j.nimb.2023.05.023.

Author contributions

The offline 2 facility was developed as described in Refs. [183] and [185]. The design, assembly and installation of the offline 2 front end gas mixing and injection system was done by Y. Nel Vila Gracia. The design, assembly and installation of the RFQ gas system was done by M. Au, Y. Nel Vila Gracia, J. Ballof and M. Bissell. The installation of MagneToF 1 was done by M. Au and R. Heinke. The installation of MagneToF 2 and the ToF drift section was done by M. Au, J. Rolewska and T. Venenciano.

Corresponding author: M. Au

CRedit author statement:

Conceptualization: M. Au, M. Athanasakis-Kaklamanakis, K. Chrysalidis, R. Heinke, B. Marsh, S.G. Wilkins, Ch.E. Düllmann, S. Rothe. Software: M. Au, L. Le, M. Athanasakis-Kaklamanakis. Investigation: M. Au, C. Bernerd, R. Mancheva, J. Rolewska, T. Venenciano. Analysis: M. Au, T. Venenciano. Supervision: K. Chrysalidis, R. Heinke, B. Marsh, Ch.E. Düllmann, S. Rothe. M. Au prepared the manuscript. All authors reviewed the manuscript.

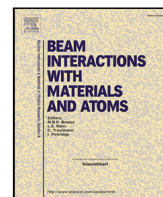
Copyright Notice

©2023 The Authors. Published by Elsevier B.V. This is an accepted version of this article published in 10.1016/j.nimb.2023.05.023. This is an open access article under the CC BY license.



Contents lists available at ScienceDirect

Nuclear Inst. and Methods in Physics Research, B

journal homepage: www.elsevier.com/locate/nimb

Developments at CERN-ISOLDE's OFFLINE 2 mass separator facility for studies of molecular ion beams

M. Au^{a,b,*}, C. Bernerd^{a,c}, Y. Nel Vila Gracia^a, M. Athanasakis-Kaklamanakis^{a,c}, J. Ballof^{a,d}, M. Bissell^a, K. Chrysalidis^a, R. Heinke^a, L. Le^a, R. Mancheva^{a,c}, B. Marsh^a, J. Rolewska^{a,e}, M. Schuett^a, T. Venenciano^{a,f}, S.G. Wilkins^{a,g}, Ch.E. Düllmann^{b,h,i}, S. Rothe^a

^a CERN, Geneva, Switzerland^b Johannes Gutenberg-Universität Mainz, Mainz, Germany^c KU Leuven, Leuven, Belgium^d FRIB, Michigan State University, East Lansing, MI, United States of America^e University of Gothenburg, Gothenburg, Sweden^f Pomona College, Claremont, United States of America^g Massachusetts Institute of Technology, Cambridge, United States of America^h GSI Helmholtzzentrum für Schwerionenforschung, Darmstadt, Germanyⁱ Helmholtz Institute Mainz, Mainz, Germany

ARTICLE INFO

Keywords:

ISOL
Molecular beams
Laser ionization
Facilities

ABSTRACT

ISOLDE's Offline 2 laboratory has been upgraded to facilitate development for the production and study of molecular ion beams. New gas injection systems have been implemented for both molecular formation in the ion source and in the radio-frequency quadrupole ion trap used for beam preparation. MagneToF detectors and time-resolved single ion counting data acquisition have been implemented for low intensity beams and studies of laser-atom or laser-molecule interactions. We present a study of the formation and ionization of BaF⁺ using the upgraded facility.

1. Introduction

Molecular beams are a growing focus of research [1–3], particularly at radioactive ion beam (RIB) facilities. Systematic studies of molecular formation, extraction, and ionization are required before new techniques can be applied to online RIB facilities such as CERN-ISOLDE [4].

For molecules with low dissociation energies or molecules that are not stable at typical target and ion source temperatures (2000 °C), molecule ionization attempts may lead to dissociation instead of ionization. An alternative method of molecule formation is to induce chemical reactions with a mass-separated ion beam and a chosen reactant in an ion trap. CERN's ISOLDE offline 2 mass separator facility (YOL2) has been upgraded to enable in-source and in-trap molecular formation. Single ion counting and time-resolved data-taking capabilities have been added.

2. Facility upgrades

YOL2 features a Frontend which delivers services (power, cooling, gas) to operate an ISOLDE-compatible target and ion source unit. The

YOL2 beamline includes ion optics, a mass-separator dipole magnet, and a radio-frequency-quadrupole cooler buncher (RFQ-cb) [5]. We present the addition of gas mixing and injection systems for the Frontend and the RFQ-cb. MagneToF detectors (ETP MagneToF 14925 [6]) have been added for single-ion counting and time-of-flight (ToF) measurements. A schematic of the upgrades is shown in Fig. 1.

The Frontend gas system allows the mixing of two different gases by partial pressures before injection into the target and ion source unit through a calibrated gas leak. The RFQ gas system allows injection of trace amounts of gas from a gas sample into a mixing reservoir before filling the reservoir with the helium typically used as buffer gas. The first MagneToF detector is installed in the beamline after mass separation. A drift section has been installed after ejection from the RFQ-cb, allowing longer flight path for ToF measurements or studies of bunched beams at MagneToF 2. For time-resolved data taking, ions on the MagneToF detectors are recorded with 500 ps resolution using a Cronologic TimeTagger [7].

* Corresponding author at: CERN, Geneva, Switzerland.
E-mail address: mia.au@cern.ch (M. Au).

<https://doi.org/10.1016/j.nimb.2023.05.023>

Received 15 February 2023; Received in revised form 26 April 2023; Accepted 4 May 2023

Available online 22 May 2023

0168-583X/© 2023 The Authors. Published by Elsevier B.V. This is an open access article under the CC BY license (<http://creativecommons.org/licenses/by/4.0/>).

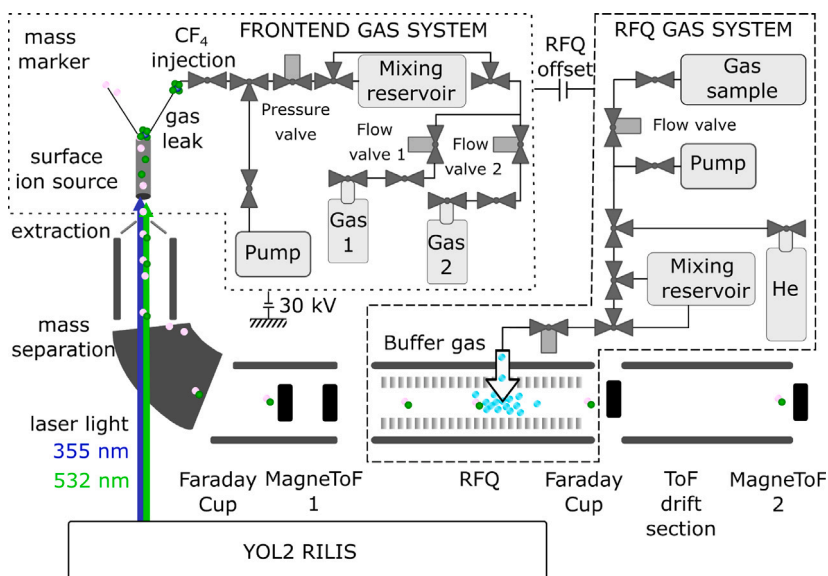


Fig. 1. Schematic of the YOL2 laboratory featuring two new gas systems, MagnetoF detectors, and a ToF section. Reactants of interest are supplied from a mass marker and a gas leak. Ions are extracted as a beam from the ion source by a potential of 30 kV and separated by m/q in the separator magnet. Mass-separated beams are sent to MagnetoF 1 or into the RFQ-cb, where the ions are cooled and bunched. Ion bunches can be studied on MagnetoF 2 after a drift section for ToF measurements.

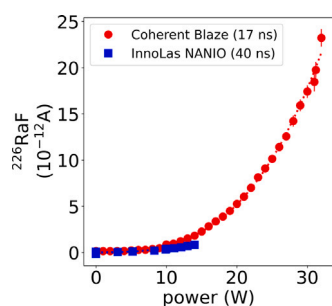


Fig. 2. Intensity of $^{226}\text{RaF}^+$ ion beam on a Faraday Cup in response to 532 nm laser power measured before transport to the ion source for lasers of two different pulse lengths at a repetition rate of 10 kHz. Third-order polynomial fits are shown.

3. Non-resonant laser effects in molecular beams

The ion source type most commonly employed at Isotope Separation On-Line (ISOL) facilities is a Resonance Ionization Laser Ion Source (RILIS), which uses laser light to step-wise resonantly excite an electron of the species of interest into the continuum, providing an efficient element-selective method of ionization [8,9]. For molecules, with rotational and vibrational degrees of freedom in addition to electronic states, the population may be distributed over a wide variety of states due to the high temperature environment in the target and ion source (2000 °C). In an online study, we observed dependence on laser pulse length and a third-order polynomial effect of laser power for the intensity of the radioactive molecular ion RaF^+ (Fig. 2). These observed dependencies motivated the systematic offline study of non-resonant laser effects using BaF^+ beams at YOL2.

The anticipated laser-related effects on molecular-ion production are summarized in Table 1 along with their expected power and wavelength dependencies. Each mechanism of light-molecule interaction is expected to depend differently on the total number of photons (laser power) and the energy of each photon (laser wavelength). In the case of dissociation, a linear dependence is expected for molecular bond strength less than the photon energy, and a quadratic dependence is expected otherwise. In the case of ionization, threshold steps would be in units of the ionization potential divided by the photon energy.

Table 1

Possible mechanisms of interaction between high-power laser light in the ion source and molecules, characterized by the observable dependence of ion beam intensity as a function of laser power and wavelength. See text for more details.

Laser-related effect	Laser power	Laser wavelength
Heating	Linear	None
Ablation	Threshold	Negligible
Dissociation	Linear	Threshold
Ionization	Quadratic or cubic	Threshold or resonant

BaF_x molecules were formed in the ion source from reactive gas injection. Excess barium was supplied as a $\text{Ba}(\text{NO}_3)_2$ standard solution deposited into a tantalum tube (mass marker). CF_4 gas was injected through a calibrated leak using the front end gas system (Fig. 1). Measurements were done with ion source heating power of 400 ± 10 W corresponding to 1700 °C, which is lower than the 2000 °C typically used in hot-cavity ion source operation. Conditions were chosen to limit the ion rate at the single-ion detector and therefore avoid saturation.

Mass scans were conducted using the YOL2 mass separator magnet with and without frequency-doubled (532 nm, 2.33 eV) and tripled (355 nm, 3.49 eV) light from an Innoslab EdgeWave Nd:YAG laser beam delivered to the ion source (Fig. 3). Ta, Ba, and BaF show increased intensity with the 355 nm light.

For Ba, with an ionization potential (IP) of 5.2 eV, and BaF (IP 4.7 eV) in a tantalum surface ion source (work function 4.3 eV), the surface ionization efficiency at the corresponding ion source temperature is expected to have an approximately linear dependence on power.

Ba^+ intensity was recorded while changing the power of 355 nm and 532 nm laser light in the ion source, as shown in Fig. 4. The bond dissociation energy of BaF into Ba+F has been measured as 5.90(44) eV, and BaF_2 into $\text{BaF}+\text{F}$ as 6.07(44) eV [10] such that ionization is favoured over dissociation. The quadratic trends in Fig. 4 show two-photon ionization for 355 nm light and a linear trend indicating heating for 532 nm light.

TaF_{1-2}^+ and TaOF_{0-2}^+ show an increase in intensity and a laser pulse-related time structure (Fig. 5). $^{181}\text{Ta}^+$ and $^{181}\text{Ta}_2^+$ fragments from dissociation of TaF_4^+ and TaF_5^+ were observed and are indicated at their corresponding effective mass where identified in Fig. 3.

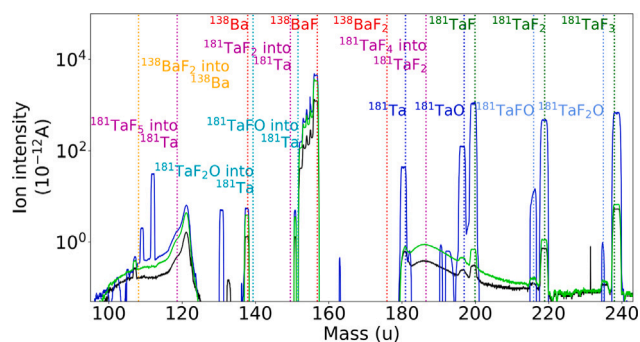


Fig. 3. A mass scan of the YOL2 mass separator magnet with 12 W of 355 nm (blue) and 532 nm (green) light in the ion source compared to the same mass scan with the laser off (black). Positions of singly-charged atomic, molecular and fragment species are shown with annotated vertical lines.

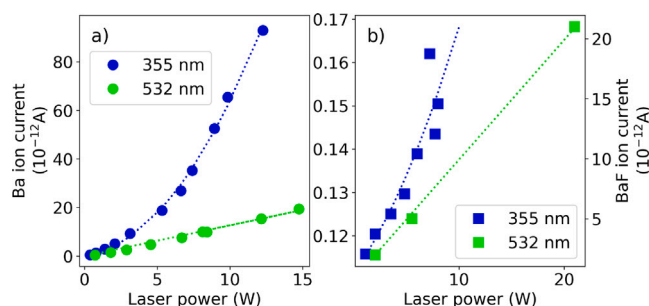


Fig. 4. The difference in laser-on and laser-off ion intensities for mass-separated beams of (a) $^{138}\text{Ba}^+$ and (b) $^{138}\text{BaF}^+$ as a function of laser power for 355 nm and 532 nm light. A second-order polynomial fit is used for 355 nm data and a linear fit is used for 532 nm data. In (b), the left vertical axis gives the value for 355 nm and the right vertical axis gives the value for 532 nm.

Species that are ionized in the extraction region between the 30 kV-ion source potential and the laboratory ground experience a fraction of the full extraction potential. Ions created in this region therefore have a different energy and are thus mass-separated with a magnetic field corresponding to this fraction of the ion source potential, resulting in peaks with narrow spread in time-of-flight as demonstrated by Heinke et al. in [11]. They then appear in the mass spectrum as broad, asymmetrical features tailing towards lower masses. In the time-domain, these ions, which are extracted immediately after creation, are therefore the first to appear at the ion detector following the laser pulse, and the bunch width is narrower than that of the ions created inside the hot cavity. The laser effect on tantalum molecules seen in Fig. 3 is observed for these extraction-ionized species on a different mass as shown in Fig. 5, indicating that some fraction are ionized outside of the ion source. Ablation can also contribute to the observed increase in ion intensity if it directly results in ions or if it increases the number of neutrals available for laser ionization.

4. Conclusions

The YOL2 facility has been upgraded to enable molecular formation with mixtures of two added gases in the ion source and with a reactive gas added to the buffer gas in the RFQ-cb. In combination with the capability to form molecules, the addition of single ion counting and time-resolved data taking enables studies of laser-related time structures and laser interaction with stable atoms and molecules as demonstrated using Ba and BaF.

High-power laser light (10s of W or more of average power) can be used for ionization of molecules in the ion source and subsequent delivery of molecular beams. The laser deposits power and can additionally increase surface ionization efficiency with an effect dependent

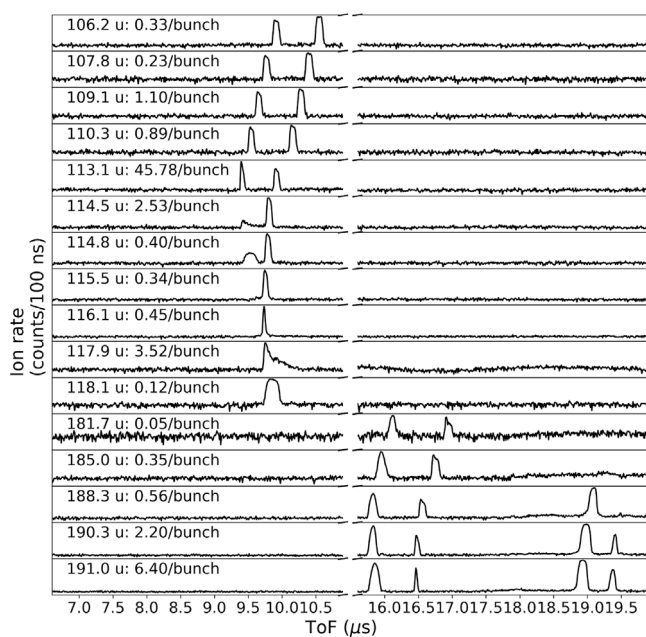


Fig. 5. Time spectra of mass-separated ion beams with respect to the laser trigger using 10 W of 355 nm laser light at a repetition rate of 10 kHz. The separator magnet set mass and the average number of ions per laser pulse (“bunch”) are indicated on the left. Vertical axes indicate the number of ions incident on the detector per laser pulse per 100 ns ToF bin in logarithmic scale.

on the ionization potential of the species. In cases where ionization occurs out of the ion source in the extraction potential, a sharp time structure related to the laser pulses is visible at mass-separating fields lower than that of the expected mass as a result of mass separation at a different ion energy.

Declaration of competing interest

The authors declare that they have no known competing financial interests or personal relationships that could have appeared to influence the work reported in this paper.

Acknowledgements

The authors thank Bernard Crepieux, Mathieu Bovigny, the ISOLDE targets and ion sources team and Simone Gilardoni for their support. This project has received funding from the European Union’s Horizon 2020 Research and Innovation Programme under grant agreement number 861198 project ‘LISA’ (Laser Ionization and Spectroscopy of Actinides) Marie Skłodowska-Curie Innovative Training Network (ITN).

References

- [1] G. Arrowsmith-Kron, M. Athanasakis-Kaklamanakis, M. Au, J. Ballof, R. Berger, A. Borschevsky, A.A. Breier, F. Buchinger, D. Budker, L. Caldwell, C. Charles, N. Dattani, R.P. de Groote, D. DeMille, T. Dickel, J. Dobaczewski, C.E. Düllmann, E. Eliav, J. Engel, M. Fan, V. Flambaum, K.T. Flanagan, A. Gaiser, R.G. Ruiz, K. Gaul, T.F. Giesen, J. Ginges, A. Gottberg, G. Gwinner, R. Heinke, S. Hoekstra, J.D. Holt, N.R. Hutzel, A. Jayich, J. Karthein, K.G. Leach, K. Madison, S. Malbrunot-Ettenauer, T. Miyagi, I.D. Moore, S. Moroch, P. Navrátil, W. Nazarewicz, G. Neyens, E. Norrgard, N. Nussgart, L.F. Pašteka, A.N. Petrov, W. Plass, R.A. Ready, M.P. Reiter, M. Reponen, S. Rothe, M. Safronova, C. Scheidenberger, A. Shindler, J.T. Singh, L.V. Skripnikov, A.V. Titov, S.-M. Udrescu, S.G. Wilkins, X. Yang, Opportunities for fundamental physics research with radioactive molecules, 2023, <http://dx.doi.org/10.48550/ARXIV.2302.02165>, URL <https://arxiv.org/abs/2302.02165>.
- [2] M.S. Safronova, D. Budker, D. Demille, D.F. Kimball, A. Derevianko, C.W. Clark, Search for new physics with atoms and molecules, Rev. Modern Phys. 90 (2) (2018) <http://dx.doi.org/10.1103/RevModPhys.90.025008>, arXiv:1710.01833.

- [3] L.V. Skripnikov, N.S. Mosyagin, A.V. Titov, V.V. Flambaum, Actinide and lanthanide molecules to search for strong CP-violation, *Phys. Chem. Chem. Phys.* 22 (33) (2020) 18374–18380, <http://dx.doi.org/10.1039/d0cp01989e>, [arXiv: 2003.10885](https://arxiv.org/abs/2003.10885).
- [4] R. Catherall, W. Andreatza, M. Breitenfeldt, A. Dorsival, G.J. Focker, T.P. Gharsa, T.J. Giles, J.L. Grenard, F. Locci, P. Martins, S. Marzari, J. Schipper, A. Shornikov, T. Stora, The ISOLDE facility, *J. Phys. G: Nucl. Part. Phys.* 44 (9) (2017) <http://dx.doi.org/10.1088/1361-6471/aa7eba>.
- [5] S. Warren, T. Giles, C.M. Pequeno, Offline 2, ISOLDE 's target, laser and beams development facility, *Nucl. Instrum. Methods Phys. Res. B* 463 (July 2019) (2020) 115–118, <http://dx.doi.org/10.1016/j.nimb.2019.07.016>.
- [6] D. Stresau, K. Hunter, W. Sheils, P. Raffin, Y. Benari, A new class of robust sub-nanosecond TOF detectors with high dynamic range, in: 54th ASMS Conference on Mass Spectroscopy, Seattle, Washington, 2006, URL <https://www.etp-ms.com/faqs/literature>.
- [7] Cronologic, TimeTagger product brief, 2022, <https://download.cronologic.de/TimeTagger/TimeTagger4-product-brief.pdf>. (Accessed 20 April 2022).
- [8] V. Fedosseev, K. Chrysalidis, T.D. Goodacre, B. Marsh, S. Rothe, C. Seiffert, K. Wendt, Ion beam production and study of radioactive isotopes with the laser ion source at ISOLDE, *J. Phys. G: Nucl. Part. Phys.* 44 (8) (2017) <http://dx.doi.org/10.1088/1361-6471/aa78e0>.
- [9] S. Rothe, B.A. Marsh, C. Mattolat, V.N. Fedosseev, K. Wendt, A complementary laser system for ISOLDE RILIS, *J. Phys. Conf. Ser.* 312 (SECTION 5) (2011) 1–6, <http://dx.doi.org/10.1088/1742-6596/312/5/052020>.
- [10] National Bureau of Standards, Bond dissociation energies in simple molecules, in: *National Standard Reference Data System, Vol. NSRDS-NBS 31, NIST, 1970*.
- [11] R. Heinke, V. Fedosseev, T. Kieck, T. Kron, B. Marsh, S. Raeder, S. Richter, S. Rothe, K. Wendt, Atom beam emersion from hot cavity laser ion sources, *Nucl. Instrum. Methods Phys. Res. B* 463 (March 2019) (2020) 449–454, <http://dx.doi.org/10.1016/j.nimb.2019.04.026>.

7. Conclusions

The work contained in this thesis comprises the development of experimental infrastructure and techniques applied to the production of isotopes in the actinide region. The presented results demonstrate the production and extraction of actinide atomic ion beams of actinium, thorium, uranium, neptunium, and plutonium, as well as actinium, thorium, uranium, neptunium and plutonium fluoride molecular ions with different considerations for the production and available isotopes of each actinide element. This work outlines to the community which actinide isotopes can be produced and studied at ISOL facilities as atoms or molecules with high-energy proton driver beams using the current state-of-the-art. The infrastructure, including single-ion counting capabilities, and the results, including information about target and ion source operational parameters, release properties, expected intensities and contamination, are already being used to conduct further experiments on the actinides [112, 158, 160].

7.1 Target and ion source operation for molecular beams

The production of RIBs using the ISOL technique requires target and ion source selection, conditions, and operational parameters that can be specifically optimized not just for each element (or molecular species), but for each particular isotope. The basic considerations discussed in Section 1.1.1 cover the selection of an appropriate target material and ion source for each species of interest. While particular operational parameters may differ depending on the species of interest, some considerations for the production of molecular ion beams have been identified in this work. For the actinide fluorides studied in this work, particularly those with two or more fluorine atoms, the ionization potentials are above the range for efficient surface ionization. The following considerations apply to the operation of hot actinide carbide targets with hot FEBIAD-type plasma ion sources, unless other target materials or ion sources are explicitly mentioned.

7.1.1 In-source molecular formation

The mechanisms of in-source molecular formation occur through reactions with residual contamination (e.g. oxides or hydroxides), the target material itself (carbides), or the deliberate injection of a reactive gas (e.g. the fluorides studied in this work). Some of these are further discussed in Publication II. Trace amounts of oxides, hydrides and hydroxides are observed even with procedures to maintain clean target and ion source environments as well as gas handling systems such that reactant compositions can be carefully controlled for each experiment. Contaminants can compete with the intended molecular formation process, reducing extraction efficiency, or alternatively can form unexpected molecular sidebands that then appear as unwanted components in the ion beams delivered for experiments. Molecular formation that occurs with the target material itself cannot be controlled by cleanliness, but causes an unavoidable additional consideration for chemical compatibility when choosing a target material. The observations provide a clear justification for the dedicated laboratories and infrastructure used for the assembly, production and handling of target and ion source units and target materials, while highlighting some of the technical challenges that must be overcome for the preparation and delivery of pure beams.

7.1.2 Injection of reactive gases

The injection of a reactive gas comes with additional parameters regarding target and ion source operation, including the volatilization of the target material, volatilization of target container or ion source materials, ion source internal pressure, ion source overloading, and failure mode considerations such as the clogging of calibrated leaks or coating of insulators.

In this work, fluorine was chosen for molecular sideband formation of the actinides for the reasons discussed in Section 1.2. For the very same reasons it volatilizes the desired actinide species, fluorine also volatilizes the actinide target materials. Uranium accepts bonds with up to six fluorine atoms, though $\text{UF}_{5,6}$ have low boiling points (530 °C and 56.5 °C, respectively) and may dissociate at 2000 °C. During operation, the distribution of uranium across its fluoride sidebands is one indication of the relative quantities of reactants available in the target and ion source. While the observed distribution in the mass-separated ion beam is also a result of molecular break up and as such is not a direct measurement of the ratios of molecular sidebands, it allows qualitative monitoring of target conditions. As an example, while increasing the partial pressure of CF_4 into the source with a UC_x target, one might observe the increase in the ratio of $\text{UF}_{3,4}^+$ compared to $\text{UF}_{0,1}^+$. At high

target temperatures, one or more of these species is likely to dominate the beam. Expected rates and further discussion of sideband distributions for UC_x targets are given in Publication II of this work.

The addition of reactive gas can similarly volatilize the materials from which the target and ion source unit are constructed. At the high temperatures required for diffusion of refractory species, few construction materials are available. The target container, transfer line, and the ion source itself are constructed of tantalum. Insulators in the VD5 FEBIAD-type plasma ion source are constructed of BeO. Tantalum fluorides are notably more volatile than the refractory metal itself (TaF_5 has a boiling point of $229.5^\circ C$ compared to $5458^\circ C$ for Ta). In this work, high rates of tantalum fluorides and oxyfluorides are observed as well as rates of BeF_2^+ , likely from the target container and ion source materials. The observation of Ta and Be as molecular fluoride ions may indicate that the reactive gas volatilizes the target and ion source construction materials.

The simultaneous volatilization of desired radioisotopes, target material, and the target and ion source construction materials by the injection of reactive gas leads to an increase in the gaseous vapours present in the ion source. In extreme conditions (high target temperatures and large amounts of reactive gas), the number of neutrals in the ion source may be much higher than the number of thermionic electrons emitted from the cathode, overwhelming the ion source and resulting in a large total ion beam but a lower ion intensity for the species of interest and a correspondingly lower extraction efficiency with respect to the in-target production rate. A second effect of the volatilization is the subsequent desorption of the volatile species onto colder surfaces. For example, the tantalum cathode may be at high temperatures to facilitate thermionic emission of electrons, simultaneously providing a high temperature environment for the formation of gaseous TaF_x . The insulators in the ion source are not actively heated and may be several hundred degrees colder, allowing some of the volatilized species to condense. In extreme conditions, the deposition can cause a conductive pathway which gives a connection between the anode body and the ion source ground potential, preventing the anode from retaining the acceleration voltage responsible for accelerating the electrons and disabling the ion source. This method of failure can prove fatal to experiments. In this work, the UC_x was observed to give higher rates of target material fluorides than the ThC_x target at comparable temperatures and reactive gas injection rates, effectively enabling the ThC_x target to be safely operated at higher temperatures, at which point tantalum fluorides begin to contribute noticeable amounts to the total beam.

The best practice identified in this work was to cool the target and ion source substantially lower than $2000^\circ C$, to temperatures in the range of 1400-

1700 °C, before increasing the amount of reactive gas added to the target. This seems to prevent a sudden burst volatilization of neutrals which coat the ion source insulators. The total ion beam intensity during ion source operation with optimized settings typically ranged between 2 and 5 μA , with both higher and lower total ion currents observed dependent on the target heating, ion source heating, pressure and composition of reactive gas injection.

7.2 Availability of actinides

7.2.1 Actinium

Actinium is now part of the catalogue of radioactive beams available at the ISOLDE facility, and can be produced and delivered using several options. The methods investigated in this work for actinium production are:

1. Extraction of actinium in atomic form from a UC_x target, using resonance laser ionization.
2. Delivery of the surface-ionized parent nuclei radium (and francium)
3. Molecular sideband extraction of actinium from a UC_x target, using CF_4 and a hot plasma (FEBIAD-type) ion source
4. Molecular sideband extraction of actinium from a ThC_x target, using CF_4 and a hot plasma (FEBIAD-type) ion source

Actinium was successfully produced in this work using all four of these methods.

The extraction of actinium isotopes as atomic ions was previously studied from a UC_x target using RILIS. This production method was confirmed in this work using the same technique, indicating the need for high temperatures (in excess of 2000 °C) to achieve rates of atomic actinium isotopes detectable at the Faraday cup level. Using this technique, actinium isotopes $^{224-231}\text{Ac}$ were produced and delivered to experiments at ISOLDE [112, 144, 145]. Though the same technique was not applied using a ThC_x target, some conclusions may be drawn from the results in this work. The observed extraction of actinium in atomic form from a carbide material (here UC_x) suggests that while the formation of actinium carbide could limit the release of actinium from ceramic carbide materials, it does not prohibit usable rates of actinium from being extracted. This conclusion allows one to consider carbide targets

for actinium production. The two materials with in-target production cross-sections of actinium nuclides are UC_x and ThC_x . FLUKA simulations predict better production cross-sections from ^{232}Th for most isotopes of Ac, except isotopes with more neutrons than ^{231}Ac . ThC_x is more refractory (melting point of $2500\text{ }^\circ\text{C}$ vs $2350\text{ }^\circ\text{C}$ for UC_x). To facilitate diffusion of refractory actinium out of a target, the highest temperatures possible without compromising the material structure are favorable. ThC_x with RILIS is therefore recommended for the production of actinium in atomic form, at temperatures as high as possible without degradation. Target and ion source designs that minimize cold spots for condensation are desirable.

In addition to the production of atomic actinium ion beams, the development and successful production of actinium fluoride molecular ion beams adds more options towards the production and study of actinium. This work shows that the technique is applicable for ISOL target conditions in the range of $2000\text{ }^\circ\text{C}$ with higher rates than resonantly laser-ionized actinium and a wider range of isotopes ($^{224-234}\text{Ac}$) observed from UC_x . From both UC_x targets and ThC_x targets, the most highly-abundant sideband was AcF_2^+ . Application of the technique for production of ^{225}Ac can contribute to the production and purification of radionuclides for targeted- α therapy. With the observed efficiencies, it could be considered to scale the rates measured in this work to expected production rates of ^{225}Ac , ^{225}Ra , and ^{225}Fr at ISOL facilities with different accelerator energy, projectile particles, or intensity, as a first approximation. In this work at the CERN-ISOLDE facility, the results translate to collection rates on the order of 10^7 AcF_2^+ particles per second with $1\text{ }\mu\text{A}$ of 1.4-GeV protons incident on a UC_x target. The sideband extraction of actinium fluorides enables experiments on actinium nuclei without radium or francium contaminants. Additionally, the molecular actinide fluoride molecules are now available for experiments.

7.2.2 Thorium

Given its refractory properties, thorium was not attempted as an atomic ion beam in this work. Instead, for some neutron-rich cases, actinium, radium, and francium ion beams can be extracted as β -decaying precursors to the desired thorium nuclei (e.g. ^{229}Th [149]). This method can be used to provide a limited selection of isotopes including $^{226-234}\text{Th}$, beyond which the actinium parent is either produced in low intensities or does not have a β -decay branch.

The molecular sideband extraction of radiogenic thorium was attempted from UC_x targets with reactive gas injection and FEBIAD ion sources, without success. From thorium carbide targets, large rates of ^{232}Th , $^{232}\text{ThF}^+$, $^{232}\text{ThF}_2^+$ and $^{232}\text{ThF}_3^+$ were observed, reaching intensities of $10\text{-}100\text{ nA}$.

7.2.3 Protactinium

Protactinium was not extracted as a resonantly laser-ionized atomic beam or as a molecular fluoride sideband from either UC_x or ThC_x targets, though all three methods were attempted. This could be due to chemisorption of protactinium on the target material surfaces, molecular formation (of e.g. protactinium carbides) with the target material, or simply due to prohibitive diffusion and desorption onto surfaces at insufficiently high temperatures.

The method of extracting radioactive parents, while not attempted in this work, could be considered for protactinium isotopes, which were attempted but not successfully extracted from a uranium carbide target as an atomic ion beam using RILIS. This is more difficult than using the method for extraction to provide thorium isotopes, in which case the actinium parent could still be directly extracted. The use of radioactive decay for protactinium nuclides requires an extractable thorium isotope, which was not achieved in this work, or an extractable actinium which decays into thorium which subsequently decays with an acceptable half life to perform studies on the protactinium daughter during an experiment. The latter case is only possible for one or two isotopes: ^{233}Ac (143 s) into ^{233}Th (21.8 min) into ^{233}Pa (27 d), and potentially ^{231}Pa , where the corresponding parent ^{233}Th has a half-life of 25.57 h.

Alternatively, external samples of long-lived protactinium isotopes such as ^{231}Pa could be considered as a means to deliver protactinium ion beams without requiring the extraction of the isotopes from bulk carbide target materials.

7.2.4 Uranium

The implementation of a uranium resonance ionization laser scheme provides a tool for identifying contamination from the target material and for monitoring the target and ion source conditions and performance through observation of the quantity of target material present as atomic vapor in the ion source. Resonance laser ionization of uranium also allows the target material itself to be used as an ion beam for setup, optimization and ion beam tuning to the experiment. In this work, it was identified that the availability of resonantly laser-ionized uranium atomic ions was limited to the uranium isotopes present in the target material ($^{238,235}\text{U}$ as well as some ^{234}U from the α -decay of ^{238}U into ^{234}Th , subsequently β -decaying into ^{234}U which has a 2.457×10^5 y half-life). While in-target production of other uranium isotopes from the ^{238}U target nucleus is predicted by FLUKA calculations, extraction and resonance laser-ionization of these radioisotopes was not successful. Since the uranium target matrix is chemically identical

to the uranium radioisotopes created as reaction products, any attempt to volatilize radiogenic uranium will inevitably volatilize the uranium target nuclei present in the UC_x . Nevertheless, RIBs of the long-lived uranium isotopes available in large quantities from UC_x targets facilitate machine setup in the actinide mass region and also enable commissioning studies using actinides, e.g. $^{235,238}\text{U}$ in Ref. [187].

^{232}Th ($Z = 90$) has fewer protons than the target nucleus ^{238}U , resulting in lower in-target production rates for isotopes of uranium ($Z = 92$). As discussed in Publication I for the production of plutonium ($Z = 94$) from UC_x , some in-target production mechanisms including radioactive decay may be able to generate a selection of available isotopes for elements of higher Z than the target nucleus. Molecular sideband extraction of uranium fluorides was attempted from a ThC_x target, without observing convincing rates. Further investigations are required.

7.2.5 Transuranium elements

Neptunium and plutonium both possess more protons than the target nucleus itself and were observed for the first time as radioactive ion beams at the ISOLDE facility. For these two elements, a range of available isotopes was identified and quantified for the ISOLDE user community, and is presented in Publication I. As a result of this work, preliminary feasibility studies for the in-source laser spectroscopy of Np and Pu were completed [158], suggesting the possibility to extract information about these transuranium nuclei through laser spectroscopy.

Both neptunium and plutonium are comparatively refractory for ISOL ion beams, but, as discussed in Publication I, the extraction efficiency of neptunium in particular is prohibitively low. The initial observations of neptunium and plutonium fluorides reported in this work are an encouraging step beyond the atomic ion beams discussed in the publication, towards higher efficiency production of neptunium and plutonium nuclides. The current limiting factor in the application of fluoride molecular sideband extraction for Np and Pu is the competing volatilization of the UC_x target material.

7.3 Radioactive molecular beams

With new and growing interest in radioactive molecules, the work presented here on the production of specific molecular sidebands gains relevance beyond the improved extraction of refractory radionuclides for nuclear physics experiments. In particular, the production of actinide molecules with electronic structures tractable by both theory and laser spectroscopy is of high interest for studies of physics beyond the standard model. RaF and AcF are two of these, and the successful production at ISOLDE opens the door wider for experiments and characterization of similar diatomic molecules—particularly fluorides—that are stable at high temperatures, using the in-source molecular formation technique. Similar fluoride sidebands beyond the actinides, such as the alkaline-earth fluorides, have been observed in the past, and the techniques for their production are relatively well-understood. To expand the catalogue of radioactive molecules, other techniques of reactant introduction could be explored. Many other radioactive molecules of interest, such as hydroxides or larger, more complex molecular structures, were not produced using the in-source molecular formation technique.

In Publication II, an alternative technique is presented for the formation of radioactive molecules from the primary mass-separated ion beam using the RFQcb devices typically used for RIB preparation. The formation of actinide oxides and hydroxides is observed using this technique, along with a preliminary characterization of some parameters influencing the production, namely the trapping or interaction time with buffer gas. These preliminary studies open a new avenue towards the deliberate production of molecular beams, with applications for molecules that are only stable at low temperatures.

8. Outlook

With the current state-of-the-art, the ISOL method reaches into the light actinide range and enables experiments on elements with proton numbers up to plutonium ($Z = 94$). $^{235-244}\text{Am}$ are likely produced with low cross-sections. ^{241}Am is long-lived and may benefit from the β -decay of ^{241}Np and ^{241}Pu . Two of these Am isotopes ($^{242,244}\text{Am}$) have the additional possibility to β -decay into $^{242,244}\text{Cm}$, which do not β -decay further to $Z = 97$, berkelium. Future advancements in high-release-efficiency target materials (e.g. nano-materials), isotope extraction techniques, and experimental sensitivity could likely extend the feasible range of experiments to $Z = 95$ (and possibly the two mentioned Cm nuclei with $Z = 96$), with the currently available target nuclei. To push further into the actinide series, samples of heavier nuclei ($^{239,240,242}\text{Pu}$, $^{241,243}\text{Am}$, and potentially even $^{242-248}\text{Cm}$) could be made available as smaller batches through reactor-based techniques (e.g. Ref. [73, 188]). While not sustainable as a regular operation, the use of external samples in place of irradiating target materials could give access to these elements of $Z > 94$ for dedicated experiments in the actinide region. This is no longer the ISOL technique, but may be considered as an alternative approach towards the refractory species (e.g. Pa, Th) that were not successfully extracted from thick targets using the ISOL method in this work. Quantification of extraction efficiencies from such external samples is needed as a first step.

Further developments are required to expand the catalogue of available radioactive ion beams and molecular species. The molecules observed here may be stable in the environment of the standard ISOL target and ion source, but require further ion source developments to optimize production and extraction while minimizing contamination. Other molecules of interest are fragile and require lower temperature environments. Additional interest in specific symmetric molecules further motivates the development of ion sources that can be operated at ambient temperatures such as the photo-cathode FEBIAD [123] discussed in Section 1.3, as well as offline developments for alternative molecular formation techniques using e.g. room temperature ion traps as discussed in Publication II.

In-source laser spectroscopy has made significant improvements in resolution through the implementation of the PI-LIST [112, 114]. This technique

can already enable resonant ionization laser spectroscopy of the actinide nuclides extracted from the target in sufficient quantities. Further consideration may be required for the direct application of the technique to spectroscopy of the radioactive molecules formed in-source. In typical ISOL conditions, molecules will possess the state distribution present at the high temperatures of the target and ion source. If multiple thermally-excited states are accessible, the population of the radioactive species may be distributed across the states, lowering the signal-to-background quality of each transition. Alternatively, selectively-ionized and mass-separated beams of such molecules cooled and bunched in a Paul trap could be delivered to experiments for high-resolution optical spectroscopy, as was demonstrated in the recent laser spectroscopy of AcF at the ISOLDE-CRIS experiment [160].

There are several current challenges facing the use of radioactive atomic or molecular species for physics beyond the standard model. The highly sensitive tabletop experiments designed for these studies typically use large amounts of long-lived isotopes to overcome low or unknown production efficiencies. The application of these atomic, molecular and optical techniques to study a radioactive ion beam requires either development of the experimental setups for implementation at a RIB facility or techniques of isotope production such as ion sources or atomic beam units with high enough efficiency to allow studies of low quantities of radioactive species. Laser ablation is often used to produce ions from a solid sample for offline study, for example from carbon in the form of graphite, amorphous (“glassy”) carbon, or graphene for the production of carbon clusters, where molecular formation results in wide mass distributions of produced molecular ions. Few radioisotopes are similarly available as macroscopic, self-supported samples. ^{238}U or ^{232}Th can be obtained in the form of metallic samples, and macroscopic quantities of some neutron-deficient uranium and thorium isotopes can be obtained as well as other nuclei produced in neutron-capture processes in high-flux research reactors. At RIB facilities, the possibility to collect samples of radioactive nuclei by ion implantation into a substrate could offer a large catalogue of isotopes. Though this approach is promising for adaptation to the high-precision studies at offline labs, many parameters of sample preparation and the ion or atom beam supply are at present still insufficiently optimized to determine efficiencies and subsequently the quantity of radioisotopes required for high-precision offline studies.

Complete List of Publications

Publications

1. M. Au, M. Athanasakis-Kaklamanakis, L. Nies, R. Heinke, K. Chrysalidis, U. Köster, P. Kunz, B. Marsh, M. Mougeot, L. Schweikhard, S. Stegemann, Y.N. Vila Gracia, Ch.E. Düllmann, S. Rothe, “Production of neptunium and plutonium nuclides from uranium carbide using 1.4-GeV protons” (2023) *Phys. Rev. C.*, 107, 064604. doi: 10.1103/PhysRevC.107.064604. arXiv:2303.12226 nucl-ex.
2. M. Au, M. Athanasakis-Kaklamanakis, L. Nies, J. Ballof, R. Berger, K. Chrysalidis, P. Fischer, R. Heinke, J. Johnson, U. Köster, D. Leimbach, B. Marsh, M. Mougeot, J. Reilly, E. Reis, M. Schlaich, Ch. Schweiger, L. Schweikhard, S. Stegemann, J. Wessolek, F. Wienholtz, S. G. Wilkins, W. Wojtaczka, Ch. E. Düllmann, S. Rothe, “In-source and in-trap formation of molecular ions in the actinide mass range at CERN-ISOLDE” (2023) *Nucl. Instrum. and Methods B.*, 541 (pp. 375-379). *Proc. EMIS XIX at RAON, 2022*. doi: 10.1016/j.nimb.2023.05.015. arXiv:2303.12215, physics.inst-det.
3. M. Au, C. Bernerd, Y.N. Vila Gracia, M. Athanasakis-Kaklamanakis, J. Ballof, M. Bissell, K. Chrysalidis, R. Heinke, L. Le, R. Mancheva, B. Marsh, J. Rolewska, M. Schuett, T. Venenciano, S.G. Wilkins, Ch. E. Düllmann, S. Rothe, “Developments at CERN-ISOLDE’s OFFLINE 2 mass separator facility for studies of molecular ion beams”, (2023) *Nucl. Instrum. and Methods B.* 541 (pp. 144-147). *Proc. EMIS XIX at RAON, 2022*. doi: 10.1016/j.nimb.2023.05.023.
4. L.V. Skripnikov, A.V. Oleynichenko, A. Zaitsevskii, N.S. Mosyagin, M. Athanasakis-Kaklamanakis, M. Au, G. Neyens, “*ab initio* study of electronic states, radiative properties of the AcF molecule” (2023) *J. Phys. Chem.*, 159, 124301 doi: 10.1063/5.0159888, arXiv:2305.06932, physics.atom-ph.
5. L. Nies, D. Atanasov, M. Athanasakis-Kaklamanakis, M. Au, K. Blaum, J. Dobaczewski, B.S. Hu, J.D. Holt, J. Karthein, I. Kulikov, Yu.A. Litvinov, D. Lunney, V. Manea, T. Miyagi, M. Mougeot, L. Schweikhard, A. Schwenk, K. Sieja, F. Wienholtz, “Isomeric excitation energy for $^{99}\text{In}^m$ from mass spectrometry reveals constant trend next to doubly magic ^{100}Sn ” (2023) *Phys. Rev. Lett.* 131, 002502, doi: 10.1103/PhysRevLett.131.022502, arXiv:2305.06932, physics.nucl-th, nucl-ex.
6. S. Udrescu, S. G. Wilkins, A. Breier, R. F. Garcia Ruiz, M. Athanasakis-Kaklamanakis, M. Au, I. Belošević, R. Berger, M. Bissell, K. Chrysalidis, T.E. Cocolios, R.P de Groote, A. Dorne, K. Flanagan, S. Franchoo, K. Gaul, S. Geldhof, T. Giesen, D. Hanstorp, R. Heinke, A. Koszorús, S. Kujanpää, L. Lalanne,

- G. Neyens, M. Nichols, H. Perrett, J. Reilly, S. Rothe, B. van den Borne, Q. Wang, J. Wessolek, X. Yang, C. Zülch, “Precision spectroscopy and laser cooling scheme of a radium-containing molecule” (2023) *accepted in Nat. Phys.*, preprint: 10.21203/rs.3.rs-2648482/v1.
7. R. Heinke, M. Au, C. Bernerd, K. Chrysalidis, T.E. Cocolios, V. Fedosseev, I. Hendriks, A. Jaradat, M. Kaja, T. Kieck, T. Kron, R. Mancheva, B.A. Marsh, S. Marzari, S. Raeder, S. Rothe, D. Studer, F. Weber, K. Wendt, “First on-line application of the high-resolution spectroscopy laser ion source PI-LIST at ISOLDE”, (2023) *Nucl. Instrum. and Methods B.*, 541 (pp. 8–12) *Proc. EMIS XIX at RAON, 2022*. doi: 10.1016/j.nimb.2023.04.057.
 8. C. Bernerd, J. D. Johnson, E. Aubert, M. Au, V. Barozier, A. P. Bernardes, P. Bertreix, F. Bruchertseifer, R. Catherall, E. Chevally, K. Chrysalidis, P. Christodoulou, T.E. Cocolios, B. Crepieux, M. Deschamps, A. Dorsival, C. Duchemin, V. Fedosseev, P. Fernier, M. Heines, R. Heinke, U. Khalid, M. Khan, Q. Khan, L. Lambert, E. Mamis, B.A. Marsh, S. Marzari, N. Menaa, M. Munos, F. Pozzi, S. Prvakova, J.P. Ramos, F. Riccardi, J.-Y. Rinchet, R.E. Rossel, T. Stora, J. Thiboud, J. Vollaie, V. Van Den Bergh, W. Wojtaczka, the CERN-MEDICIS collaboration, “Production of innovative radioisotopes for medical applications at the CERN-MEDICIS facility” (2023), *Nucl. Instrum. and Methods B.*, 542 (pp. 137–143) *Proc. EMIS XIX at RAON, 2022*. doi: 10.1016/j.nimb.2023.05.008.
 9. M. Schuett, M. Au, M. Bissell, N. Bidault, A. Koliatos, L. Le, N. Azaryan, R. Heinke, K. Chrysalidis, S. Rothe, “Developments at the CERN-ISOLDE Offline 2 mass separator” (2023) *Nucl. Instrum. and Methods B.*, 541, (pp. 82-85). *Proc. EMIS XIX at RAON, 2022*. doi: 10.1016/j.nimb.2023.04.053.
 10. S. Stegemann, D. Atanasov, M. Au, E. Grenier-Boley, M. Butcher, M. Duraffourg, E. Fadakis, T. Feniet, Y.N. Vila Gracia, T. Giles, J. Konki, L. Le, R. Lică, P. Martins, E. Matheson, C. Mihai, R. Martinez Muniz, C. Neacșu, G. Pascovici, K.A. Szczurek, S. Warren, S. Rothe, “The CERN-ISOLDE fast tape station” (2023) *Nucl. Instrum. and Methods B.*, 541, (pp. 169-172). *Proc. EMIS XIX at RAON, 2022*. doi: 10.1016/j.nimb.2023.04.018.
 11. S. Rothe, M. Au, J. Ballof, E. Barbero, M. Bissell, A. Boucherie, M. Bovigny, K. Chrysalidis, B. Crepieux, J. Cruikshank, E. Fadakis, R. Heinke, F. Josa, L. Le, A. Koliatos, E. Piselli, E. Reis, V. Samothrakis, M. Schütt, L. Lambert, D. Leimbach, S. Marzari, M. Owen, S. Stegemann, Y.N. Vila Gracia, “Targets and ion sources at CERN-ISOLDE—Facilities and developments” (2023) *Nucl. Instrum. and Methods B.*, 542, (pp. 38–44). *Proc. EMIS XIX at RAON, 2022*. doi: 10.1016/j.nimb.2023.05.058.
 12. C.S. Sumithrarachchi, Y. Liu, S.N. Rogers, S. Schwarz, G. Bollen, N. Gamage, A. Henriques, A. Lapiere, R. Ringle, I. Yandow, A.C.C. Villari, K.A. Domnanich, S. Satija, G.W. Severin, M. Au, J. Ballof, Y.N. Vila Gracia, M. Owen, E. Reis, S. Rothe, S. Stegemann, “The new Batch Mode Ion Source for stand-alone operation at the Facility for Rare Isotope Beams (FRIB)” (2023) *Nucl. Instrum. and Methods B.*, 541 (pp. 301-304). *Proc. EMIS XIX at RAON, 2022*. doi: 10.1016/j.nimb.2023.05.061.
 13. J. Ballof, N. Nussgart, P. Lalain, M. Au, R. Heinke, D. Leimbach, S. Stegemann, M. Schütt, S. Rothe, Jaideep T. Singh, “Progress towards the FRIB-EDM3-Frontend:

- A tool to provide radioactive molecules from isotope harvesting for fundamental symmetry studies” (2023) *Nucl. Instrum. and Methods B.*, 541, (pp. 224-227). *Proc. EMIS XIX at RAON, 2022*. doi: 10.1016/j.nimb.2023.04.049.
14. G. Arrowsmith-Kron, M. Athanasakis-Kaklamanakis, M. Au, J. Ballof, R. Berger, A. Borschevsky, A. A. Breier, F. Buchinger, D. Budker, L. Caldwell, C. Charles, N. Dattani, R.P. de Groote, D. DeMille, T. Dickel, J. Dobaczewski, Ch. E. Düllmann, E. Eliav, J. Engel, M. Fan, V. Flambaum, K. T. Flanagan, A. Gaiser, R. Garcia Ruiz, K. Gaul, T. F. Giesen, J. Ginges, A. Gottberg, G. Gwinner, R. Heinke, S. Hoekstra, J. D. Holt, N. R. Hutzler, A. Jayich, J. Kartheim, K. G. Leach, K. Madison, S. Malbrunot-Ettenauer, T. Miyagi, I. D. Moore, S. Moroch, P. Navrátil, W. Nazarewicz, G. Neyens, E. Norrgard, N. Nusgart, L. F. Pašteka, A. N. Petrov, W. Plass, R. A. Ready, M. Pascal Reiter, M. Reponen, S. Rothe, M. Safronova, C. Scheidenberger, A. Shindler, J. T. Singh, L. V. Skripnikov, A. V. Titov, S. Udrescu, S.G. Wilkins, X. Yang, “Opportunities for Fundamental Physics Research with Radioactive Molecules”, (2023) *submitted to Rep. Prog. Phys.* arXiv:2302.02165.
 15. M. Urquiza-González, M. Au, C. Bernerd, M. Bissell, B. van den Borne, K. Chrysalidis, T. E. Cocolios, V. N. Fedosseev, K. T. Flanagan, R. G. Garcia Ruiz, S. Geldhof, R. P. de Groote, Á. Koszorús, D. Hanstorp, M. Heines, R. Heinke, K. Hens, O.S. Khwairakpam, S. Kujanpää, L. Lalanne, B. A. Marsh, G. Neyens, M. Nichols, H. Perrett, D. Pitman-Weymouth, J. Reilly, V. Sonnenschein, K. Wendt, J. Wessolek, S. G. Wilkins, X. F. Yang, “Benchmark evaluation for a single frequency continuous wave OPO seeded pulsed dye amplifier for high-resolution laser spectroscopy” (2023) *Proc. SPIE 12399, Solid State Lasers XXXII: Technology and Devices 123990M*, doi: 10.1117/12.2646665.
 16. J. Ballof, M. Au, E. Barbero, K. Chrysalidis, Ch. E. Düllmann, V. Fedosseev, E. Granados, R. Heinke, B. A. Marsh, M. Owen, S. Rothe, T. Stora, A. Yakushev, “A cold electron-impact ion source driven by a photo-cathode – New opportunities for the delivery of radioactive molecular beams?” (2022) *J. Phys. - Conf. Series*. doi: 10.1088/1742-6596/2244/1/012072.
 17. S. Sels, F.M. Maier, M. Au, P. Fischer, C. Kanitz, V. Lagaki, S. Lechner, E. Leisten-schneider, D. Leimbach, E.M. Lykiardopoulou, A. A. Kwiatkowski, T. Manovitz., G. Neyens, S. Rothe, L. Schweikhard, M. Vilen, R. N. Wolf, S. Malbrunot-Ettenauer. “Doppler and sympathetic ion cooling for the investigation of short-lived radionuclides” (2022) *Phys. Rev. Res.* 4, 033229. doi: 10.1103/PhysRevResearch.4.033229.
 18. C. Babcock, T. Day Goodacre, P. Amani, M. Au, P. Bricault, M. Brownell, B. Cade, K. Chen, L. Egoriti, J. Johnson, W. Paley, A. Gottberg. “Offline target and ion source studies for TRIUMF-ARIEL” (2019) *Nucl. Instrum. and Methods B.*, 463 (pp. 464-467) *Proc. EMIS 2018*. doi: 10.1016/j.nimb.2019.04.023.

Proposals

1. M. Au. A. Borschevsky, K. Chrysalidis, R. Crosa-Rossa, Ch. E. Düllmann, R. Heinke, A.H. Jaradat, M. Kaja, B.A. Marsh, I. Moore, A. Raggio, S. Rothe, D. van Eerten, C. Walther, “In-source laser resonance ionization spectroscopy of neptunium and plutonium”, (2022) CERN-INTC-2022-028, Letter of Intent INTC-I-243, CDS No. 2809416.

2. M. Au, M. Athanasakis-Kaklamanakis, J. Ballof, R. Heinke, B. A. Marsh, M. Mougeot, L. Nies, B. Reich, S. Rothe, S. Stegemann “Target and ion source development for LISA”, (8 Nov 2021) Beam time request, CERN, EDMS No. 2669220.
3. M. Au, M. Athanasakis-Kaklamanakis, J. Ballof, R. Heinke, B. A. Marsh, M. Mougeot, L. Nies, B. Reich, S. Rothe, S. Stegemann “Pre-irradiated target investigations under the LISA ITN project at ISOLDE”, (17 March 2021) Beam time request, CERN, EDMS No. 2509744.
4. M. Au, M. Athanasakis-Kaklamanakis, S. Rothe, “A mass spectrometer for molecular ion beam development at ISOLDE OFFLINE”, (19 Aug 2021) SY departmental project proposal, CERN, EDMS No. 2617173.
5. G. Neyens, M. Athanasakis-Kaklamanakis, M. Au, S. Rothe, Ch. E. Düllmann, K. Flanagan, I. Moore, “New opportunities with radioactive molecules” (2023) NuPECC Long Range Plan 2024 contribution, <https://indico.ph.tum.de/event/7050/contributions/>.
6. S. A. Bennett, D. K. Sharp, T. Wright, M. Au, P. A. Butler, A. Camaiani, D. J. Clarke, A. J. Dolan, S. J. Freeman, L. P. Gaffney, K. Garrett, S. A. Giuliani, A. Heinz, H. T. Johansson, B. R. Jones, B. Jonson, A. Kawecka, B. P. Kay, J. Klimo, M. Kowalska, M. Labiche, I. Lazarus, P. T. MacGregor, B. A. Marsh, M. Managlia, G. Martínez-Pinedo, T. Nilsson, J. Ojala, B. Olaizola, R. D. Page, O. Poleshchuk, R. Raabe, S. Reeve, B. Reich, A. Rodriguez, S. Rothe and A. G. Smith, H. Törnqvist, A. Youssef, “Probing the fission and radiative decay of the $^{235}\text{U}+n$ system using (d,pf) and $(d,p\gamma)$ reactions” (2023) CERN-INTC-2023-019, Letter of Intent INTC-P-659, CDS No. 2845988.
7. K. Chrysalidis, R. Heinke, M. Au, C. Bernerd, A. H. Jaradat, U. Köster, R. Mancheva, B. A. Marsh, E. Reis, M. Schütt, S. Rothe, S. Stegemann, J. Wessolek, “Yield measurements for lanthanide elements with Ta-foil target and a LIST ion source” (2022) CERN-INTC-2022-042, Letter of Intent INTC-I-246, CDS No. 2834598.
8. M. Athanasakis-Kaklamanakis, S. Wilkins, M. Au, R. Berger, A. Borschevsky, K. Chrysalidis, T.E. Cocolios, R.P. de Groot, Ch.E. Düllmann, K.T. Flanagan, R.F. Garcia Ruiz, S. Geldhof, R. Heinke, T.A. Isaev, J. Johnson, A. Kiuberis, Á. Koszorús, L. Lalanne, M. Mougeot, G. Neyens, L. Nies, J. Reilly, S. Rothe, L. Schweikhard, A.R. Vernon, X.F. Yang, “Laser ionization spectroscopy of AcF” (2021) CERN-INTC-2021-053, Proposal INTC-P-615, CDS No. 2782407.
9. S. Rothe, M. Au, R. Lica, S. Stegemann, “A dedicated tapestation for machine development at ISOLDE”, (19 Aug 2021) SY departmental project proposal, CERN, EDMS No. 2617167.
10. M. Athanasakis-Kaklamanakis, S. G. Wilkins, T.E. Cocolios, K. T. Flanagan, R. F. Garcia Ruiz, G. Neyens, X. F. Yang, M. Au, R. Berger, M. L. Bissell, A. Borschevsky, A. Breier, A. Brinson, R. P De Groot, Ch. E Düllmann, K. Gaul, S. Geldhof, T. F. Giesen, F. P. Gustafsson, J. Kartheim, Á Koszorús, S. Lechner, S. Malbrunot-Ettenauer, S. Rothe, S. Sels, J. Stohner, S. Udrescu, P. Van Duppen, A. R. Vernon, M. Vilén, “Radioactive molecules at ISOLDE” (2021) CERN-INTC-2021-017, Letter of Intent INTC-I-227, CDS No.2748712.

11. T. Wright, D.K. Sharp, M. Au, S.A. Bennett, P.A. Butler, A. Camaiani, S. J. Freeman, L.P. Gaffney, K. Garrett, S.A. Giuliani, A. Heinz, H.T. Johansson, B. Jonson, B.P. Kay, J. Klimo, M. Kowalska, M. Labiche, I. Lazarus, B. Marsh, T. Nilsson, B. Olaizola, R.D. Page, G. Martínez-Pinedo, R. Raabe, B. Reich, A. Rodriguez, S. Rothe and A.G. Smith, A. Youssef “Fission properties probed via measurements of transfer-induced fission with actinide beams in inverse kinematics using the ISOLDE Solenoidal Spectrometer” (2021) CERN-INTC-2021-009, Letter of Intent INTC-I-224, CDS No. 2748661.
12. R. Heinke, B. Andel, A.N. Andreyev, M. Au, A.E. Barzakh, A.J. Brinson, K. Chrysalidis, T.E. Cocolios, B.S. Cooper, J. Cubiss, H. De Witte, K. Dockx, D.V. Fedorov, V.N. Fedosseev, K.T. Flanagan, R.F. Garcia Ruiz, F.P. Gustafsson, R. Heinke, J. Johnson, M. Kadja, V.Leask, R. Lica, B.A. Marsh, P.L. Molkanov G. Neyens, H.A. Perrett, S. Raeder, B. Reich, C.M. Ricketts, S. Rothe, M.D. Seliverstov, S.M. Udrescu, P. Van Duppen, A.R. Vernon, E. Verstraelen, K. Wendt, J. Wessolek, S.G. Wilkins, W. Wojtaczka, X. F. Yang, “Investigation of octupole deformation in neutron-rich actinium using high-resolution in-source laser spectroscopy” (2020) CERN-INTC-2020-029, Proposal INTC-P-556, CDS No. 2717945.

Bibliography

- [1] N. G. Connelly, T. Damhus, R. M. Hartshorn, A. T. Hutton (Eds.), IUPAC Red Book, RSC Publishing, 2005, Ch. IR-3, pp. 51–52. doi:10.1515/pac-2014-0718.
- [2] F. Kondev, M. Wang, W. Huang, S. Naimi, G. Audi, The NUBASE2020 evaluation of nuclear physics properties, Chinese Physics C 45 (3) (2021) 030001. doi:10.1088/1674-1137/abddae.
- [3] E. M. Holmbeck, R. Surman, A. Frebel, G. C. McLaughlin, M. R. Mumpower, T. M. Sprouse, T. Kawano, N. Vassh, T. C. Beers, Characterizing r-Process Sites through Actinide Production, in: Journal of Physics: Conference Series, Vol. 1668, IOP Publishing, 2020, p. 012020. arXiv:2001.08792, doi:10.1088/1742-6596/1668/1/012020.
- [4] M. R. Mumpower, T. Kawano, T. M. Sprouse, N. Vassh, E. M. Holmbeck, R. Surman, P. Möller, β -delayed Fission in r-process Nucleosynthesis, The Astrophysical Journal 869 (1) (2018) 14. arXiv:1802.04398, doi:10.3847/1538-4357/aaeaca.
- [5] A. N. Andreyev, K. Nishio, K. H. Schmidt, Nuclear fission: A review of experimental advances and phenomenology, Reports on Progress in Physics 81 (1) (2018) 61. doi:10.1088/1361-6633/aa82eb.
- [6] T. Kajino, G. J. Mathews, Impact of new data for neutron-rich heavy nuclei on theoretical models for r-process nucleosynthesis, Reports on Progress in Physics 80 (2017). doi:10.1088/1361-6633/aa6a25.
- [7] K. H. Schmidt, B. Jurado, Review on the progress in nuclear fission - Experimental methods and theoretical descriptions, Reports on Progress in Physics 81 (10) (2018) 64. doi:10.1088/1361-6633/aacfa7.
- [8] V. Radchenko, A. Morgenstern, A. Jalilian, C. Ramogida, C. S. Cutler, C. Duchemin, C. Hoehr, F. Haddad, F. Bruchertseifer, H. Gausemel, H. Yang, J. A. Osso, K. Washiyama, K. Czerwinski, K. Leufgen, M. Pruszynski, O. Valz-dorf, P. Causey, P. Schaffer, R. Perron, M. Samsonov, D. S. Wilbur, T. Stora, Y. Li, Production and supply of alpha particles emitting radionuclides for Targeted Alpha Therapy (TAT), Journal of Nuclear Medicine (2021). doi:10.2967/jnumed.120.261016.
- [9] E. R. Birnbaum, M. E. Fassbender, M. G. Ferrier, K. D. John, T. Mastren, Actinides in Medicine, John Wiley and Sons, Ltd, 2018, pp. 1–21. doi:10.1002/9781119951438.eibc2563.

- [10] A. K. H. Robertson, C. F. Ramogida, P. Schaffer, V. Radchenko, Development of ^{225}Ac Radiopharmaceuticals: TRIUMF Perspectives and Experiences, *Current Radiopharmaceuticals* 11 (3) (2018) 156–172. doi:10.2174/1874471011666180416161908.
- [11] A. Kudo, *Plutonium in the Environment*, Elsevier Science, 2001.
- [12] J. Lee, *Nuclear Reactor Physics and Engineering*, John Wiley and Sons, Inc., 2020. doi:10.1002/9781119582342.
- [13] J. Erler, N. Birge, M. Kortelainen, W. Nazarewicz, E. Olsen, A. M. Perhac, M. Stoitsov, The limits of the nuclear landscape, *Nature* 486 (7404) (2012) 509–512. doi:10.1038/nature11188.
- [14] D. R. McAlister, E. P. Horwitz, Chromatographic generator systems for the actinides and natural decay series elements, *Radiochimica Acta* 99 (3) (2011) 151–159. doi:10.1524/ract.2011.1804.
- [15] S. Hasan, M. A. Prelas, Molybdenum-99 production pathways and the sorbents for 99Mo/99mTc generator systems using (n, γ) 99Mo: a review, *SN Applied Sciences* 2 (11) (2020) 1–28. doi:10.1007/s42452-020-03524-1.
- [16] G. Currie, J. Wheat, R. Davidson, H. Kiat, Radionuclide production, *Radiographer* 58 (3) (2011) 46–52. doi:10.1002/j.2051-3909.2011.tb00155.x.
- [17] R. Catherall, W. Andreazza, M. Breitenfeldt, A. Dorsival, G. J. Focker, T. P. Gharsa, T. J. Giles, J. L. Grenard, F. Locci, P. Martins, S. Marzari, J. Schipper, A. Shornikov, T. Stora, The ISOLDE facility, *Journal of Physics G: Nuclear and Particle Physics* 44 (9) (2017) 1. doi:10.1088/1361-6471/aa7eba.
- [18] CERN, ISOLDE, <https://isolde.cern>, [Online; accessed 01.07.2023] (2023).
- [19] J. Dilling, R. Krücken, L. Merminga, *ISAC and ARIEL: The TRIUMF radioactive beam facilities and the scientific program*, Springer Dordrecht Heidelberg New York London, 2014. doi:10.1007/978-94-007-7963-1.
- [20] TRIUMF, TRIUMF: Canada’s Particle Accelerator Centre, <https://www.triumf.ca>, [Online; accessed 01.07.2023] (2023).
- [21] S. Gales, GANIL-SPIRAL2: a new era, *Journal of Physics: Conference Series* 267 (1) (2011) 012009. doi:10.1088/1742-6596/267/1/012009.
- [22] GANIL SPIRAL2, GANIL, <https://www.ganil-spiral2.eu>, [Online; accessed 01.07.2023] (2023).
- [23] Y. J. Kim, Current status of experimental facilities at RAON, *Nuclear Instruments and Methods in Physics Research Section B: Beam Interactions with Materials and Atoms* 463 (2020) 408–414. doi:10.1016/j.nimb.2019.04.041.
- [24] RAON, IBS, Institute for Basic Science, <https://risp.ibs.re.kr/>, [Online; accessed 01.07.2023] (2020).
- [25] G. de Angelis, the SPES collaboration, G. Prete, A. Andrighetto, M. Manziolaro, S. Corradetti, D. Scarpa, M. Rossignoli, A. Monetti, M. Lollo, M. Calderolla, J. Vasquez, D. Zafiroopoulos, L. Sarchiapone, D. Benini, P. Favaron, M. Rigato, R. Pegoraro, D. Maniero, L. Calabretta, M. Comunian, M. Maggiore, A. Lombardi, L. Piazza, A. M. Porcellato, C. Roncolato, G. Bisoffi, A. Pisent, A. Galatà,

- M. Giacchini, G. Bassato, S. Canella, F. Gramegna, J. Valiente, J. Bermudez, P. F. Mastinu, J. Esposito, J. Wyss, A. Russo, S. Zanella, The SPES Radioactive Ion Beam facility of INFN, *Journal of Physics: Conference Series* 580 (1) (2015) 012014. doi:10.1088/1742-6596/580/1/012014.
- [26] INFN Istituto Nazionale di Fisica Nucleare Laboratori Nazionali di Legnaro, SPES Project, <https://web.infn.it/spes/>, [Online; accessed 01.07.2023] (2023).
- [27] H. A. Abderrahim, P. Baeten, D. D. Bruyn, J. Heyse, P. Schuurmans, J. Wagemans, MYRRHA, a Multipurpose hYbrid Research Reactor for High-end Applications, *Nuclear Physics News* 20 (1) (2010) 24–28. doi:10.1080/10506890903178913.
- [28] MYRRHA, ISOL@MYRRHA, <https://myrrha.be/myrrha-applications/nuclear-science/isolmyrrha>, [Online; accessed 01.07.2023] (2023).
- [29] S. Franchoo, The Alto Tandem and Isol Facility at IPN Orsay, 2014, Ch. 6, p. 020041. doi:10.7566/JSPSC.6.020041.
- [30] Irène Joliot-Curie – IJCLab, Plateforme ALTO Accélérateur Linéaire et Tandem à Orsay, <https://alto.ijclab.in2p3.fr>, [Online; accessed 01.07.2023] (2023).
- [31] J. Äystö, T. Eronen, A. Jokinen, A. Kankainen, I. D. Moore, K. Penttilä, Three decades of research using IGISOL technique at the University of Jyväskylä, Springer Dordrecht Heidelberg New York London, 2014. doi:10.1007/978-94-007-5555-0.
- [32] University of Jyväskylä, Nuclear physics facilities, <https://www.jyu.fi/science/en/physics/research/infrastructures/accelerator-laboratory/nuclear-physics-facilities>, [Online; accessed 01.07.2023] (2022).
- [33] D. Castelvecchi, Long-awaited accelerator ready to explore origins of elements, *Nature* 605 (May) (2022) 201—203. doi:10.1038/d41586-022-00711-5.
- [34] Michigan State University, FRIB | Facility for Rare Isotope Beams | Michigan State University, <https://frib.msu.edu>, [Online; accessed 01.07.2023] (2023).
- [35] Y. Leifels, K. Große, GSI-FAIR SCIENTIFIC REPORT 2022 An overview of the 2022 achievements in science and technology, Tech. rep., GSI Helmholtzzentrum für Schwerionenforschung GmbH, Darmstadt, Germany (2023). doi:10.15120/GSI-2023-00462.
- [36] GSI Helmholtzzentrum für Schwerionenforschung GmbH, GSI - Aktuelles, <https://www.gsi.de/>, [Online; accessed 01.07.2023] (2023).
- [37] Y. Yano, The RIKEN RI Beam Factory Project: A status report, *Nuclear Instruments and Methods in Physics Research, Section B: Beam Interactions with Materials and Atoms* 261 (1-2 SPEC. ISS.) (2007) 1009–1013. doi:10.1016/j.nimb.2007.04.174.
- [38] RIKEN Nishina Center for Accelerator-Based Science, RIBF | Introduction to RI Beam Factory and Users' Information, <https://www.nishina.riken.jp/ribf/>, [Online; accessed 01.07.2023] (2023).
- [39] N. Abrosimov, G. Borukhovich, A. Laptev, V. Marchenkov, G. Petrov, O. Shcherbakov, Y. Tuboltsev, V. Yurchenko, Neutron time-of-flight spectrometer GNEIS at the GATCHINA 1 GeV proton synchrocyclotron, *Nuclear Instruments and Methods in Physics Research Section A: Accelerators, Spectrometers, Detectors and Associated Equipment* 242 (1) (1985) 121–133. doi:10.1016/0168-9002(85)90896-4.

- [40] PNPI, Petersburg Nuclear Physics Institute, <http://www.pnpi.nrcki.ru>, [Online; accessed 01.07.2023] (2023).
- [41] D. J. Morrissey, B. M. Sherrill, In-Flight Separation of Projectile Fragments, Springer Berlin Heidelberg, 2004, Ch. 1, pp. 113–135. doi:10.1007/978-3-540-44490-9_4.
- [42] C. Duchemin, J. P. Ramos, T. Stora, E. Ahmed, E. Aubert, N. Audouin, E. Barbero, V. Barozier, A. P. Bernardes, P. Bertreix, A. Boscher, F. Bruchertseifer, R. Catherall, E. Chevallay, P. Christodoulou, K. Chrysalidis, T. E. Cocolios, J. Comte, B. Crepieux, M. Deschamps, K. Dockx, A. Dorsival, V. N. Fedosseev, P. Fernier, R. Formento-Cavaier, S. El Idrissi, P. Ivanov, V. M. Gadelshin, S. Gilardoni, J. L. Grenard, F. Haddad, R. Heinke, B. Juif, U. Khalid, M. Khan, U. Köster, L. Lambert, G. Lilli, G. Lunghi, B. A. Marsh, Y. M. Palenzuela, R. Martins, S. Marzari, N. Mena, N. Michel, M. Munos, F. Pozzi, F. Riccardi, J. Riegert, N. Riggaz, J. Y. Rinchet, S. Rothe, B. Russell, C. Saury, T. Schneider, S. Stegemann, Z. Talip, C. Theis, J. Thiboud, N. P. van der Meulen, M. van Stenis, H. Vincke, J. Voltaire, N. T. Vuong, B. Webster, K. Wendt, S. G. Wilkins, CERN-MEDICIS: A Review Since Commissioning in 2017, *Frontiers in Medicine* 8 (July) (2021) 1–11. doi:10.3389/fmed.2021.693682.
- [43] O. Kofoed-Hansen, K. Nielsen, Short-lived krypton isotopes and their daughter substances, *Physical Review Journals* 82 (96) (1951) 499. doi:10.1103/PhysRev.82.96.2.
- [44] CERN-ISOLDE, The ISOLDE yield database, version 0.2, <https://cern.ch/isolde-yields>, [Online; accessed 01.03.2022] (2021).
- [45] J. Ballof, C. Seiffert, B. Crepieux, C. E. Düllmann, M. Delonca, M. Gai, A. Gottberg, T. Kröll, R. Lica, M. Madurga Flores, Y. Martinez Palenzuela, T. M. Mendonca, M. Owen, J. P. Ramos, S. Rothe, T. Stora, O. Tengblad, F. Wienholtz, Radioactive boron beams produced by isotope online mass separation at CERN-ISOLDE, *European Physical Journal A* 55 (5) (2019). doi:10.1140/epja/i2019-12719-1.
- [46] K. Johnston, J. Schell, J. G. Correia, M. Deicher, H. P. Gunlaugsson, A. S. Fenta, E. David-Bosne, A. R. Costa, D. C. Lupascu, The solid state physics programme at ISOLDE: Recent developments and perspectives, *Journal of Physics G: Nuclear and Particle Physics* 44 (10) (2017). doi:10.1088/1361-6471/aa81ac.
- [47] A. Jancso, J. G. Correia, A. Gottberg, J. Schell, M. Stachura, D. Szunyogh, S. Pallada, D. C. Lupascu, M. Kowalska, L. Hemmingsen, TDPAC and β -NMR applications in chemistry and biochemistry, *Journal of Physics G: Nuclear and Particle Physics* 44 (6) (2017). doi:10.1088/1361-6471/aa666b.
- [48] H. Fynbo, O. S. Kirseboom, O. Tengblad, ISOLDE decay station for decay studies of interest in astrophysics and exotic nuclei, *Journal of Physics G: Nuclear and Particle Physics* 44 (4) (2017). doi:10.1088/1361-6471/aa5e09.
- [49] D. Lunney, Extending and refining the nuclear mass surface with ISOLTRAP, *Journal of Physics G: Nuclear and Particle Physics* 44 (6) (2017). doi:10.1088/1361-6471/aa6752.
- [50] R. N. Wolf, F. Wienholtz, D. Atanasov, D. Beck, K. Blaum, C. Borgmann, F. Herfurth, M. Kowalska, S. Kreim, Y. A. Litvinov, D. Lunney, V. Manea, D. Neidherr,

- M. Rosenbusch, L. Schweikhard, J. Stanja, K. Zuber, ISOLTRAP's multi-reflection time-of-flight mass separator/spectrometer, *International Journal of Mass Spectrometry* 349-350 (1) (2013) 123–133. doi:10.1016/j.ijms.2013.03.020.
- [51] M. Mukherjee, D. Beck, K. Blaum, G. Bollen, J. Dilling, S. George, F. Herfurth, A. Herlert, A. Kellerbauer, H. J. Kluge, S. Schwarz, L. Schweikhard, C. Yazidjian, ISOLTRAP: An on-line Penning trap for mass spectrometry on short-lived nuclides, *The European Physical Journal A* 35 (1) (2008) 1–29. doi:10.1140/epja/i2007-10528-9.
- [52] V. Fedosseev, K. Chrysalidis, T. D. Goodacre, B. Marsh, S. Rothe, C. Seiffert, K. Wendt, Ion beam production and study of radioactive isotopes with the laser ion source at ISOLDE, *Journal of Physics G: Nuclear and Particle Physics* 44 (8) (2017) 1. doi:10.1088/1361-6471/aa78e0.
- [53] T. E. Cocolios, H. H. Al Suradi, J. Billowes, I. Budinčević, R. P. De Groote, S. De Schepper, V. N. Fedosseev, K. T. Flanagan, S. Franchoo, R. F. Garcia Ruiz, H. Heylen, F. Le Blanc, K. M. Lynch, B. A. Marsh, P. J. Mason, G. Neyens, J. Papuga, T. J. Procter, M. M. Rajabali, R. E. Rossel, S. Rothe, G. S. Simpson, A. J. Smith, I. Strashnov, H. H. Stroke, D. Verney, P. M. Walker, K. D. Wendt, R. T. Wood, The Collinear Resonance Ionization Spectroscopy (CRIS) experimental setup at CERN-ISOLDE, *Nuclear Instruments and Methods in Physics Research, Section B: Beam Interactions with Materials and Atoms* 317 (PART B) (2013) 565–569. doi:10.1016/j.nimb.2013.05.088.
- [54] R. Neugart, J. Billowes, M. L. Bissell, K. Blaum, B. Cheal, K. T. Flanagan, G. Neyens, W. Nörtershäuser, D. T. Yordanov, Collinear laser spectroscopy at ISOLDE: New methods and highlights, *Journal of Physics G: Nuclear and Particle Physics* 44 (6) (2017). doi:10.1088/1361-6471/aa6642.
- [55] A. D. Pietro, K. Riisager, P. V. Duppen, Physics with post-accelerated beams at ISOLDE: Nuclear reactions, *Journal of Physics G: Nuclear and Particle Physics* 44 (4) (2017). doi:10.1088/1361-6471/aa6088.
- [56] P. A. Butler, J. Cederkall, P. Reiter, Nuclear-structure studies of exotic nuclei with MINIBALL, *Journal of Physics G: Nuclear and Particle Physics* 44 (4) (2017). doi:10.1088/1361-6471/aa5c4e.
- [57] K. Wimmer, Nucleon transfer reactions with radioactive beams, *Journal of Physics G: Nuclear and Particle Physics* 45 (3) (2018). doi:10.1088/1361-6471/aaa2bf.
- [58] Y. Kadi, Y. Blumenfeld, W. V. Delsolaro, M. A. Fraser, M. Huyse, A. P. Koufidou, J. A. Rodriguez, F. Wenander, Post-accelerated beams at ISOLDE, *Journal of Physics G: Nuclear and Particle Physics* 44 (8) (2017). doi:10.1088/1361-6471/aa78ca.
- [59] J. P. Ramos, Thick solid targets for the production and online release of radioisotopes: The importance of the material characteristics – A review, *Nuclear Instruments and Methods in Physics Research, Section B: Beam Interactions with Materials and Atoms* 463 (January 2019) (2020) 201–210. doi:10.1016/j.nimb.2019.05.045.
- [60] A. Gottberg, Target materials for exotic ISOL beams, *Nuclear Instruments and Methods in Physics Research, Section B: Beam Interactions with Materials and Atoms* 376 (2016) 8–15. doi:10.1016/j.nimb.2016.01.020.

- [61] R. Kirchner, Release studies of elementary and metal-fluoride ions at the GSI on-line mass separator, *Nuclear Instruments and Methods in Physics Research, Section B: Beam Interactions with Materials and Atoms* 126 (1-4) (1997) 135–140. doi:10.1016/S0168-583X(96)01028-2.
- [62] U. Köster, Yields and spectroscopy of radioactive isotopes at LOHENGRIN and ISOLDE, Doctoral thesis, Technische Universität München, presented on 30 Dec 1999 (2000).
URL <https://cds.cern.ch/record/494272>
- [63] U. Köster, P. Carbonez, A. Dorsival, J. Dvorak, R. Eichler, S. Fernandes, H. Frånberg, J. Neuhausen, Z. Novackova, R. Wilfinger, A. Yakushev, (Im-)possible ISOL beams, in: *European Physical Journal: Special Topics*, Vol. 150, Springer-Verlag, 2007, pp. 285–291. doi:10.1140/epjst/e2007-00326-1.
- [64] U. Köster, O. Arndt, E. Bouquerel, V. N. Fedoseyev, H. Frånberg, A. Joinet, C. Jost, I. S. Kerkines, R. Kirchner, Progress in ISOL target-ion source systems, *Nuclear Instruments and Methods in Physics Research Section B: Beam Interactions with Materials and Atoms* 266 (19-20) (2008) 4229–4239. doi:10.1016/J.NIMB.2008.05.152.
- [65] T. Bjørnstad, E. Hagebø, P. Hoff, O. C. Jonsson, E. Kugler, H. L. Ravn, S. Sundell, B. Vosicki, Methods for production of intense beams of unstable nuclei: New developments at ISOLDE, *Physica Scripta* 34 (6) (1986) 578–590. doi:10.1088/0031-8949/34/6A/013.
- [66] H. Franberg, Production of exotic , short lived carbon isotopes in ISOL-type facilities., Ph.D. thesis, Universität Bern (2008).
URL <http://cds.cern.ch/record/1136904>
- [67] H. Frånberg, M. Ammann, H. W. Gäggeler, U. Köster, Chemical investigations of isotope separation on line target units for carbon and nitrogen beams, *Review of Scientific Instruments* 77 (3) (2006) 1–5. doi:10.1063/1.2171672.
- [68] C. Seiffert, Production of radioactive molecular beams for CERN-ISOLDE, Doctoral thesis, Technische Universität Darmstadt (2015).
URL <https://cds.cern.ch/record/2064456>
- [69] G. Arrowsmith-Kron, M. Athanasakis-Kaklamanakis, M. Au, J. Ballof, R. Berger, A. Borschevsky, A. A. Breier, F. Buchinger, D. Budker, L. Caldwell, C. Charles, N. Dattani, R. P. de Groote, D. DeMille, T. Dickel, J. Dobaczewski, C. E. Düllmann, E. Eliav, J. Engel, M. Fan, V. Flambaum, K. T. Flanagan, A. Gaiser, R. G. Ruiz, K. Gaul, T. F. Giesen, J. Ginges, A. Gottberg, G. Gwinner, R. Heinke, S. Hoekstra, J. D. Holt, N. R. Hutzler, A. Jayich, J. Karthein, K. G. Leach, K. Madison, S. Malbrunot-Ettenauer, T. Miyagi, I. D. Moore, S. Moroch, P. Navrátil, W. Nazarewicz, G. Neyens, E. Norrgard, N. Nusgart, L. F. Paštaka, A. N. Petrov, W. Plass, R. A. Ready, M. P. Reiter, M. Reponen, S. Rothe, M. Safronova, C. Scheidenberger, A. Shindler, J. T. Singh, L. V. Skripnikov, A. V. Titov, S.-M. Udrescu, S. G. Wilkins, X. Yang, Opportunities for Fundamental Physics Research with Radioactive Molecules, *Reports on Progress in Physics* (submitted) (2023).
- [70] M. S. Safronova, D. Budker, D. Demille, D. F. Kimball, A. Derevianko, C. W. Clark, Search for new physics with atoms and molecules, *Reviews of Modern Physics* 90 (2) (2018). arXiv:1710.01833, doi:10.1103/RevModPhys.90.025008.

- [71] M. Athanasakis-Kaklamanakis, S. G. Wilkins, T. E. Cocolios, K. T. Flanagan, R. F. G. Ruiz, G. Neyens, X. F. Yang, M. Au, R. Berger, M. L. Bissell, A. Borschevsky, A. A. Breier, A. Brinson, R. P. De Groote, C. E. Düllmann, K. Gaul, S. Geldhof, T. F. Giesen, F. P. Gustafsson, J. Karthein, Á. Koszorús, S. Lechner, S. Malbrunot-Ettenauer, S. Rothe, S. Sels, J. Stohner, S. Udrescu, P. Van Duppen, A. R. Vernon, M. Vilén, Radioactive molecules at ISOLDE, Tech. rep., CERN, Letter of Intent to the ISOLDE and Neutron Time-of-Flight Committee, Geneva (2020).
URL <https://cds.cern.ch/record/2748712>
- [72] M. Athanasakis-Kaklamanakis, S. G. Wilkins, A. A. Breier, G. Neyens, King-Plot Analysis of Isotope Shifts in Simple Diatomic Molecules, *Physical Review X* 13 (1) (2023) 11015. doi:10.1103/PhysRevX.13.011015.
- [73] J. D. Johnson, M. Heines, F. Bruchertseifer, E. Chevallay, T. E. Cocolios, K. Dockx, C. Duchemin, S. Heinitz, R. Heinke, S. Hurier, L. Lambert, B. Leenders, H. Skliarova, T. Stora, W. Wojtaczka, Resonant laser ionization and mass separation of ^{225}Ac , *Scientific Reports* 13 (1) (2023) 1–11. doi:10.1038/s41598-023-28299-4.
- [74] R. Eder, H. Grawe, E. Hagebø, P. Hoff, E. Kugler, H. L. Ravn, K. Steffensen, The production yields of radioactive ion-beams from fluorinated targets at the ISOLDE on-line mass separator, *Nuclear Inst. and Methods in Physics Research, B* 62 (4) (1992) 535–540. doi:10.1016/0168-583X(92)95387-7.
- [75] J. Ballof, Radioactive Molecular Beams at CERN-ISOLDE, Doctoral thesis, Johannes Gutenberg-Universität Mainz, CERN-THESIS-2021-226 (2021).
URL <https://cds.cern.ch/record/2797475>
- [76] M. Au, J. Ballof, Molecular sidebands for radioactive ion beam extraction (July 2022). doi:10.5281/zenodo.6884293.
- [77] S. M. Udrescu, A. J. Brinson, R. F. G. Ruiz, K. Gaul, R. Berger, J. Billowes, C. L. Binnersley, M. L. Bissell, A. A. Breier, K. Chrysalidis, T. E. Cocolios, B. S. Cooper, K. T. Flanagan, T. F. Giesen, R. P. de Groote, S. Franchoo, F. P. Gustafsson, T. A. Isaev, A. Koszorús, G. Neyens, H. A. Perrett, C. M. Ricketts, S. Rothe, A. R. Vernon, K. D. A. Wendt, F. Wienholtz, S. G. Wilkins, X. F. Yang, Isotope shifts of radium monofluoride molecules, *Phys. Rev. Lett.* 127 (2021) 033001. doi:10.1103/PhysRevLett.127.033001.
- [78] R. F. Garcia Ruiz, R. Berger, J. Billowes, C. L. Binnersley, M. L. Bissell, A. A. Breier, A. J. Brinson, K. Chrysalidis, T. E. Cocolios, B. S. Cooper, K. T. Flanagan, T. F. Giesen, R. P. de Groote, S. Franchoo, F. P. Gustafsson, T. A. Isaev, A. Koszorús, G. Neyens, H. A. Perrett, C. M. Ricketts, S. Rothe, L. Schweikhard, A. R. Vernon, K. D. A. Wendt, F. Wienholtz, S. G. Wilkins, X. F. Yang, Spectroscopy of short-lived radioactive molecules, *Nature* 581 (May) (2020) 396–400. doi:10.1038/s41586-020-2299-4.
- [79] N. R. Hutzler, Polyatomic molecules as quantum sensors for fundamental physics, *Quantum Science and Technology* 5 (4) (2020). arXiv:2008.03398, doi:10.1088/2058-9565/abb9c5.

- [80] F. Herfurth, J. Dilling, A. Kellerbauer, G. Bollen, S. Henry, H. J. Kluge, E. Lamour, D. Lunney, R. B. Moore, C. Scheidenberger, S. Schwarz, G. Sikler, J. Szerypo, A linear radiofrequency ion trap for accumulation, bunching, and emittance improvement of radioactive ion beams, *Nuclear Instruments and Methods in Physics Research, Section A: Accelerators, Spectrometers, Detectors and Associated Equipment* 469 (2) (2001) 254–275. [arXiv:0011021](#), [doi:10.1016/S0168-9002\(01\)00168-1](#).
- [81] M. Fan, C. A. Holliman, X. Shi, H. Zhang, M. W. Straus, X. Li, S. W. Buechele, A. M. Jayich, Optical Mass Spectrometry of Cold RaOH^+ and RaOCH_3^+ , *Physical Review Letters* 126 (2) (2021) 023002. [arXiv:arXiv:2007.11614v1](#), [doi:10.1103/PhysRevLett.126.023002](#).
- [82] L. V. Skripnikov, N. S. Mosyagin, A. V. Titov, V. V. Flambaum, Actinide and lanthanide molecules to search for strong CP-violation, *Physical Chemistry Chemical Physics* 22 (33) (2020) 18374–18380. [doi:10.1039/d0cp01989e](#).
- [83] G. Penyazkov, L. V. Skripnikov, A. V. Oleynichenko, A. V. Zaitsevskii, Effect of the neutron quadrupole distribution in the TaO^+ cation, *Chemical Physics Letters* 793 (February) (2022) 1–4. [doi:10.1016/j.cpllett.2022.139448](#).
- [84] V. V. Flambaum, V. A. Dzuba, Sensitivity of the isotope shift to the distribution of nuclear charge density, *Physical Review A* 100 (3) (2019) 32511. [doi:10.1103/PhysRevA.100.032511](#).
- [85] Planck Collaboration, Adam, R., Ade, P. A. R., Aghanim, N., Akrami, Y., Alves, M. I. R., Argüeso, F., Arnaud, M., Arroja, F., Ashdown, M., Aumont, J., Baccigalupi, C., Ballardini, M., Banday, A. J., Barreiro, R. B., Bartlett, J. G., Bartolo, N., Basak, S., Battaglia, P., Battaner, E., Battye, R., Benabed, K., Benoît, A., Benoit-Lévy, A., Bernard, J.-P., Bersanelli, M., Bertin-court, B., Bielewicz, P., Bikmaev, I., Bock, J. J., Böhringer, H., Bonaldi, A., Bonavera, L., Bond, J. R., Borrill, J., Bouchet, F. R., Boulanger, F., Bucher, M., Burenin, R., Burigana, C., Butler, R. C., Calabrese, E., Cardoso, J.-F., Carvalho, P., Casaponsa, B., Castex, G., Catalano, A., Challinor, A., Chamballu, A., Chary, R.-R., Chiang, H. C., Chluba, J., Chon, G., Christensen, P. R., Church, S., Clemens, M., Clements, D. L., Colombi, S., Colombo, L. P. L., Combet, C., Comis, B., Contreras, D., Couchot, F., Coulais, A., Crill, B. P., Cruz, M., Curto, A., Cuttaia, F., Danese, L., Davies, R. D., Davis, R. J., de Bernardis, P., de Rosa, A., de Zotti, G., Delabrouille, J., Delouis, J.-M., Désert, F.-X., Di Valentino, E., Dickinson, C., Diego, J. M., Dolag, K., Dole, H., Donzelli, S., Doré, O., Douspis, M., Ducout, A., Dunkley, J., Dupac, X., Efstathiou, G., Eisenhardt, P. R. M., Elsner, F., Enßlin, T. A., Eriksen, H. K., Falgarone, E., Fantaye, Y., Farhang, M., Feeney, S., Fergusson, J., Fernandez-Cobos, R., Feroz, F., Finelli, F., Florido, E., Forni, O., Frailis, M., Fraisse, A. A., Franceschet, C., Franceschi, E., Frejsel, A., Frolov, A., Galeotta, S., Galli, S., Ganga, K., Gauthier, C., Génova-Santos, R. T., Gerbino, M., Ghosh, T., Giard, M., Giraud-Héraud, Y., Giusarma, E., Gjerløw, E., González-Nuevo, J., Górski, K. M., Grainge, K. J. B., Gratton, S., Gregorio, A., Gruppuso, A., Gudmundsson, J. E., Hamann, J., Handley, W., Hansen, F. K., Hanson, D., Harrison, D. L., Heavens, A., Helou, G., Henrot-Versillé, S., Hernández-Monteagudo, C., Herranz, D., Hildebrandt, S. R., Hivon, E., Hobson, M., Holmes, W. A., Hornstrup, A., Hovest, W., Huang, Z., Huffenberger, K. M., Hurier, G., Ilić, S., Jaffe, A. H., Jaffe, T. R., Jin, T., Jones, W. C., Juvela, M., Karakci, A., Keihänen, E., Keskitalo, R., Khamitov, I., Kiiveri, K., Kim, J., Kisner,

T. S., Kneissl, R., Knoche, J., Knox, L., Krachmalnicoff, N., Kunz, M., Kurki-Suonio, H., Lacasa, F., Lagache, G., Lähteenmäki, A., Lamarre, J.-M., Langer, M., Lasenby, A., Lattanzi, M., Lawrence, C. R., Le Jeune, M., Leahy, J. P., Lellouch, E., Leonardi, R., León-Tavares, J., Lesgourgues, J., Levrier, F., Lewis, A., Liguori, M., Lilje, P. B., Lilley, M., Linden-Vørnle, M., Lindholm, V., Liu, H., López-Cañiego, M., Lubin, P. M., Ma, Y.-Z., Macías-Pérez, J. F., Maggio, G., Maino, D., Mak, D. S. Y., Mandolesi, N., Mangilli, A., Marchini, A., Marcos-Caballero, A., Marinucci, D., Maris, M., Marshall, D. J., Martin, P. G., Martinelli, M., Martínez-González, E., Masi, S., Matarrese, S., Mazzotta, P., McEwen, J. D., McGehee, P., Mei, S., Meinhold, P. R., Melchiorri, A., Melin, J.-B., Mendes, L., Mennella, A., Migliaccio, M., Mikkelsen, K., Millea, M., Mitra, S., Miville-Deschênes, M.-A., Molinari, D., Moneti, A., Montier, L., Moreno, R., Morgante, G., Mortlock, D., Moss, A., Mottet, S., Münchmeyer, M., Munshi, D., Murphy, J. A., Narimani, A., Naselsky, P., Nastasi, A., Nati, F., Natoli, P., Negrello, M., Netterfield, C. B., Nørgaard-Nielsen, H. U., Noviello, F., Novikov, D., Novikov, I., Olamaie, M., Oppermann, N., Orlando, E., Oxborrow, C. A., Paci, F., Pagano, L., Pajot, F., Paladini, R., Pandolfi, S., Paoletti, D., Partridge, B., Pasian, F., Patanchon, G., Pearson, T. J., Peel, M., Peiris, H. V., Pelkonen, V.-M., Perdureau, O., Perotto, L., Perrott, Y. C., Perrotta, F., Pettorino, V., Piacentini, F., Piat, M., Pierpaoli, E., Pietrobon, D., Plaszczyński, S., Pogosyan, D., Pointecouteau, E., Polenta, G., Popa, L., Pratt, G. W., Prézeau, G., Prunet, S., Puget, J.-L., Rachen, J. P., Racine, B., Reach, W. T., Rebolo, R., Reinecke, M., Remazeilles, M., Renault, C., Renzi, A., Ristorcelli, I., Rocha, G., Roman, M., Romelli, E., Rosset, C., Rossetti, M., Rotti, A., Roudier, G., Rouillé d'Orfeuil, B., Rowan-Robinson, M., Rubiño-Martín, J. A., Ruiz-Granados, B., Rumsey, C., Rusholme, B., Said, N., Salvatelli, V., Salvati, L., Sandri, M., Sanghera, H. S., Santos, D., Saunders, R. D. E., Sauvé, A., Savelainen, M., Savini, G., Schaefer, B. M., Schammel, M. P., Scott, D., Seiffert, M. D., Serra, P., Shellard, E. P. S., Shimwell, T. W., Shiraishi, M., Smith, K., Souradeep, T., Spencer, L. D., Spinelli, M., Stanford, S. A., Stern, D., Stolyarov, V., Stompor, R., Strong, A. W., Sudiwala, R., Sunyaev, R., Sutter, P., Sutton, D., Suur-Uski, A.-S., Sygnet, J.-F., Tauber, J. A., Tavagnacco, D., Terenzi, L., Texier, D., Toffolatti, L., Tomasi, M., Tornikoski, M., Tramonte, D., Tristram, M., Troja, A., Trombetti, T., Tucci, M., Tuovinen, J., Türler, M., Umama, G., Valenziano, L., Valiviita, J., Van Tent, F., Vassallo, T., Vibert, L., Vidal, M., Viel, M., Vielva, P., Villa, F., Wade, L. A., Walter, B., Wandelt, B. D., Watson, R., Wehus, I. K., Welikala, N., Weller, J., White, M., White, S. D. M., Wilkinson, A., Yvon, D., Zacchei, A., Zibin, J. P., Zonca, A., Planck 2015 results - i. overview of products and scientific results, *Astronomy and Astrophysics* 594 (2016) A1. doi:10.1051/0004-6361/201527101.

- [86] Planck Collaboration, P. A. R. Ade, N. Aghanim, M. Arnaud, M. Ashdown, J. Aumont, C. Baccigalupi, A. J. Banday, R. B. Barreiro, N. Bartolo, E. Battaner, R. Battye, K. Benabed, A. Benoît, A. Benoit-Lévy, J. P. Bernard, M. Bersanelli, P. Bielewicz, J. J. Bock, A. Bonaldi, L. Bonavera, J. R. Bond, J. Borrill, F. R. Bouchet, M. Bucher, C. Burigana, R. C. Butler, E. Calabrese, J. F. Cardoso, A. Catalano, A. Challinor, A. Chamballu, H. C. Chiang, P. R. Christensen, S. Church, D. L. Clements, S. Colombi, L. P. L. Colombo, C. Combet, F. Couchot, A. Coulais, B. P. Crill, A. Curto, F. Cuttaia, L. Danese, R. D. Davies, R. J. Davis, P. de Bernardis, A. de Rosa, G. de Zotti, J. Delabrouille, F. X. Désert, J. M. Diego, H. Dole, S. Donzelli, O. Doré, M. Douspis, A. Ducout, X. Dupac, G. Efstathiou, F. Elsner, T. A. Enßlin, H. K. Eriksen, J. Fergusson, F. Finelli,

- O. Forni, M. Frailis, A. A. Fraisse, E. Franceschi, A. Frejsel, S. Galeotta, S. Galli, K. Ganga, M. Giard, Y. Giraud-Héraud, E. Gjerløw, J. González-Nuevo, K. M. Górski, S. Gratton, A. Gregorio, A. Gruppuso, J. E. Gudmundsson, F. K. Hansen, D. Hanson, D. L. Harrison, A. Heavens, G. Helou, S. Henrot-Versillé, C. Hernández-Monteagudo, D. Herranz, S. R. Hildebrandt, E. Hivon, M. Hobson, W. A. Holmes, A. Hornstrup, W. Hovest, Z. Huang, K. M. Huffenberger, G. Hurier, A. H. Jaffe, T. R. Jaffe, W. C. Jones, M. Juvela, E. Keihänen, R. Keskitalo, T. S. Kisner, J. Knoche, M. Kunz, H. Kurki-Suonio, G. Lagache, A. Lähteenmäki, J. M. Lamarre, A. Lasenby, M. Lattanzi, C. R. Lawrence, R. Leonardi, J. Lesgourgues, F. Levrier, A. Lewis, M. Liguori, P. B. Lilje, M. Linden-Vørnle, M. López-Caniego, P. M. Lubin, Y. Z. Ma, J. F. Macías-Pérez, G. Maggio, D. Maino, N. Mandolesi, A. Mangilli, A. Marchini, M. Maris, P. G. Martin, M. Martinelli, E. Martínez-González, S. Masi, S. Matarrese, P. McGehee, P. R. Meinhold, A. Melchiorri, L. Mendes, A. Mennella, M. Migliaccio, S. Mitra, M. A. Miville-Deschênes, A. Moneti, L. Montier, G. Morgante, D. Mortlock, A. Moss, D. Munshi, J. A. Murphy, A. Narimani, P. Naselsky, F. Nati, P. Natoli, C. B. Netterfield, H. U. Nørgaard-Nielsen, F. Noviello, D. Novikov, I. Novikov, C. A. Oxborrow, F. Paci, L. Pagano, F. Pajot, D. Paoletti, F. Pasian, G. Patanchon, T. J. Pearson, O. Perdureau, L. Perotto, F. Perrotta, V. Pettorino, F. Piacentini, M. Piat, E. Pierpaoli, D. Pietrobon, S. Plaszczynski, E. Pointecouteau, G. Polenta, L. Popa, G. W. Pratt, G. Prézeau, S. Prunet, J. L. Puget, J. P. Rachen, W. T. Reach, R. Rebolo, M. Reinecke, M. Remazeilles, C. Renault, A. Renzi, I. Ristorcelli, G. Rocha, C. Rosset, M. Rossetti, G. Roudier, M. Rowan-Robinson, J. A. Rubiño-Martín, B. Rusholme, V. Salvatelli, M. Sandri, D. Santos, M. Savelainen, G. Savini, B. M. Schaefer, D. Scott, M. D. Seiffert, E. P. S. Shellard, L. D. Spencer, V. Stolyarov, R. Stompor, R. Sudiwala, R. Sunyaev, D. Sutton, A. S. Suur-Uski, J. F. Sygnet, J. A. Tauber, L. Terenzi, L. Toffolatti, M. Tomasi, M. Tristram, M. Tucci, J. Tuovinen, L. Valenziano, J. Valiviita, B. Van Tent, M. Viel, P. Vielva, F. Villa, L. A. Wade, B. D. Wandelt, I. K. Wehus, M. White, D. Yvon, A. Zacchei, A. Zonca, Planck 2015 results. XIV. Dark energy and modified gravity, *Astronomy and Astrophysics* 594 (2016) A14. [arXiv:1502.01590](https://arxiv.org/abs/1502.01590), [doi:10.1051/0004-6361/201525814](https://doi.org/10.1051/0004-6361/201525814).
- [87] M. Dine, A. Kusenko, Origin of the matter-antimatter asymmetry, *Rev. Mod. Phys.* 76 (2003) 1–30. [doi:10.1103/RevModPhys.76.1](https://doi.org/10.1103/RevModPhys.76.1).
- [88] T. Mannel, Theory and Phenomenology of CP Violation, *Nuclear Physics B - Proceedings Supplements* 167 (2007) 170–174. [doi:10.1016/j.nuclphysbps.2006.12.083](https://doi.org/10.1016/j.nuclphysbps.2006.12.083).
- [89] A. D. Sakharov, Violation of CP invariance, C asymmetry, and baryon asymmetry of the universe, *Soviet Physics Uspekhi* 34 (5) (1991) 392. [doi:10.1070/PU1991v034n05ABEH002497](https://doi.org/10.1070/PU1991v034n05ABEH002497).
- [90] J. M. Pendlebury, S. Afach, N. J. Ayres, C. A. Baker, G. Ban, G. Bison, K. Bodek, M. Burghoff, P. Geltenbort, K. Green, W. C. Griffith, M. Van Der Grinten, Z. D. Grujić, P. G. Harris, V. Hélaine, P. Iaydjiev, S. N. Ivanov, M. Kasprzak, Y. Kermaidic, K. Kirch, H. C. Koch, S. Komposch, A. Kozela, J. Krempel, B. Lauss, T. Lefort, Y. Lemièrre, D. J. May, M. Musgrave, O. Naviliat-Cuncic, F. M. Piegsa, G. Pignol, P. N. Prashanth, G. Quémener, M. Rawlik, D. Rebreyend, J. D. Richardson, D. Ries, S. Rocca, D. Rozpedzik, A. Schnabel, P. Schmidt-Wellenburg, N. Severijns, D. Shiers, J. A. Thorne, A. Weis, O. J. Winston, E. Wursten, J. Zejma, G. Zsigmond, Revised experimental upper limit on the electric dipole moment of

- the neutron, *Physical Review D - Particles, Fields, Gravitation and Cosmology* 92 (9) (2015) 1–22. [arXiv:1509.04411](#), [doi:10.1103/PhysRevD.92.092003](#).
- [91] V. V. Flambaum, I. B. Samsonov, H. B. T. Tan, Limits on CP-violating hadronic interactions and proton EDM from paramagnetic molecules, *Journal of High Energy Physics* 2020 (10) (Oct. 2020). [doi:10.1007/jhep10\(2020\)077](#).
- [92] T. A. Collaboration, J. Baron, W. C. Campbell, D. DeMille, J. M. Doyle, G. Gabrielse, Y. V. Gurevich, P. W. Hess, N. R. Hutzler, E. Kirilov, I. Kozyryev, B. R. O’Leary, C. D. Panda, M. F. Parsons, E. S. Petrik, B. Spaun, A. C. Vutha, A. D. West, Order of magnitude smaller limit on the electric dipole moment of the electron, *Science* 343 (6168) (2014) 269–272. [doi:10.1126/science.1248213](#).
- [93] V. Andreev, D. G. Ang, D. DeMille, J. M. Doyle, G. Gabrielse, J. Haefner, N. R. Hutzler, Z. Lasner, C. Meisenhelder, B. R. O’Leary, C. D. Panda, A. D. West, E. P. West, X. Wu, Improved limit on the electric dipole moment of the electron, *Nature* 562 (7727) (2018) 355–360. [doi:10.1038/s41586-018-0599-8](#).
- [94] N. Severijns, M. Beck, O. Naviliat-Cuncic, Tests of the standard electroweak model in nuclear beta decay, *Reviews of Modern Physics* 78 (3) (2006) 991–1040. [doi:10.1103/RevModPhys.78.991](#).
- [95] T. S. Roussy, L. Caldwell, T. Wright, W. B. Cairncross, Y. Shagam, K. B. Ng, N. Schlossberger, S. Y. Park, A. Wang, J. Ye, E. A. Cornell, An improved bound on the electron’s electric dipole moment, *Science* 381 (6653) (2023) 46–50. [doi:10.1126/science.adg4084](#).
- [96] D. DeMille, J. M. Doyle, A. O. Sushkov, Probing the frontiers of particle physics with tabletop-scale experiments, *Science* 357 (6355) (2017) 990–994. [doi:10.1126/science.aal3003](#).
- [97] V. Flambaum, M. Pospelov, A. Ritz, Y. Stadnik, Sensitivity of EDM experiments in paramagnetic atoms and molecules to hadronic cp violation, *Physical Review D* 102 (3) (Aug. 2020). [doi:10.1103/physrevd.102.035001](#).
- [98] I. Kozyryev, N. R. Hutzler, Precision Measurement of Time-Reversal Symmetry Violation with Laser-Cooled Polyatomic Molecules, *Physical Review Letters* 119 (13) (2017) 1–6. [arXiv:1705.11020](#), [doi:10.1103/PhysRevLett.119.133002](#).
- [99] N. R. Hutzler, A. Borschevsky, D. Budker, D. DeMille, V. V. Flambaum, G. Gabrielse, R. F. G. Ruiz, A. M. Jayich, L. A. Orozco, M. Ramsey-Musolf, M. Reece, M. S. Safronova, J. T. Singh, M. R. Tarbutt, T. Zelevinsky, Searches for new sources of CP violation using molecules as quantum sensors (2020) 1–5 [arXiv:2010.08709](#).
- [100] V. Flambaum, I. Samsonov, H. T. Tan, Effects of cp-violating internucleon interactions in paramagnetic molecules, *Physical Review D* 102 (11) (Dec 2020). [doi:10.1103/physrevd.102.115036](#).
- [101] Y. V. Stadnik, V. A. Dzuba, V. V. Flambaum, Improved Limits on Axionlike-Particle-Mediated P,T-Violating Interactions between Electrons and Nucleons from Electric Dipole Moments of Atoms and Molecules, *Physical Review Letters* 120 (1) (2018) 013202. [doi:10.1103/PhysRevLett.120.013202](#).

- [102] V. V. Flambaum, Enhanced nuclear Schiff moment and time-reversal violation in Th 229 -containing molecules, *Physical Review C* 99 (3) (2019) 35501. [arXiv:1808.03629](#), [doi:10.1103/PhysRevC.99.035501](#).
- [103] R. Kirchner, A. Piotrowski, Thermal ionization in a hot cavity, *Nuclear Instruments and Methods* 153 (1) (1978) 291–292. [doi:10.1016/0029-554X\(78\)90653-5](#).
- [104] R. Kirchner, Ion sources for radioactive beams and related problems (Review) (invited), *Review of Scientific Instruments* 67 (3) (1996) 928–933. [doi:10.1063/1.1146774](#).
- [105] R. Kirchner, Review of ISOL target-ion-source systems, *Nuclear Instruments and Methods in Physics Research, Section B: Beam Interactions with Materials and Atoms* 204 (2003) 179–190. [doi:10.1016/S0168-583X\(02\)01900-6](#).
- [106] M. Huyse, Ionization in a hot cavity, *Nuclear Instruments and Methods in Physics Research* 215 (1) (1983) 1–5. [doi:10.1016/0167-5087\(83\)91284-X](#).
- [107] M. Turek, A. Droédziel, K. Pysznik, D. Mączka, B. Słowiński, Simulations of ionization in a hot cavity surface ion source, *Review of Scientific Instruments* 83 (2) (2012) 023303. [doi:10.1063/1.3685247](#).
- [108] R. Heinke, E. Chevallay, K. Chrysalidis, T. E. Cocolios, C. Duchemin, V. N. Fedosseev, S. Hurier, L. Lambert, B. Leenders, B. A. Marsh, N. P. van der Meulen, P. Sprung, T. Stora, M. Tosato, S. G. Wilkins, H. Zhang, Z. Talip, Efficient Production of High Specific Activity Thulium-167 at Paul Scherrer Institute and CERN-MEDICIS, *Frontiers in Medicine* 8 (2021). [doi:10.3389/fmed.2021.712374](#).
- [109] S. Rothe, T. Day Goodacre, D. V. Fedorov, V. N. Fedosseev, B. A. Marsh, P. L. Molkanov, R. E. Rossel, M. D. Seliverstov, M. Veinhard, K. D. Wendt, Laser ion beam production at CERN-ISOLDE: New features - More possibilities, *Nuclear Instruments and Methods in Physics Research, Section B: Beam Interactions with Materials and Atoms* 376 (2016) 91–96. [doi:10.1016/j.nimb.2016.02.024](#).
- [110] X. F. Yang, S. J. Wang, S. G. Wilkins, R. F. Ruiz, Laser spectroscopy for the study of exotic nuclei, *Progress in Particle and Nuclear Physics* 129 (2023) 104005. [doi:10.1016/j.pnpnp.2022.104005](#).
- [111] B. A. Marsh, T. Day Goodacre, S. Sels, Y. Tsunoda, B. Andel, A. N. Andreyev, N. A. Althubiti, D. Atanasov, A. E. Barzakh, J. Billowes, K. Blaum, T. E. Cocolios, J. G. Cubiss, J. Dobaczewski, G. J. Farooq-Smith, D. V. Fedorov, V. N. Fedosseev, K. T. Flanagan, L. P. Gaffney, L. Ghys, M. Huyse, S. Kreim, D. Lunney, K. M. Lynch, V. Manea, Y. Martinez Palenzuela, P. L. Molkanov, T. Otsuka, A. Pastore, M. Rosenbusch, R. E. Rossel, S. Rothe, L. Schweikhard, M. D. Seliverstov, P. Spagnoletti, C. Van Beveren, P. Van Duppen, M. Veinhard, E. Verstraelen, A. Welker, K. Wendt, F. Wienholtz, R. N. Wolf, A. Zadornaya, K. Zuber, Characterization of the shape-staggering effect in mercury nuclei, *Nature Physics* 14 (12) (2018) 1163–1167. [doi:10.1038/s41567-018-0292-8](#).
- [112] R. Heinke, M. Au, C. Bernerd, K. Chrysalidis, T. E. Cocolios, V. N. Fedosseev, I. Hendriks, A. A. Jaradat, M. Kaja, T. Kieck, T. Kron, R. Mancheva, B. A. Marsh, S. Marzari, S. Raeder, S. Rothe, D. Studer, F. Weber, K. Wendt, First on-line application of the high-resolution spectroscopy laser ion source PI-LIST at ISOLDE, *Nuclear Instruments and Methods in Physics Research Section B: Beam Interactions with Materials and Atoms* 541 (2023) 8–12. [doi:10.1016/J.NIMB.2023.04.057](#).

- [113] D. A. Fink, S. D. Richter, B. Bastin, K. Blaum, R. Catherall, T. E. Cocolios, D. V. Fedorov, V. N. Fedosseev, K. T. Flanagan, L. Ghys, A. Gottberg, N. Imai, T. Kron, N. Lecesne, K. M. Lynch, B. A. Marsh, T. M. Mendonca, D. Pauwels, E. Rapisarda, J. P. Ramos, R. E. Rossel, S. Rothe, M. D. Seliverstov, M. Sjödin, T. Stora, C. Van Beveren, K. D. Wendt, First application of the Laser Ion Source and Trap (LIST) for on-line experiments at ISOLDE, *Nuclear Instruments and Methods in Physics Research, Section B: Beam Interactions with Materials and Atoms* 317 (PART B) (2013) 417–421. doi:10.1016/j.nimb.2013.06.039.
- [114] R. Heinke, T. Kron, S. Raeder, T. Reich, P. Schönberg, M. Trümper, C. Weichhold, K. Wendt, High-resolution in-source laser spectroscopy in perpendicular geometry: Development and application of the PI-LIST, *Hyperfine Interactions* 238 (1) (2017). doi:10.1007/s10751-016-1386-2.
- [115] P. Kunz, G. Huber, G. Passler, N. Trautmann, Efficient three-step, two-color ionization of plutonium using a resonance enhanced 2-photon transition into an autoionizing state, *European Physical Journal D* 29 (2) (2004) 183–188. doi:10.1140/epjd/e2004-00024-4.
- [116] N. Kneip, C. E. Düllmann, V. Gadelshin, R. Heinke, C. Mokry, S. Raeder, J. Runke, D. Studer, N. Trautmann, F. Weber, K. Wendt, Highly selective two-step laser ionization schemes for the analysis of actinide mixtures, *Hyperfine Interactions* 241 (1) (2020) 1–7. doi:10.1007/s10751-020-01712-4.
- [117] M. Block, M. Laatiaoui, S. Raeder, Recent progress in laser spectroscopy of the actinides, *Progress in Particle and Nuclear Physics* 116 (2021) 0–1. arXiv:2010.11941, doi:10.1016/j.pnpnp.2020.103834.
- [118] L. Penescu, R. Catherall, J. Lettry, T. Stora, Development of high efficiency Versatile Arc Discharge Ion Source at CERN ISOLDE, *Review of Scientific Instruments* 81 (2) (2010) 1–5. doi:10.1063/1.3271245.
- [119] R. Kirchner, E. Roeckl, Investigation of small-volume gaseous discharge ion sources for isotope separation on-line, *Nuclear Instruments and Methods* 131 (2) (1975) 371–374. doi:10.1016/0029-554X(75)90342-0.
- [120] F. Maldonado, Comprehensive ionization model development for the FEBIAD ion source and its application for TRIUMF’s radioactive ion beam program, Doctoral thesis, University of Victoria (2022).
- [121] L. C. Penescu, Techniques to produce and accelerate radioactive ion beams, Doctoral thesis, Polytechnic Institute Bucharest, presented 2009 (2009). URL <https://cds.cern.ch/record/2259078>
- [122] J. Ballof, K. Chrysalidis, C. E. Düllmann, V. Fedosseev, E. Granados, D. Leimbach, B. A. Marsh, J. P. Ramos, A. Ringvall-Moberg, S. Rothe, T. Stora, S. G. Wilkins, A. Yakushev, A concept for the extraction of the most refractory elements at CERN-ISOLDE as carbonyl complex ions, *European Physical Journal A* 58 (5) (2022) 1–18. doi:10.1140/epja/s10050-022-00739-1.
- [123] J. Ballof, M. Au, E. Barbero, K. Chrysalidis, C. E. Düllmann, V. Fedosseev, E. Granados, R. Heinke, B. A. Marsh, M. Owen, S. Rothe, T. Stora, A. Yakushev, A cold electron-impact ion source driven by a photo-cathode - New opportunities for the delivery of radioactive molecular beams?, *Journal of Physics: Conference Series* 2244 (1) (2022). doi:10.1088/1742-6596/2244/1/012072.

- [124] D. Stresau, K. Hunter, W. Sheils, P. Raffin, Y. Benari, A new class of robust sub-nanosecond ToF detectors with high dynamic range, 54th ASMS Conference on Mass Spectroscopy, Seattle, Washington (2006).
URL <https://www.etp-ms.com/faqs/literature>
- [125] Cronologic, TimeTagger Product Brief, <https://download.cronologic.de/TimeTagger/TimeTagger4-product-brief.pdf>, accessed: 2022-04-20 (2022).
- [126] A. Voss, V. Sonnenschein, P. Campbell, B. Cheal, T. Kron, I. D. Moore, I. Pohjalainen, S. Raeder, N. Trautmann, K. Wendt, High-resolution laser spectroscopy of long-lived plutonium isotopes, *Physical Review A* 95 (3) (2017) 1–11. arXiv: 1703.01845, doi:10.1103/PhysRevA.95.032506.
- [127] H. J. Kluge, Penning trap mass spectrometry of radionuclides, *International Journal of Mass Spectrometry* 349-350 (1) (2013) 26–37. doi:10.1016/j.ijms.2013.04.017.
- [128] F. Wienholtz, D. Beck, K. Blaum, C. Borgmann, M. Breitenfeldt, R. B. Cakirli, S. George, F. Herfurth, J. D. Holt, M. Kowalska, S. Kreim, D. Lunney, V. Manea, J. Menéndez, D. Neidherr, M. Rosenbusch, L. Schweikhard, A. Schwenk, J. Simonis, J. Stanja, R. N. Wolf, K. Zuber, Masses of exotic calcium isotopes pin down nuclear forces, *Nature* 498 (7454) (2013) 346–349. doi:10.1038/nature12226.
- [129] L. Nies, D. Atanasov, M. Athanasakis-Kaklamanakis, M. Au, K. Blaum, J. Dobaczewski, B. S. Hu, J. Holt, J. Kartheim, I. Kulikov, Y. A. Litvinov, D. Lunney, V. Manea, T. Miyagi, M. Mougeot, L. Schweikhard, A. Schwenk, K. Sieja, F. Wienholtz, Isomeric excitation energy for $^{99}\text{In}^m$ from mass spectrometry reveals constant trend next to doubly magic ^{100}Sn , Accepted in *Physical Review Letters* (2023).
- [130] P. Fischer, L. Schweikhard, Multiple-ion-ejection multi-reflection time-of-flight mass spectrometry for single-reference mass measurements with lapping ion species, *Review of Scientific Instruments* 91 (2) (2020) 023201. doi:10.1063/1.5131582.
- [131] S. Stegemann, D. Atanasov, M. Au, E. Grenier-Boley, M. Butcher, M. Duraffourg, E. Fadakis, T. Feniet, Y. N. Gracia, T. Giles, J. Konki, L. Le, R. Lică, P. Martins, E. Matheson, C. Mihai, R. M. Muniz, C. Neacșu, G. Pascovici, K. A. Szczurek, S. Warren, S. Rothe, The CERN-ISOLDE fast tape station, *Nuclear Instruments and Methods in Physics Research, Section B: Beam Interactions with Materials and Atoms* 541 (May) (2023) 169–172. doi:10.1016/j.nimb.2023.04.018.
- [132] I. Pohjalainen, I. D. Moore, T. Kron, S. Raeder, V. Sonnenschein, H. Tomita, N. Trautmann, A. Voss, K. Wendt, In-gas-cell laser ionization studies of plutonium isotopes at IGISOL, *Nuclear Instruments and Methods in Physics Research, Section B: Beam Interactions with Materials and Atoms* 376 (2016) 233–239. doi:10.1016/j.nimb.2016.02.019.
- [133] M. Au, B. Reich, S. Rothe, V. Fedosseev, Pre-irradiated target investigations under the LISA ITN project at ISOLDE, Tech. rep., CERN (March 2021).
URL <https://edms.cern.ch/document/2509744/1>
- [134] C. Duchemin, T. Cocolios, M. Fedosseev, B. Marsh, S. Rothe, T. Stora, Radionuclide inventory in targets irradiated at ISOLDE before LS2 in view of long half-life actinide collections at CERN-MEDICIS, Tech. rep., CERN (2020).

- [135] M. Au, M. Athanasakis-Kaklamanakis, J. Ballof, R. Heinke, B. Marsh, M. Mougeot, L. Nies, B. Reich, S. Rothe, S. Stegemann, Target and ion source development for laser ionization and spectroscopy of the actinides, Tech. rep., CERN (Dec 2021). URL <https://edms.cern.ch/document/2669220/1>
- [136] H. De Witte, A. N. Andreyev, S. Dean, S. Franchoo, M. Huyse, O. Ivanov, U. Köster, W. Kurcewicz, J. Kurpeta, A. Plochocki, K. Van De Vel, J. Van De Walle, P. Van Duppen, Alpha-decay of neutron-deficient ^{200}Fr and heavier neighbours, *European Physical Journal A* 23 (2) (2005) 243–247. doi:10.1140/epja/i2004-10077-9.
- [137] G. J. Deblonde, M. Zavarin, A. B. Kersting, The coordination properties and ionic radius of actinium: A 120-year-old enigma, *Coordination Chemistry Reviews* 446 (2021) 214130. doi:10.1016/j.ccr.2021.214130.
- [138] R. Heinke, B. Andel, A. N. Andreyev, M. Au, A. E. Barzakh, A. J. Brinson, K. Chrysalidis, T. E. Cocolios, B. S. Cooper, J. Cubiss, H. D. Witte, K. Dockx, D. V. Fedorov, V. N. Fedosseev, K. T. Flanagan, R. F. G. Ruiz, F. P. Gustafsson, J. Johnson, M. Kadja, V. Leask, R. Lică, B. A. Marsh, P. L. Molkanov, G. Neyens, H. A. Perrett, S. Raeder, B. Reich, C. M. Ricketts, S. Rothe, M. D. Seliverstov, S. M. Udrescu, P. Van Duppen, A. R. Vernon, E. Verstraelen, K. Wendt, J. Wessolek, S. G. Wilkins, W. Wojtaczka, X. F. Yang, Investigation of octupole deformation in neutron-rich actinium using high-resolution in-source laser spectroscopy, Tech. rep., CERN, Proposal to the ISOLDE and Neutron Time-of-Flight Committee, Geneva (2020). URL <https://cds.cern.ch/record/2717945>
- [139] R. Eychenne, M. Chérel, F. Haddad, F. Guérard, J. F. Gestin, Overview of the most promising radionuclides for targeted alpha therapy: The “hopeful eight”, *Pharmaceutics* 13 (6) (2021). doi:10.3390/pharmaceutics13060906.
- [140] A. Guglielmetti, R. Bonetti, G. Ardisson, V. Barci, T. Giles, M. Hussonnois, J. L. Du, C. L. Naour, V. L. Mikheev, L. Pasinetti, H. Ravn, S. Tretyakova, D. Trubert, New measurement of exotic decay of ^{225}Ac by ^{14}C emission, *European Physical Journal A* 12 (2002) 383–386. doi:10.1007/s10050-001-8661-5. URL <https://hal.in2p3.fr/in2p3-00011028>
- [141] K. Dockx, F. Bruchertseifer, T. E. Cocolios, M. Dierckx, V. N. Fedosseev, A. Fenwick, T. Giles, D. Hougbo, S. Judge, J. Keightley, B. A. Marsh, Y. Martinez, A. Morgenstern, A. Pearce, L. Popescu, A. P. Robinson, S. Rothe, S. Stegemann, T. Stora, Towards reliable production of ^{225}Ac for medical applications: Systematic analysis of the production of Fr, Ra and Ac beams, Tech. rep., CERN, Letter of Intent to the ISOLDE and Neutron Time-of-Flight Committee, Geneva (2017). URL <https://cds.cern.ch/record/2241281>
- [142] E. Jajčičinová, K. Dockx, T. Cocolios, B. Cooper, K. Chrysalidis, D. Fedorov, V. Fedosseev, K. Flanagan, M. Griseri, D. Hougbo, A. Kellerbauer, S. Kraemer, B. Marsh, L. Popescu, J. Ramos, S. Rothe, M. Seliverstov, S. Sels, G. Smith, S. Stegemann, M. Stryczyk, V. Verelst, Impact of the laser ionisation and temperature on the Actinium production from UCx target, Zenodo, 2023, Ch. 24, pp. 84–86. doi:10.5281/zenodo.7913190.
- [143] S. Rothe, M. Klein, RILIS Database— an ionization scheme database for laser ion sources (2021). URL <https://cern.ch/riliselements>

- [144] A. Andreyev, B. . Andel, S. Antalic, A. E. Barzakh, T. Berry, M. J. G Borge, J. A. Briz, A. Broniš, T. E. Cocolios, K. Chrysalidis, J. G. Cubiss, H. De Witte, K. Dockx, D. V. Fedorov, V. N. Fedosseev, L. M. Fraile, L. Gaffney, G. Georgiev, P. T. Greenlees, L. J. Harkness-Brennan, R. Heinke, A. Illana, J. Johnson, D. T. Joss, D. S. Judson, U. Koester, J. Konki, J. Kurcewicz, I. Lazarus, R. Lică, M. Madurga, N. Marginean, B. A. Marsh, C. Mihai, P. L. Molkanov, P. Mosat, E. Nacher, A. Negret, K. Nishio, R. D. Page, S. Pascu, A. Perea, V. Pucknell, P. Rahkila, E. Rapisarda, S. Rothe, M. D. Seliverstov, A. Stott, C. Sotty, M. Stryczyk, O. Tengblad, I. Tsekhanovich, P. Van Duppen, V. Vedia, R. Wadsworth, N. Warr, S. G. Wilkins, Y. Watanabe, Y. Hirayama, M. Mukai, S. Iimura, H. Watanabe, A. Algora, P. Jones, Feasibility studies towards the systematic investigation of the β -delayed fission in the neutron-rich actinides., Tech. rep., CERN, Letter of Intent to the ISOLDE and Neutron Time-of-Flight Committee (2020).
URL <https://cds.cern.ch/record/2717968>
- [145] R. Heinke, A. Jaradat, Implementation of PI-LIST at ISOLDE, Tech. rep., EU H2020 LISA MSCA ITN (Oct. 2022). doi:10.5281/zenodo.7824897.
- [146] B. Eichler, S. Hübener, H. Rossbach, Adsorption flüchtiger Metalle auf metallischen Oberflächen und ihre Anwendung in der Kernchemie: Berechnung der Enthalpie der dissoziativen Chemisorption von Monooxiden der Seltenerdmetalle und Actinoide, Tech. rep., Rossendorf Fachinformations-Zentrum. Zentral-Inst., Dresden (1986).
URL <https://cds.cern.ch/record/176614>
- [147] N. Edelstein, J. Fuger, L. Morss, J. Katz, The Chemistry of the Actinide and Transactinide Elements, Springer, 2006.
- [148] I. Pohjalainen, I. D. Moore, S. Geldhof, V. Rosecker, J. Sterba, T. Schumm, Gas cell studies of thorium using filament dispensers at IGISOL, Nuclear Instruments and Methods in Physics Research, Section B: Beam Interactions with Materials and Atoms 484 (March) (2020) 59–70. doi:10.1016/j.nimb.2020.08.012.
- [149] S. Kraemer, J. Moens, M. Athanasakis-Kaklamanakis, S. Bara, K. Beeks, P. Chhetri, K. Chrysalidis, A. Claessens, T. E. Cocolios, J. M. Correia, H. De Witte, R. Ferrer, S. Geldhof, R. Heinke, N. Hosseini, M. Huyse, U. Köster, Y. Kudryavtsev, M. Laatiaoui, R. Lica, G. Magchiels, V. Manea, C. Merckling, L. M. C. Pereira, S. Raeder, T. Schumm, S. Sels, P. G. Thirof, S. M. Tunhuma, P. V. D. Bergh, P. Van Duppen, A. Vantomme, M. Verlinde, R. Villarreal, U. Wahl, Observation of the radiative decay of the ^{229}Th nuclear clock isomer, Nature 617 (May) (2022) 706–710. arXiv:2209.10276, doi:10.1038/s41586-023-05894-z.
- [150] P. Naubereit, T. Gottwald, D. Studer, K. Wendt, Excited atomic energy levels in protactinium by resonance ionization spectroscopy, Physical Review A 98 (2) (2018) 1–6. doi:10.1103/PhysRevA.98.022505.
- [151] S. Cotton, Lanthanide and Actinide Chemistry, John Wiley and Sons, Ltd, 2006. doi:10.1002/0470010088.
- [152] M. R. Savina, B. H. Isselhardt, A. Kucher, R. Trappitsch, B. V. King, D. Ruddle, R. Gopal, I. Hutcheon, High Useful Yield and Isotopic Analysis of Uranium by Resonance Ionization Mass Spectrometry, Analytical Chemistry 89 (11) (2017) 6224–6231. doi:10.1021/acs.analchem.7b01204.

- [153] M. Au, M. Athanasakis-Kaklamanakis, L. Nies, J. Ballof, R. Berger, K. Chrysalidis, P. Fischer, R. Heinke, J. Johnson, U. Köster, D. Leimbach, B. Marsh, M. Mougeot, B. Reich, J. Reilly, E. Reis, M. Schlaich, C. Schweiger, L. Schweikhard, S. Stegemann, J. Wessolek, F. Wienholtz, S. G. Wilkins, W. Wojtaczka, C. E. Düllmann, S. Rothe, In-source and in-trap formation of molecular ions in the actinide mass range at CERN-ISOLDE, *Nucl. Instrum. Methods B* 541 (2023) 375–379. doi:10.1016/j.nimb.2023.05.015.
- [154] M. Laatiaoui, W. Lauth, H. Backe, M. Block, D. Ackermann, B. Cheal, P. Chhetri, C. E. Düllmann, P. Van Duppen, J. Even, R. Ferrer, F. Giacoppo, S. Götz, F. P. Heßberger, M. Huyse, O. Kaleja, J. Khuyagbaatar, P. Kunz, F. Lautenschläger, A. K. Mistry, S. Raeder, E. M. Ramirez, T. Walther, C. Wraith, A. Yakushev, Atom-at-a-time laser resonance ionization spectroscopy of nobelium, *Nature* 538 (7626) (2016) 495–498. doi:10.1038/nature19345.
- [155] P. Kunz, J. Lassen, C. Andreoiu, F. H. Garcia, Transuranium isotopes at ISAC/TRIUMF, *Nuclear Instruments and Methods in Physics Research, Section B: Beam Interactions with Materials and Atoms* 534 (November 2022) (2023) 90–96. doi:10.1016/j.nimb.2022.11.006.
- [156] M. Au, M. Athanasakis-Kaklamanakis, L. Nies, R. Heinke, K. Chrysalidis, U. Köster, P. Kunz, B. Marsh, M. Mougeot, L. Schweikhard, S. Stegemann, Y. V. Gracia, C. E. Düllmann, S. Rothe, Production of neptunium and plutonium nuclides from uranium carbide using 1.4-GeV protons, *Phys. Rev. C* 107 (6) (2023) 064604. doi:10.1103/PhysRevC.107.064604.
- [157] M. Kaja, Resonance laser ionization of neptunium isotopes, Doctoral thesis, Johannes Gutenberg-Universität Mainz, in preparation (2000).
- [158] M. Au, A. Borschevsky, K. Chrysalidis, R. Crosa-Rossa, C. Düllmann, R. Heinke, A. Jaradat, M. Kaja, B. Marsh, I. Moore, A. Raggio, S. Rothe, S. Stegemann, D. van Eerten, C. Walther, In-source laser resonance ionization spectroscopy of neptunium and plutonium, Tech. rep., CERN, Letter of Intent to the ISOLDE and Neutron Time-of-Flight Committee, Geneva (2022). URL <https://cds.cern.ch/record/2809416>
- [159] V. V. Flambaum, D. Demille, M. G. Kozlov, Time-reversal symmetry violation in molecules induced by nuclear magnetic quadrupole moments, *Physical Review Letters* 113 (10) (2014). doi:10.1103/PhysRevLett.113.103003.
- [160] M. Athanasakis-Kaklamanakis, S. G. Wilkins, M. Au, R. Berger, A. Borschevsky, K. Chrysalidis, T. E. Cocolios, R. P. De Groote, K. T. Flanagan, R. F. G. Ruiz, S. Geldhof, R. Heinke, T. A. Isaev, J. Johnson, A. Kiuberis, L. Lalanne, M. Mougeot, G. Neyens, L. Nies, J. Reilly, S. Rothe, L. Schweikhard, A. R. Vernon, X. F. Yang, Laser ionization spectroscopy of AcF, Tech. rep., CERN, Letter of Intent to the ISOLDE and Neutron Time-of-Flight Committee (2021).
- [161] L. V. Skripnikov, A. V. Oleynichenko, A. Zaitsevskii, N. S. Mosyagin, M. Athanasakis-Kaklamanakis, M. Au, G. Neyens, *ab initio* study of electronic states and radiative properties of the AcF molecule, *Journal of Physical Chemistry* 159 (2023) 124301. doi:10.1063/5.0159888.
- [162] J. E. Gaiser, Charmonium Spectroscopy from Radiative Decays of the J/Psi and Psi Prime, Ph. D. dissertation, Stanford University (1982).

- [163] A. Nylandsted Larsen, G. Bortels, B. Denecke, Satellite peaks in high-resolution alpha-particle spectra of decay-chain members measured with silicon surface-barrier detectors, *Nuclear* 219 (1984) 339–346.
- [164] M. Basunia, Nuclear Data Sheets for A=213, *Nuclear Data Sheets* 181 (2022) 475–585. doi:10.1016/j.nds.2022.03.002.
- [165] F. Kondev, E. McCutchan, B. Singh, K. Banerjee, S. Bhattacharya, A. Chakraborty, S. Garg, N. Jovancevic, S. Kumar, S. Rathi, T. Roy, J. Lee, R. Shearman, Nuclear Data Sheets for A=217, *Nuclear Data Sheets* 147 (2018) 382–458. doi:10.1016/j.nds.2018.01.002.
- [166] A. Kumar Jain, S. Singh, S. Kumar, J. K. Tuli, Nuclear Data Sheets for A = 221, *Nuclear Data Sheets* 108 (4) (2007) 883–922. doi:10.1016/j.nds.2007.03.002.
- [167] J. Chen, F. Kondev, Nuclear Data Sheets for A = 209, *Nuclear Data Sheets* 126 (2015) 373–546. doi:10.1016/j.nds.2015.05.003.
- [168] C. Ahdida, D. Bozzato, D. Calzolari, F. Cerutti, N. Charitonidis, A. Cimmino, A. Coronetti, G. L. D’Alessandro, A. D. Servelle, L. S. Esposito, R. Froeschl, R. G. Alía, A. Gerbershagen, S. Gilardoni, D. Horváth, G. Hugo, A. Infantino, V. Kouskoura, A. Lechner, B. Lefebvre, G. Lerner, M. Magistris, A. Manousos, G. Moryc, F. O. Ruiz, F. Pozzi, D. Prelicpean, S. Roesler, R. Rossi, M. S. Gilarte, F. S. Pujol, P. Schoofs, V. Stránský, C. Theis, A. Tsinganis, R. Versaci, V. Vlachoudis, A. Waets, M. Widorski, New Capabilities of the FLUKA Multi-Purpose Code, *Frontiers in Physics* (9) (2022) 788253.
- [169] G. Battistoni, T. Boehlen, F. Cerutti, P. Chin, L. Esposito, A. Fassò, A. Ferrari, A. Lechner, A. Empl, A. Mairani, A. Mereghetti, P. G. Ortega, J. Ranft, S. Roesler, P. Sala, V. Vlachoudis, G. Smirnov, Overview of the FLUKA code, *Annals of Nuclear Energy* (82) (2015) 10–18.
- [170] J. F. Ziegler, J. P. Biersack, *The Stopping and Range of Ions in Matter*, Springer US, Boston, MA, 1985, Ch. Chapter, pp. 93–129. doi:10.1007/978-1-4615-8103-1_3.
- [171] M. Berger, J. Coursey, M. Zucker, J. Chang, Stopping-Power and Range Tables for Electrons, Protons, and Helium Ions, <https://www.nist.gov/pml/stopping-power-range-tables-electrons-protons-and-helium-ions>, [Online; accessed 05.03.2023] (2017). doi:10.18434/T4NC7P.
- [172] C. Bernerd, J. Johnson, E. Aubert, M. Au, V. Barozier, P. Bertreix, F. Bruchertseifer, R. Catherall, E. Chevally, K. Chrysalidis, P. Christodoulou, T. E. Cocolios, B. Crepieux, M. Deschamps, A. Dorsival, C. Duchemin, V. Fedosseev, P. Fernier, M. Heines, R. Heinke, U. Khalid, M. Khan, Q. Khan, L. Lambert, E. Mamis, B. A. Marsh, S. Marzari, N. Mena, M. Munos, F. Pozzi, S. Prvakova, J. P. Ramos, F. Riccardi, R. E. Rossel, T. Stora, J. Thiboud, J. Vollaie, V. V. D. Bergh, W. Wojtaczka, Production of innovative radionuclides for medical applications at the CERN-MEDICIS facility, *Nuclear Inst. and Methods in Physics Research, B* 542 (June) (2023) 137–143. doi:10.1016/j.nimb.2023.05.008.
- [173] C. Maples, Nuclear data sheets for A = 223, *Nuclear Data Sheets* 22 (2) (1977) 243–274. doi:10.1016/S0090-3752(77)80007-0.
- [174] B. Singh, D. Abriola, C. Baglin, V. Demetriou, T. Johnson, E. McCutchan, G. Mukherjee, S. Singh, A. Sonzogni, J. Tuli, Nuclear Data Sheets for A = 211, *Nuclear Data Sheets* 114 (6) (2013) 661–749. doi:10.1016/j.nds.2013.05.001.

- [175] E. Laser, M. and Merz, Über die fluorierung von Protaktinium, *Journal of Inorganic Nuclear Chemistry* 31 (1969) 349–360.
- [176] NIST, NIST Chemistry Webbook, <https://webbook.nist.gov/chemistry/>, [Online; accessed 25.01.2022] (2023). doi:10.18434/T4D303.
- [177] R. Kiper, Physicochemical properties of substances, <http://chemister.ru>, [Online, accessed 25.05.2023] (2022).
- [178] J. G. Malm, B. Weinstock, E. E. Weaver, The Preparation and Properties of NpF_5 ; a Comparison with PuF_5 , *Journal of Physical Chemistry* 62 (12) (1958) 1506–1508. doi:10.1021/j150570a009.
- [179] Office for Special Political Affairs, The world’s requirements for energy: the role of nuclear energy, in: *Proceedings of the International Conference on the Peaceful Uses of Atomic Energy*, Vol. Volume 1, UN, 1956, pp. viii, 479 p.
URL <http://digitallibrary.un.org/record/3903820>
- [180] W. T. Carnall, G. R. Choppin (Eds.), *Plutonium Chemistry*, American Chemical Society, 1983. doi:10.1021/bk-1983-0216.
- [181] B. Weinstock, J. G. Malm, The properties of plutonium hexafluoride, *Journal of Inorganic and Nuclear Chemistry* 2 (5) (1956) 380–394. doi:10.1016/0022-1902(56)80092-4.
- [182] A. E. Florin, I. R. Tannenbaum, J. F. Lemons, Preparation and properties of plutonium hexafluoride and identification of plutonium(VI) oxyfluoride, *Journal of Inorganic and Nuclear Chemistry* 2 (5) (1956) 368–379. doi:10.1016/0022-1902(56)80091-2.
- [183] S. Rothe, M. Au, J. Ballof, E. Barbero, M. Bissell, A. Boucherie, M. Bovigny, Targets and ion sources at CERN-ISOLDE — Facilities and developments, *Nuclear Instruments and Methods in Physics Research, Section B: Beam Interactions with Materials and Atoms* 542 (June) (2023) 38–44. doi:10.1016/j.nimb.2023.05.058.
- [184] M. Schuett, M. Au, M. Bissell, N. Bidault, A. Koliatos, L. Le, N. Azaryan, R. Heinke, K. Chrysalidis, S. Rothe, Developments at the CERN-ISOLDE Offline 2 mass separator, *Nuclear Instruments and Methods in Physics Research, Section B: Beam Interactions with Materials and Atoms* 541 (May) (2023) 82–85. doi:10.1016/j.nimb.2023.04.053.
URL <https://doi.org/10.1016/j.nimb.2023.04.053>
- [185] S. Warren, T. Giles, C. M. Pequeno, Offline 2, ISOLDE ’s target, laser and beams development facility, *Nuclear Inst. and Methods in Physics Research, B* 463 (July 2019) (2020) 115–118. doi:10.1016/j.nimb.2019.07.016.
- [186] M. Au, M. Athanasakis-Kaklamanakis, S. Rothe, A mass spectrometer for molecular ion beam development at ISOLDE OFFLINE, Tech. rep., CERN (Aug 2021).
URL <https://edms.cern.ch/document/2617173/1>
- [187] S. Bennett, D. Sharp, T. Wright, Probing the fission and radiative decay of the $^{235}\text{u}+n$ system using (d,pf) and $(d,p\gamma)$ reactions, Tech. rep., CERN, Letter of Intent to the ISOLDE and Neutron Time-of-Flight Committee, Geneva (2023).
URL <https://cds.cern.ch/record/2845988>

- [188] C. S. Sumithrarachchi, Y. Liu, S. N. Rogers, S. Schwarz, G. Bollen, N. Gamage, The new Batch Mode Ion Source for stand-alone operation at the Facility for Rare Isotope Beams (FRIB), Nuclear Instruments and Methods in Physics Research, Section B: Beam Interactions with Materials and Atoms 541 (March) (2023) 301–304. doi:10.1016/j.nimb.2023.05.061.

